

Dissertation  
submitted to the  
Combined Faculties for the Natural Sciences and for Mathematics  
of the Ruperto-Carola University of Heidelberg, Germany  
for the degree of  
Doctor of Natural Sciences

presented by  
MSc Ivonne Morales  
Born in Monterrey, México

Oral examination: April 14, 2011

# Functional Analysis of Potential Phosphorylation Sites in the HIV-1 p6<sup>Gag</sup> Domain

Referees:

Prof. Dr. Hans-Georg Kräusslich

PD Dr. Jacomine Krijnse-Locker

## Summary

The human immunodeficiency virus type 1 (HIV-1) interacts with multiple host components and usurps cellular regulatory mechanisms, such as phosphorylation to help direct different events of its replication cycle. Protein phosphorylation is a posttranslational modification widely used by the cell to convey specific messages in response to specific stimuli and allows the coordination of a myriad of cellular processes in a timely and specific manner. The C-terminal p6 domain of the HIV-1 Gag protein, besides carrying the PTAP L-domain required to mediate virus release, is subject to phosphorylation. Although p6 has been identified to exist as the major phosphoprotein in HIV-1 particles, an in-depth study of the functional role of p6 phosphorylation has not been conducted to date. Thus, these observations prompted us to perform a comprehensive analysis of the consequences of potential p6 phosphorylation in the HIV-1 replication cycle.

Information derived from phosphorylation prediction programs and from HIV-1 subtype sequence alignments allowed us to select the p6 residues: T8, S14, T23 and S25 for mutational analysis. None of these residues, except for T8, had an effect in virus maturation, production, or replication capacity. We observed a partial enhancement in virus release by a T8D mutant—designed to mimick a phosphorylated state—that is likely due to a slightly greater affinity for the cellular interaction partner, Tsg101. We coupled our mutational analysis with the power of mass spectrometry to identify phosphorylated residues in p6. Multiple phosphoresidues were detected: T21, T22/23, S40, S43, and S51 and some appear to occur at specific processing stages of the Gag precursor protein.

Surprisingly, a p6 T8N mutant behaved similar to the wildtype virus both in release and in single-round infection. Biochemical and structural studies revealed that this mutant is engages the ESCRT machinery, most likely through Tsg101. This interaction putatively occurs with a 5-fold lower affinity that is sufficient to mediate the recruitment of the ESCRT machinery to sites of virus assembly and budding. This finding elicits further characterization of the complex which would be especially relevant in the design of p6-Tsg101 peptide inhibitors. In addition, we speculate that the PNAP motif, present in a few other viruses and

eukaryotic proteins might have preferentially evolved into a motif of higher affinity, namely the PT/SAP motif.

This study has advanced our knowledge of the phosphorylation state of HIV-1 p6 and suggests potential functional consequences of this modification. In addition, it reveals an unprecedented interaction between a PNAP late domain and Tsg101, highlighting the structural flexibility that might exist to accommodate other residues at the T8 position, which would be an important consideration in the design of peptide inhibitors. Finally, it provides a potential instance of viral late domain motif evolution.

## Zusammenfassung

Das humane Immundefizienz-Virus Typ 1 (HIV-1) kann mit vielen Proteinen und anderen Komponenten seiner Wirtszelle interagieren und so zelluläre Regulationsmechanismen wie die Phosphorylierung für seinen Replikationszyklus ausnutzen. Die Phosphorylierung von Proteinen ist eine translationale Modifikation, die von der Zelle genutzt wird, um spezifische Reiz-Signale weiterzuleiten und die zeitliche und spezifische Koordination unzähliger zellulärer Prozesse zu gewährleisten.

Das p6 Protein am C-Terminus von HIV-1 Gag besitzt nicht nur eine PTAP *late domain* sondern ist auch Ziel vieler Phosphorylierungen in der Wirtszelle. Obwohl p6 schon als das am häufigsten phosphorylierte Protein in HIV-1 Partikel identifiziert wurde, sind bis heute keine vertiefenden Analysen über die Funktion dieser p6 Modifikationen durchgeführt worden. Deshalb widmet sich die vorliegende Arbeit der ausführlichen Untersuchung der Auswirkung von möglichen Phosphorylierungs-Stellen in p6 auf den HIV-1 Replikationszyklus. Mit Hilfe von Bioinformatik-Programmen zur Identifikation von möglichen Phosphorylierungsstellen und zusätzlichen HIV-1 Subtypen Sequenz Analysen konnten vier konservierte und möglicherweise phosphorylierte Aminosäuren in p6 identifiziert werden: T8, S14, T23 und S25, die dann detailliert durch Mutationsanalysen untersucht wurden.

Bis auf die Aminosäure Threonin an Position 8 hatte keine der anderen drei zuvor identifizierten Aminosäuren einen Effekt auf die Replikation, Virusreifung oder Virusproduktion. Wir konnten eine leichte Erhöhung der Virusfreisetzung im Vergleich zu anderen Mutationen bei der T8D Mutante beobachten, die extra konstruiert wurde, um die Phosphorylierung an dieser Position nachzuahmen. Dieser Effekt kam vermutlich durch eine höhere Bindungsaffinität dieser Mutante zum zellulären Interaktionspartner Tsg101 zustande. Zusätzlich zur Mutationsanalyse haben wir mittels Massenspektrometrie die Phosphorylierungsstellen in p6 genau bestimmt. Dabei wurden mehrere Phosphorylierungspositionen ermittelt: T21, T22/23, S40, S43 und S51 von denen einige vermutlich nur zu bestimmten Zeiten der Prozessierung des Gag Vorläuferproteins in Erscheinung treten.

Überraschenderweise verhielt sich die p6 T8N Mutante in der Virusfreisetzung und Infektion genau wie Wildtyp. Biochemische Untersuchungen und Strukturanalysen zeigten, dass das mutierte Virus mit dem ESCRT Komplex interagieren können, sehr wahrscheinlich über Tsg101. Diese Interaktion geschieht sehr wahrscheinlich mit einer 5-fach geringeren Affinität als mit Wildtyp Virus, diese reicht aber aus für die Rekrutierung des ESCRT Komplexes zum Ort des Viruszusammenbaus und dem Virusaustritt. Diese Beobachtung ist ein erster Schritt für die weitere Charakterisierung dieser Interaktion, die besonders wichtig für die Entwicklung von p6-Tsg101 Peptid-Inhibitoren ist.

Zusätzlich dazu könnte man spekulieren, dass sich das PNAP Motiv, das in einigen wenigen anderen Viren und auch zellulären Proteinen vorhanden ist, evolutionär zum PT/SAP Motiv mit höherer Bindungsaffinität entwickelt hat.

Die vorliegende Arbeit könnte den aktuellen Wissensstand bezüglich der Phosphorylierung des HIV-1 p6 Proteins erweitern und zeigt darüberhinaus die möglichen funktionalen Folgen dieser Modifikationen auf. Zusätzlich dazu konnte eine neue Interaktion zwischen einer PNAP *late domain* und Tsg101 identifiziert werden, was die strukturelle Flexibilität und Anpassungsfähigkeit der Aminosäure an der Position T8 betont. Diese neuen Erkenntnisse sind sehr wichtig für die Entwicklung von Peptid-Inhibitoren. Darüberhinaus wurde hier in dieser Arbeit eine Möglichkeit für die evolutionäre Veränderung und Entwicklung einer viralen *late domain* aufgedeckt.

## Table of contents

Summary .....	1
Zusammenfassung.....	5
Table of contents.....	7
List of figures .....	11
1 Introduction.....	13
1.1 The Human Immunodeficiency Virus type 1 (HIV-1).....	14
1.2 The HIV-1 replication cycle.....	15
1.3 The mechanism of HIV-1 exit .....	17
1.3.1 Virus assembly at the plasma membrane and bud formation.....	17
1.3.2 Bud scission .....	19
1.4 The Tsg101 UEV-PTAP interaction.....	30
1.5 Phosphorylation as a posttranslational modification usurped by HIV-1.....	36
1.5.1 Kinase structure and levels of substrate specificity .....	36
1.5.2 Phosphorylation of HIV-1 proteins.....	39
1.5.3 HIV-1 p6 as the major phosphoprotein in virus particles.....	41
Goal of the study .....	42
2 Materials and Methods .....	43
2.1 Materials and instruments .....	43
2.2 Buffers and reagents .....	44
2.3 Primers .....	46
2.4 Plasmids.....	49
2.5 Cell lines.....	50
2.6 Antibodies.....	50

2.7	Molecular Biological methods .....	51
2.7.1	Transformation and plasmid amplification .....	51
2.7.2	DNA sequencing .....	52
2.7.3	Polymerase chain reaction (PCR) .....	52
2.7.4	Restriction digest and ligation .....	53
2.7.5	DNA electrophoresis .....	53
2.7.6	FRB and FKBP expression plasmids .....	54
2.7.7	Generation of p6 single point mutants .....	54
2.7.8	Generation of an infectious pNL4-3 clone containing uncoupled gag-pol frames and p6 mutant derivatives .....	54
2.8	Biochemical Methods .....	55
2.8.1	SDS-Polyacrylamide Gel Electrophoresis (SDS-PAGE) and Western Blot .....	55
2.8.2	Silver staining .....	56
2.8.3	Enzyme-Linked Immunosorbent Assay (p24-ELISA) .....	56
2.8.4	Tsg101 UEV domain purification .....	57
2.8.5	Peptides .....	58
2.8.6	Phosphopeptide mass spectrometry analysis .....	58
2.8.7	Isothermal Titration Calorimetry (ITC) .....	59
2.9	Cell Biological Methods .....	59
2.9.1	Cell culture .....	59
2.9.2	Transfection of cells .....	60
2.9.3	RNA interference .....	60
2.9.4	Analysis of heterodimerizer-mediated Gag-FKBP release .....	61
2.9.5	Isolation of human peripheral blood mononuclear cells (PBMCs) .....	62
2.9.6	Thin-section electron microscopy of cell samples .....	62
2.10	Virological methods .....	63
2.10.1	Virus propagation and purification by OptiPrep gradient .....	63

2.10.2	Analysis of HIV-1 particle release .....	63
2.10.3	Infectivity assay .....	64
2.10.4	Replication kinetics of HIV-1 and p6 mutant derivatives .....	64
3	Results.....	65
3.1	Identification and selection of predicted and conserved phosphorylated residues in the p6 <sup>Gag</sup> domain of HIV-1 .....	65
3.2	Effect of p6 mutants in HIV-1 release and viral protein processing.....	68
3.3	Infectivity and replication capacity of HIV-1 p6 mutants.....	70
3.4	Analysis of a p6 T8E mutant .....	74
3.5	Comprehensive analysis of predicted phosphorylation sites in HIV-1 p6.....	76
3.5.1	Uncoupling the overlapping <i>gag</i> and <i>pol</i> reading frames.....	77
3.5.2	Effect of frameshift displacement on virus maturation and particle production .....	78
3.5.3	Effect of frameshift displacement on virus infectivity .....	79
3.5.4	Generation of uncoupled viruses carrying extensive mutations in HIV-1 p6.....	80
3.6	p6 phosphopeptide analysis by Mass Spectrometry.....	82
3.7	Effect of a p6 T8N mutant in the HIV-1 replication cycle.....	93
3.7.1	Morphology of p6 T8N mutant virion analyzed by electron microscopy.....	96
3.8	Characterization of the interaction properties between the p6 T8N mutant and the Tsg101 UEV domain.....	98
3.8.1	Analysis of the crystal structure of the Tsg101 UEV domain in complex with a PNAP p6 peptide .....	98
3.9	Binding affinity between a PNAP p6 peptide and Tsg101 UEV .....	101
4	Discussion .....	106
4.1	Comprehensive analysis of HIV-1 p6 <sup>Gag</sup> phosphorylation .....	107
4.2	Uncoupling of the <i>gag</i> and <i>pol</i> overlapping reading frames to perform extensive mutations in p6 <sup>Gag</sup> .....	109
4.3	p6 phosphopeptide analysis by mass spectrometry .....	113
4.4	Interaction properties between a p6 T8N mutant and the Tsg101 UEV domain .....	115

4.5	Future directions .....	119
5	References .....	121
	Appendix A: Analysis of the role of E3 ubiquitin ligase recruitment in retrovirus formation.....	129
	List of publications.....	134
6	List of Abbreviations .....	135
	Acknowledgements .....	139

## List of figures

FIGURE 1.1. HIV-1 GENOME ORGANIZATION AND VIRION STRUCTURAL FEATURES. ....	15
FIGURE 1.2. SCHEMATIC OF THE HIV-1 REPLICATION CYCLE. ....	17
FIGURE 1.3 HIV-1 P6 MUTANTS HAVE A PRONOUNCED DEFECT IN RELEASE. ....	19
FIGURE 1.4. THE LATE DOMAINS OF DIFFERENT ENVELOPED VIRUSES. ....	21
FIGURE 1.5 THE ROLE OF THE ESCRT COMPLEX IN PROTEIN SORTING AND MVB BIOGENESIS. ....	23
FIGURE 1.6 MOLECULAR COMPONENTS OF THE ESCRT COMPLEX. ....	26
FIGURE 1.7 THE DIFFERENT ESCRT ENTRY PATHWAYS USED BY THE THREE VIRAL LATE DOMAINS. ....	30
FIGURE 1.8 Tsg101 UEV SEQUENCE AND SECONDARY STRUCTURE. ....	32
FIGURE 1.9 BINDING OF THE HIV-1 PTAP PEPTIDE. ....	33
FIGURE 1.10 STRUCTURE OF THE COMPLEX BETWEEN THE Tsg101 UEV DOMAIN AND Ub. ....	34
FIGURE 1.11 Tsg101 UEV CAN SIMULTANEOUSLY BIND A PTAP PEPTIDE AND Ub. ....	35
FIGURE 1.12 PROTEIN KINASE STRUCTURE WITH ATP AND AMINO ACID PHOSPHORYLATION REACTION. ....	37
FIGURE 3.1 EFFECT OF P6 MUTANTS IN VIRUS PRODUCTION AND GAG PROTEIN PROCESSING. ....	68
FIGURE 3.2 COMPARISON OF THE LEVELS OF HIV-1 PRODUCED BY THE T8 MUTANTS. ....	69
FIGURE 3.3 SINGLE-ROUND INFECTIVITY OF HIV-1 P6 MUTANTS. ....	70
FIGURE 3.4 REPLICATION KINETICS OF HIV-1 P6 MUTANTS. ....	72
FIGURE 3.5 REPLICATION KINETICS OF HIV-1 P6 MUTANTS IN PRIMARY LYMPHOCYTES. ....	73
FIGURE 3.6 EFFECT OF A P6 T8E MUTANT ON HIV-1 RELEASE AND GAG PROCESSING. ....	74
FIGURE 3.7 EFFECT OF THE HIV-1 P6 T8N AND T8Q MUTANTS ON VIRUS RELEASE AND GAG PROCESSING. ....	75
FIGURE 3.8. THE HIV-1 FRAMESHIFT DETERMINANTS. ....	76
FIGURE 3.9 SCHEMATIC OF THE STRATEGY USED TO UNCOUPLE THE HIV-1 GAG- AND POL-READING FRAMES. ....	77
FIGURE 3.10 INFLUENCE OF FRAMESHIFT DISPLACEMENT ON VIRUS MATURATION AND RELEASE. ....	78
FIGURE 3.11 ANALYSIS OF FRAMESHIFT DISPLACEMENT ON VIRUS INFECTIVITY. ....	79
FIGURE 3.12 SCHEMATIC OF THE THREE FRAGMENTS CONTAINING MULTIPLE MUTATIONS IN P6. ....	80
FIGURE 3.13. CHARACTERIZATION OF VIRUS MATURATION AND PRODUCTION BY THE UNCOUPLED P6 MUTANT VIRUSES. ....	81
FIGURE 3.14. SELECTION OF VIRUS PROTEIN BANDS FOR MASS SPECTROMETRY ANALYSIS. ....	83
FIGURE 3.15 LIST OF PEPTIDES OBTAINED FROM THE MASS SPECTROMETRY ANALYSIS OF HIV-1 PROTEINS. ....	86
FIGURE 3.16 WESTERN BLOT ANALYSIS OF HIV-1-DERIVED P6 PRODUCTS. ....	88
FIGURE 3.17 MASS SPECTROMETRY ANALYSIS OF P6 POSTTRANSLATIONAL MODIFICATIONS. ....	89
FIGURE 3.18 SCHEMATIC OF IDENTIFIED PHOSPHORESIDUES IN HIV-1 PROTEINS BY MS ANALYSIS. ....	90
FIGURE 3.19 PHOSHOPEPTIDE ENRICHMENT ANALYSIS OF P6 PHOSPHORYLATION. ....	91
FIGURE 3.20 WESTERN BLOT ANALYSIS OF HIV-1-DERIVED P6 PRODUCTS. ....	92

FIGURE 3.21 EFFECT OF THE P6 T8N MUTANT IN VIRAL INFECTIVITY. ....	94
FIGURE 3.22 EFFECT OF TSG101 KNOCKDOWN ON THE RELEASE EFFICIENCY OF THE P6 T8N MUTANT VIRUS.....	96
FIGURE 3.23 VISUALIZATION OF P6 T8N VIRIONS BY THIN-SECTION ELECTRON MICROSCOPY. ....	97
FIGURE 3.24 GEL FILTRATION PURIFIED TSG101 UEV. ....	99
FIGURE 3.25 TSG101 UEV CRYSTAL STRUCTURE. ....	100
FIGURE 3.26 CRYSTAL STRUCTURE OF THE TSG101 UEV-PTAP COMPLEX.....	101
FIGURE 3.27 SCHEMATIC REPRESENTATION OF A POWER COMPENSATION CALORIMETER.....	102
FIGURE 3.28 ISOTHERMAL TITRATION CALORIMETRY OF THE TSG101 UEV-P6 PEPTIDE INTERACTION. ....	105

# 1 Introduction

Composed of only a genome and protein, viruses cannot subsist by themselves and therefore rely on a host to replicate. Thus, parasitizing a susceptible host cell and overtaking its intracellular components is an absolute requirement for their survival and propagation. These tiny infectious agents, which range in size from 20 nm to about 400 nm, have evolved multiple ways to recognize, bind to and enter their hosts, providing some with the ability to infect a wide range of hosts. Moreover, once they have gained access into the host cell's interior, they can efficiently usurp the cell's cytoskeletal components and use them as trafficking roads on which they can reach specific regions and organelles within the cell. Viruses may even use the cell's replication machinery to copy their own genetic information while they entirely rely on the host's translation machinery to give rise to the components necessary to build and assemble new progeny virions. Newly formed virions are then ready to exit the cell—either through lysis of the host cell or by budding through cellular membranes—and continue their further propagation.

Overall, viruses have evolved elegant ways to take advantage of the subtlety with which cellular networks function. For instance, posttranslational modification of cellular proteins conveys specific messages to the cell and makes it possible to orchestrate a myriad of cellular processes. Likewise, some viral proteins have adopted the capability to undergo modification, granting the virus access to cellular pathways that facilitate its travel through and out of the cell.

This study mainly addresses the cellular biology of the Human Immunodeficiency Virus type 1 (HIV-1)-host cell interactions and focuses on the potential role of phosphorylation during different stages of its replication cycle.

## 1.1 *The Human Immunodeficiency Virus type 1 (HIV-1)*

In the early 1980s, a rare epidemic characterized by a pronounced impairment in immune function was reported in countries all over the world. This deficiency was termed Acquired Immunodeficiency Syndrome (AIDS) and was observed to be often accompanied by a series of opportunistic infections, such as *Pneumocystis carinii* infection and Kaposi's sarcoma (52). It was in 1983 when the Human Immunodeficiency Virus type 1 (HIV-1) was identified as the retrovirus causing AIDS (7, 46). HIV-1 has caused the death of an estimated 1.8 million people worldwide in 2009 alone. According to the most recent UNAIDS report, there are 33.3 million people living with HIV-1, of whom 22.5 million are living in sub-Saharan Africa(141).

A member of the Retroviridae, HIV-1 is an enveloped lentivirus that carries two copies of a single-stranded RNA genome of about 9700 nucleotides in length of positive polarity. The overall genome organization is depicted in Figure 1.1. The viral genome of all simple retroviruses gives rise to 3 main genes: *group specific antigen (gag)*, *polymerase (pol)* and *envelope (env)*. In addition to these three main genes, the HIV-1 genome encodes for the accessory proteins *nef* (negative factor), *vif* (virion infectivity factor), *vpr* (viral protein R), *vpu* (viral protein U), *tat* (transactivator) and *rev* (regulator of virion) which play important roles during HIV-1 pathogenesis. The *gag* gene encodes the main structural component of the virion, Gag. During virus maturation, Gag is proteolytically processed into the proteins matrix (MA), capsid (CA), nucleocapsid (NC), spacer peptides 1 and 2 (SP1 and SP2) and the p6 protein. The *pol* gene gives rise to 3 enzymes: protease (PR), reverse transcriptase (RT), and integrase (IN), while the *env* gene encodes for the surface (SU) and transmembrane (TM) glycoproteins that coat the surface of the viral lipid envelope (30, 63). The illustration in Figure 1.1 shows both the arrangement of the major and regulatory viral components encoded by the viral genome, as well as a model for virus structure in both the immature and cleaved, mature form.

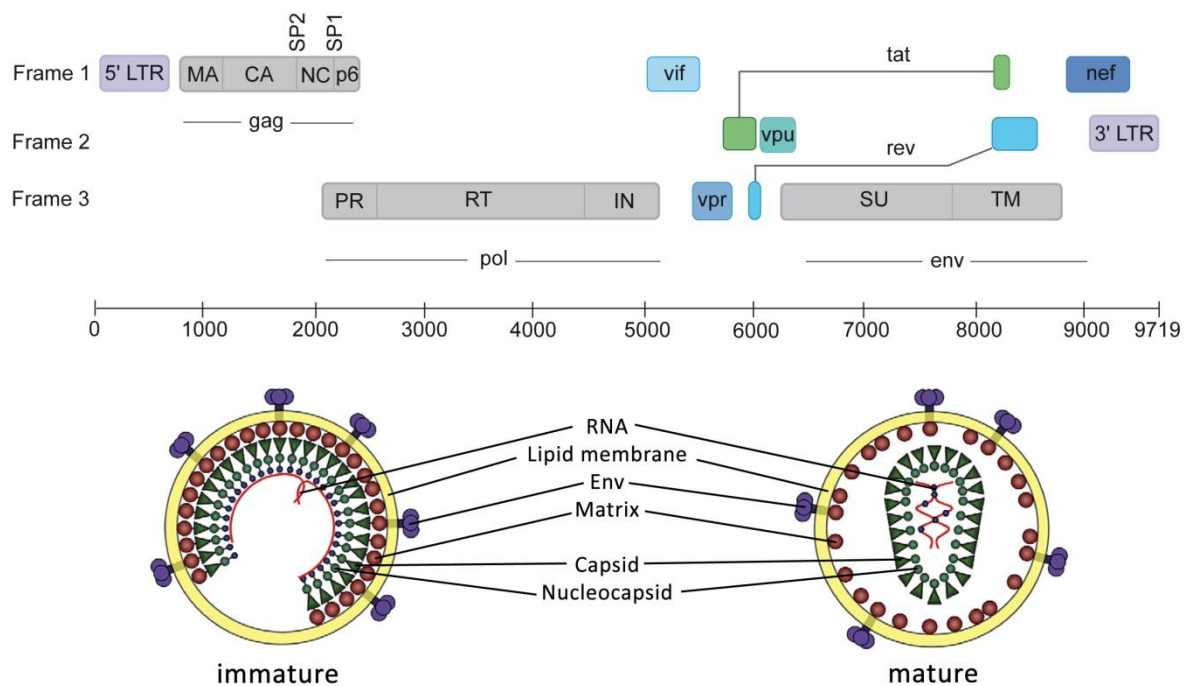


**Figure 1.1. HIV-1 genome organization and virion structural features.**

Above, the HIV-1 genome encodes 3 main genes: *gag*, *pol*, and *env*, as well as the accessory proteins *vif*, *vpr*, *vpu*, *tat*, *rev*, and *nef*. The RNA transcripts that give rise to these proteins are generated as unspliced (*gag* and *pol*), singly spliced (*env*, *vif*, *vpr*, *vpu*) or multiply spliced (*tat*, *rev*, *nef*). For *tat* and *rev*, the 5' and 3' exon splice junction sites are marked by a bold line. Sequences found at both the 5' and 3' ends of the genome contain the long-terminal repeats (LTRs), regions that dictate viral RNA synthesis and integration, while genome packaging into new progeny virions is directed by the packaging signal *psi* at the 5' terminus of the transcript. The HIV-1 genome in this illustration is based on the HXB2 isolate. Below, a schematic of the structural features of the two virus forms: immature (left) and mature (right). The immature virus is characterized by a thick layer of uncleaved *gag* polyproteins underlying the virion membrane, whereas proteolytic processing of the *gag* polyproteins during maturation gives rise to a cone-shaped core that encloses the viral RNA and additional viral proteins. This processing step renders the virus infectious. Adapted from (47, 86).

## 1.2 The HIV-1 replication cycle

The HIV-1 replication cycle occurs as a series of steps depicted in Figure 1.2. The first step involved in granting the virus access into the host cell cytoplasm is mediated by the binding of the envelope surface (SU) glycoprotein gp120 to the cellular receptor CD4 and the coreceptor CXCR4 or CCR5, depending on viral tropism. Engagement of both receptor and coreceptor leads to conformational changes in gp120 that expose the transmembrane (TM) glycoprotein, gp41. In turn, gp41 undergoes a structural rearrangement that creates a 6-bundled helix, bringing together the lipid bilayer of the virion and the host cell plasma membrane leading to fusion of the two membranes, thus allowing the viral core to be released into the cytoplasm (41, 51, 91). Nevertheless, recent evidence suggests that HIV-1

primarily relies on endocytic uptake to reach the cytoplasm (98). Once in the cytoplasm, HIV cores disassemble rapidly in a process known as uncoating. During this process, a reverse transcription complex (RTC) comprised of NC (nucleocapsid), RT (reverse transcriptase), IN (integrase), Vpr and viral RNA forms and reverse transcription of the viral RNA takes place. The product of the reverse transcription reaction is a full-length, double-stranded linear DNA version of the genome, flanked at each end by two long-terminal repeats (LTRs) that are important for integration of the proviral DNA into the host genome and for viral RNA expression (41, 63, 85). The viral protein-DNA complex, now referred to as the preintegration complex (PIC) is transported across the nuclear membrane in a process that might be facilitated by the Vpr and/or IN proteins. Once inside the nucleus, the viral IN protein acts to insert the linear DNA into the host cell chromosome (63). The integrated viral DNA, known as the provirus, serves as the template for the synthesis of the viral RNAs. HIV transcripts can be unspliced, singly spliced or multiply spliced. The unspliced and singly spliced transcripts are transported by the viral Rev protein from the nucleus to the cytoplasm (91). The unspliced RNA is used to make Gag and Gag-Pol proteins and also serves as the genome. The singly spliced RNA is used to make the Env glycoproteins which are synthesized in the ER followed by their transport to the plasma membrane via the secretory pathway (41, 63). The Gag and Gag-Pol polyprotein precursors are synthesized on cytoplasmic ribosomes and the newly synthesized polyproteins recruit two copies of the single-stranded viral genome (87) before travelling to the plasma membrane. At the plasma membrane, the assembly of the Gag proteins generates curvature that leads to formation of a bud. During budding, the viral Env glycoproteins are incorporated into the nascent particles. The budding step is completed as the particle pinches off from the plasma membrane (41). Concomitant with or shortly after budding, the viral protease mediates virus particle maturation through cleavage of the Gag and Gag-Pol polyproteins, leading to formation of an electron-dense MA layer beneath the envelope and a conical capsid core at the center of the particle (91).

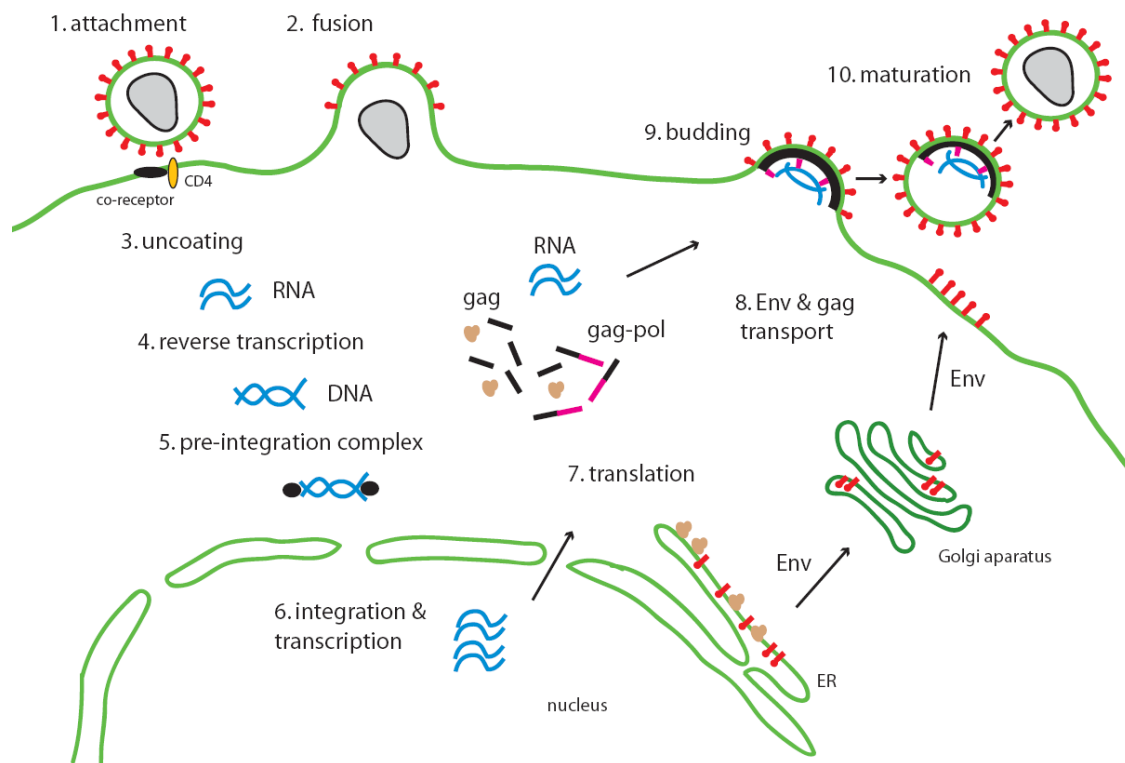


**Figure 1.2. Schematic of the HIV-1 replication cycle.**

Virus entry into the host cell cytoplasm is mediated by the initial binding of the viral gp120 envelope protein with the host's cellular receptor and coreceptor CD4 and CXCR4, respectively. This interaction results in a series of rearrangements that permit the envelope transmembrane protein, gp41 to mediate fusion of the viral membrane with the host cell membrane. Once it has gained access into the cytoplasm, the viral core is uncoated and reverse transcription of the viral RNA takes place within a reverse transcription complex (RTC). This reaction generates a full-length double-stranded DNA copy of the viral genome that remains associated with viral proteins (shown as the black dots) in the form of a pre-integration complex (PIC). This complex is then transported into the nucleus where the viral protein IN catalyzes the insertion of the proviral DNA into the host genome. Viral transcripts are exported into the cytoplasm where Gag and Gag-Pol precursor proteins are made. In contrast, the Env proteins are made in the rough endoplasmic reticulum (rER) (where the brown dots represent ribosomes) and travel via the secretory pathway to reach the plasma membrane. The Gag and Gag-Pol precursors associate with viral RNA transcripts in the cytoplasm before they reach the plasma membrane, where they assemble and induce bud formation. Nascent viral particles are ultimately released from the cell by the action of ESCRT proteins, which sever the membrane stalk connecting the virion to the host membrane. During the budding process, the immature virion undergoes proteolytic processing by the viral protease resulting in the formation of a conical capsid shell that surrounds the viral genome.

## 1.3 The mechanism of HIV-1 exit

### 1.3.1 Virus assembly at the plasma membrane and bud formation

In natural target cells of HIV-1, such as T cells and macrophages, the major site of virus particle assembly and budding is the plasma membrane (106, 149). The viral Gag

protein directs both of these processes, in fact, assembly of Gag alone at the plasma membrane results in the production of immature, non-infectious virions (50), indicating that Gag itself contains sufficient information to mediate the entire budding process. Ivanchenko et al (73), recently investigated the kinetics with which the assembly and budding reaction take place. By making use of GFP-tagged HIV-1 virions, they found that the fluorescence intensities of individual gag clusters changes in 3 phases—phase I was characterized by an increase in fluorescence intensity during the first minutes after nucleation of an assembly site was detected; in phase II, the fluorescence signal intensity remained stationary or constant, while during phase III a decay in the fluorescence intensity was observed. Overall, these phases can be translated into an assembly reaction of the Gag shell at the plasma membrane that requires around 8-9 minutes and culminates in the release of the nascent virus particles 16 minutes later(73)

Synthesis of the Gag polyproteins takes place in the cytoplasm of the infected cell and they must therefore find a way to reach the plasma membrane to initiate assembly. It is still a matter of debate how Gag precursor proteins are transported to the plasma membrane. Some evidence suggests that active transport of Gag might not be required for assembly since disrupting cytoskeletal components has no major effect on the appearance of HIV-1 Gag at the plasma membrane or virus yield (79). Alternatively, it has been suggested that host transport proteins such as GGA (golgi-localized, gamma ear-containing, ADP ribosylation factor-binding) or Arf (ADP ribosylation factor) mediate Gag movement to the plasma membrane (77). It is also still undefined whether Gag is transported as monomers or oligomers to the plasma membrane, but a recent study by Kutluay et al (87) found Gag to be present as monomers or low-order multimers during its association with viral RNA in the cytoplasm. Moreover, high-order Gag multimerization required membrane binding, suggesting this event occurs once Gag reaches the plasma membrane. Despite these uncertainties regarding Gag assembly, the process by which Gag associates with the plasma membrane has been more extensively characterized. The matrix (MA) domain of HIV-1 Gag contains a cluster of basic residues and an N-terminus that is co-translationally myristylated (11, 106, 146). Both of these features are critical for its affinity and binding to areas of the plasma membrane that contain the negatively charged phospholipid, phosphatidylinositol-(4,5)-bisphosphate or PI(4,5)P<sub>2</sub>. A study conducted by Ono (106) showed that PI(4,5)P<sub>2</sub> is

essential for both efficient Gag membrane binding and specific localization to the plasma membrane. Furthermore, MA binding of PI(4,5)P<sub>2</sub> triggers myristate exposure, anchoring Gag to the lipid bilayer while sequestering a PI(4,5)P<sub>2</sub> unsaturated acyl chain inside the MA molecules (126). The Gag-PI(4,5)P<sub>2</sub> interaction is thought to help partition Gag to lipid-raft-like microdomains (126). This notion would be in agreement with the fact that the HIV-1 viral envelope is enriched in cholesterol and sphingolipids relative to the host cell plasma membrane (16).

## 1.3.2 Bud scission

### 1.3.2.1.1 *The role of viral late domains in virus budding*

It is likely that Gag lattice formation at the membrane and lipid interactions provide the energy necessary to bend the membrane and enwrap the nascent virion. Early during Gag assembly and lattice formation, specific cellular proteins are recruited to the budding site to catalyze the release of nascent HIV-1 particles. This task is fulfilled through the p6 domain of the viral Gag protein.

The first hint that this region of HIV-1 Gag was involved in the release process came from a study by Göttlinger et al 20 years ago (53). Mutation of specific p6 sequences within the context of a full-length HIV-1 molecular clone resulted in impaired virus production. Visualization of this defect by electron microscopy (EM) showed that budding virus particles remained attached to the host membrane through a thin membrane stalk (53) (Figure 1.3).

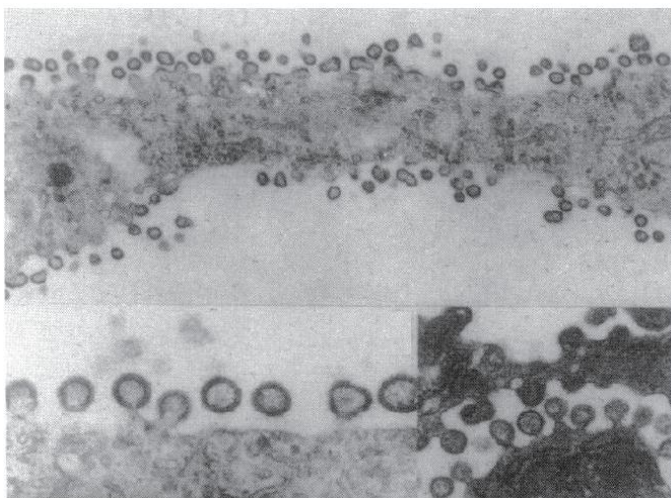


**Figure 1.3 HIV-1 p6 mutants have a pronounced defect in release.**

Electron microscopy image of HIV-1 virions that carry mutations in p6 Gag. The membrane of both host cell and nascent virion remain connected through a thin membranous stalk. Adapted from (53).

A few years later, Huang et al., pinpointed this phenotype to a P-T-A-P motif at the N-terminus of p6 where the threonine can also occur as a serine. Residues within this motif are critical for efficient virus release, while mutations outside this motif have little or no effect in virus particle production (64). Importantly, these studies laid the foundations for the discovery of similar and novel motifs in other retroviruses. For instance, the rous sarcoma virus (RSV) was found to encode a motif of a P-P-P-Y type that was shown to be required for budding (150, 153). This same motif was found to occur in the mason-pfizer monkey virus (MPMV) gag as well as in the p12 protein of moloney-murine leukemia virus (MuLV). In all instances, this motif was shown to be involved in virus production (154, 155). Interestingly, a motif of yet another type was uncovered in the lentivirus equine infectious anemia virus (EIAV). This motif corresponded to a Y-P-X-L present in its p9 protein (119). These 3 different types of motifs, namely PTAP, PPXY, and YPXL became collectively known as late (L)-domains for their role in the late stages of the virus replication cycle. More recently, a new viral L-domain was identified in a paramyxovirus (131). The core sequence of this motif consists of the residues FPIV (131). Notably, besides retroviruses, other enveloped viruses such as vesicular stomatitis virus (VSV)—a rhabdovirus—and Ebola virus—a filovirus—contain both PPPY and PT/SAP L-domains (31, 58, 76, 96). Years later after the characterization of the first L-domain in HIV-1, Strack et al, uncovered the presence of a second L-domain of the YPXL type at the C-terminus of the p6 domain (136). Additional L-domains have also been identified in MPMV and RSV (37, 54). Figure 1.4 illustrates the position, number and type of L-domains present in several enveloped viruses.

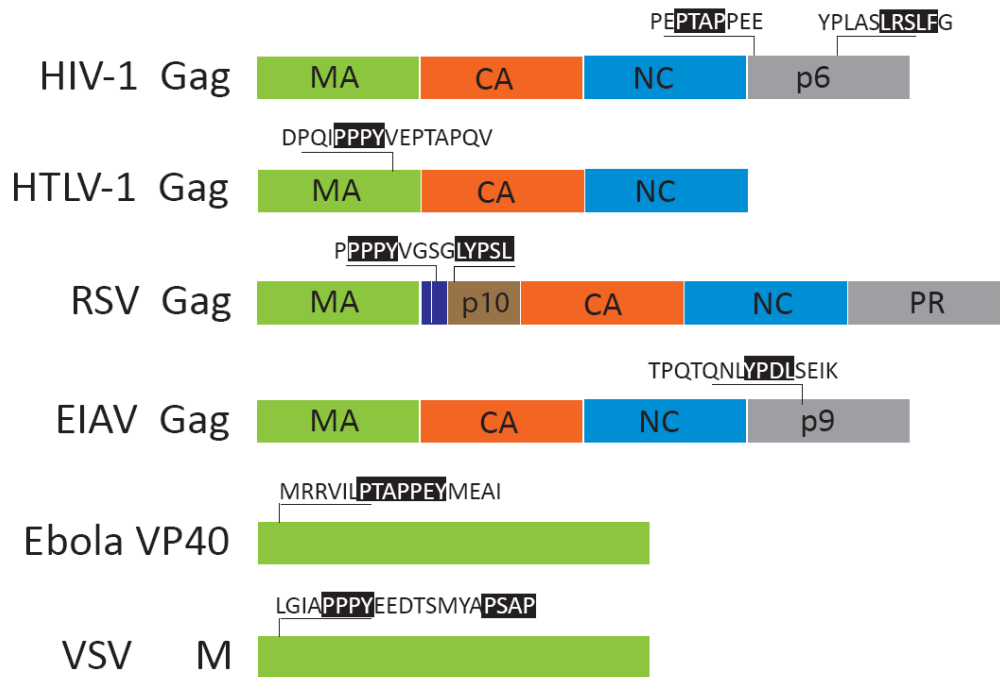


**Figure 1.4. The late domains of different enveloped viruses.**

Divergent enveloped viruses have been found to contain late domains in their structural proteins. The position and number of late domains vary from one virus family to another or even within virus species. Adapted from (12, 100).

The fact that viral L-domain function is position-independent even in the context of different retroviruses suggests that L-domains may function as protein modules (110). Thus, it seemed likely that these domains bound to and recruited host factors to the site of virus budding (43). Indeed, the first reported interaction between a cellular protein and a retroviral L-domain was shown for RSV (48). A series of studies followed in which potential interaction partners were identified for the different L-domain-containing enveloped viruses. A consensus of such studies determined that PPXY L-domains interact with the WW domains of E3 ubiquitin ligases of the Nedd4 (neuronal precursor cell-expressed developmentally downregulated 4) family (35, 48, 59, 83). This family of ubiquitin ligases has a common modular architecture: they contain an N-terminal C2 domain, a central WW domain and a C-terminal HECT (homologous to E6-AP carboxyl terminus) domain involved in cellular targeting, substrate recognition and ubiquitin conjugation, respectively (72). The YPXL late domain of EIAV and HIV-1 interact with the adaptor protein AIP1/Alix (ALG-2 (apoptosis-linked gene 2)-interacting protein X) protein (136) while PT/SAP L-domains interact with the

tumor susceptibility gene 101 (Tsg101) (49, 96, 144). Tsg101 forms part of a protein complex termed the endosomal sorting complex required for transport (ESCRT) that is involved in the sorting of ubiquitinated membrane proteins targeted for degradation in the lumen of the lysosome (80). Alix on the other hand, is an adaptor/scaffolding protein that plays a more indirect role in the ESCRT pathway in contrast to its putative yeast homolog Bro1, which is required for proper endosomal sorting in yeast (124). These findings sparked an interest to further characterize the interactions between viral L-domains and their cellular partner(s), especially since these are critical for the efficient release of nascent viral particles. At the same time, it led to the development of models by which the final scission step between the viral and the host cell membrane is thought to occur. The following section will describe the cellular machinery usurped by HIV-1 to mediate the final scission step that leads to its separation from the host cell membrane.

#### ***1.3.2.1.2 The Endosomal Sorting Complex Required for Transport (ESCRT) machinery***

ESCRT complex components were initially identified as part of an effort to study organelle biogenesis and assembly by using the yeast vacuole of *Saccharomyces cerevisiae* as a model system (121). In that study, a set of yeast protein mutants, termed class E vps mutants, appeared to be defective in the sorting process and displayed a characteristic morphology by electron microscopy (EM). Class E vps proteins appeared to be sequestered within a multilamellar endosome-like compartment that was distinct from the vacuole (121, 122). This compartment became known as the “class E compartment” and the genes involved in this morphology as “class E VPS (vacuolar protein sorting) genes” (121). Further characterization of the class E genes revealed that they are highly conserved from yeast to humans, and its components were subsequently isolated and structurally and biochemically characterized into four subcomplexes termed ESCRT-0, -I, -II, and -III. Together, they constitute the ESCRT complex, so named for its role in the protein sorting pathway (68, 80). The ESCRT complex has a principal role in the downregulation of receptor-mediated cell signaling. It recognizes and sorts endocytosed ubiquitinated plasma membrane signaling receptors into multivesicular bodies (MVBs) that eventually fuse with a lysosome, where

proteases degrade MVB contents. The ESCRT complex subdivides this task among its four subunits—ESCRT-0 recognizes and recruits cargo to early endosomes, ESCRT-I and -II sequester cargo into MVBs and ESCRT-III is thought to catalyze the final scission step that releases the budding MVB into the lumen of the late endosome. Recycling of the ESCRT components is mediated by the ATP-dependent Vps4 as depicted in Figure 1.5 (120, 127).

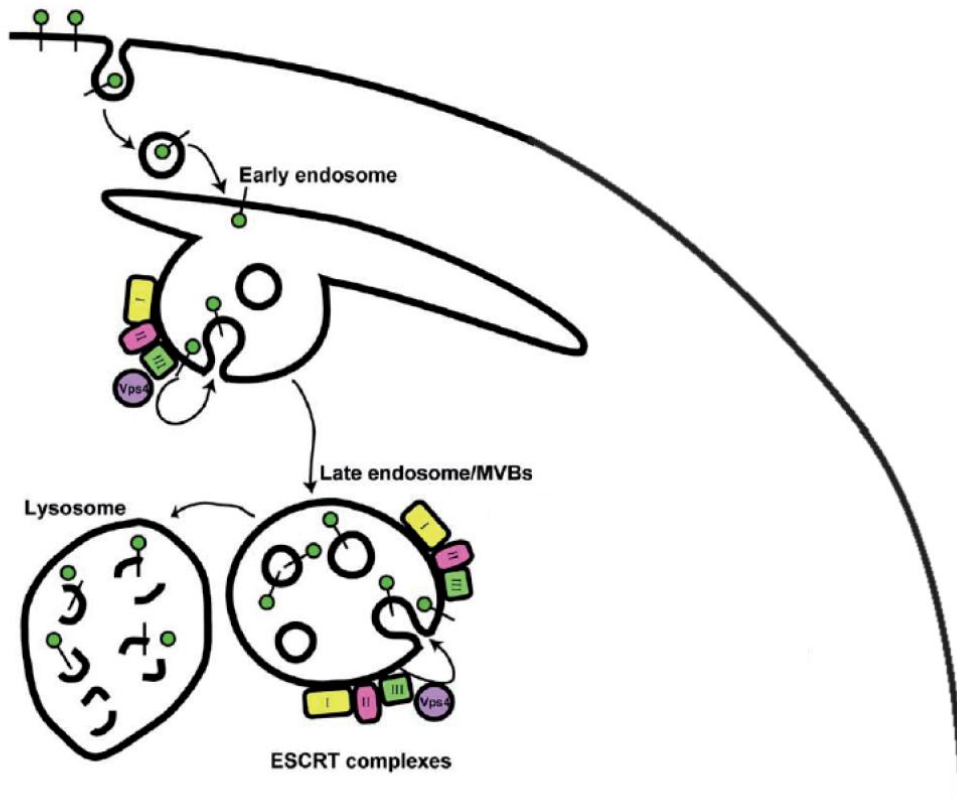


**Figure 1.5 The role of the ESCRT complex in protein sorting and MVB biogenesis.**

(A) Ubiquitylated cell-signaling receptors that need to be downregulated are sorted into intraluminal vesicles (ILVs) within endosomal-derived multivesicular bodies (MVBs). Subsequent fusion of the MVB with the lysosome results in the proteasomal degradation of the ILV content. The endosomal sorting complex required for transport (ESCRT) plays a major role in the recognition and sorting of ubiquitylated cargo. Ubiquitylated transmembrane proteins are recognized by the ubiquitin-recognition motifs present in ESCRT-0, ESCRT-I and ESCRT-II components. Assembly of these ESCRT components at the limiting membrane of the endosome results in initial deformation of the membrane followed by scission of the membrane bud neck mediated by ESCRT-III assembly and Vps4 ATP hydrolyzing activity. ESCRT components are then disassembled and recycled back into the cytosol by the action of Vps4. Adapted from (27).

The fact that proteins involved in the ESCRT pathway also seemed to participate in retroviral budding (see section 1.3.2.1.1) led to the realization that the ESCRT pathway might be hijacked by viral components to mediate their exit from the cell. This observation seemed plausible due to the fact that MVB biogenesis and viral budding are topologically equivalent processes, where budding is directed away from the cytosol. Moreover, it was also observed

that cytokinesis, a process employing the same topology during separation of a mother cell to generate a new daughter cell, also requires the participation of ESCRT components (23). These observations highlight the role of the ESCRTs in a variety of cellular processes that seem to include autophagy (69).

#### **1.3.2.1.2.1 ESCRT-0: cargo recruitment**

This complex consists of the subunits Hrs (hepatocyte growth-factor-regulated tyrosine kinase substrate) and STAM (signal-transducing adaptor molecule), Vps27 and Hse1 in yeast (120, 124). Hrs additionally contains a FYVE zinc-finger domain that is specific for binding the endosomal lipid phosphatidyl inositol 3-phosphate (PtdIns(3)P) and a PT/SXAP motif through which it binds the ESCRT-I component, Tsg101 (Vps23 in yeast) (81). The Hrs/STAM complex is thought to be recruited to the early endosomal membrane by PtdIns(3)P binding. Once at the endosomal membrane, Hrs recruits clathrin, resulting in restricted localization of Hrs that helps to concentrate cargo within a specific area of the endosome (124). The complex binds ubiquitylated cargo through their ubiquitin-interacting motifs (UIMs) (124, 127). Membrane-bound Hrs/STAM serves as a docking site for recruitment of the ESCRT-I complex via interaction between the ESCRT-I component, Tsg101 and a PT/SXAP motif in the C-terminus of Hrs.

#### **1.3.2.1.2.2 ESCRT-I and II: stabilization of the membrane bud**

The ESCRT-I was initially characterized in yeast and later in mammalian cells. It consists of a constitutively assembled complex of four subunits existing in a 1:1:1:1 ratio: Tsg101/Vps23, Vps28, Vps37 and Mvb12 (120). The crystal structure of the yeast ESCRT-I revealed that the complex exists as a 13 nm-long stalk connected to a 5 nm-long headpiece (84). The Tsg101 subunit contains a catalytically-inactive ubiquitin E2-variant domain (UEV) that binds to the PT/SXAP motifs in ESCRT-0, viral L-domains, such as that in HIV-1 p6 and ubiquitylated cargo (49, 68, 69, 120), contributing to recruitment of this complex to the endosomal membrane. In yeast, contact to the ESCRT-II complex is mediated through the C-terminal helical region in Vps28.

ESCRT-II is composed of one molecule each of EAP30/Vps22, EAP45/Vps36 and two molecules of EAP20/Vps25. Like ESCRT-0 and ESCRT-I it has ubiquitin-binding activity through EAP45/Vps36. ESCRT-0, -I and -II, all recognize and bind the same isoleucine (Ile) 44 hydrophobic patch in ubiquitin. The complex has a rigid, Y-shaped core and the overall structure has a maximal dimension of about 15 nm (70). Contact to the ESCRT-III complex is facilitated by Vps25 in ESCRT-II to the ESCRT-III component Vps20 (human CHMP6). It is not clear, however, how human VPS28 (in ESCRT-I) might bind to EAP45/Vps36. Although essential for endosomal sorting in yeast, the ESCRT-II complex is dispensable for HIV-1 budding and probably also for cytokinesis (69, 88).

#### **1.3.2.1.2.3 ESCRT-III: scission of the bud**

Subunits within the ESCRT-III complex are highly charged, with an N-terminal basic and a C-terminal acidic region. Unlike ESCRT-I and -II subunits, ESCRT-III proteins exist as inactive monomers in the cytosol. Upon activation, these subunits undergo conformational changes that allow them to interact with other ESCRT-III subunits to form a large protein lattice of unknown stoichiometry on the membrane (120, 127). The yeast ESCRT-III consists of four subunits: Vps20 (CHMP (charged multivesicular body proteins) 6 in humans) Snf7/Vps32 (CHMP4A, B and C), Vps24 (CHMP3) and Vps2 (CHMP2A, and B). The subunit that nucleates assembly on membranes is Vps20, which is N-terminally myristoylated and is thought to interact directly with the endosomal membrane. Vps20 binds to the Vps25 subunit of ESCRT-II, which functions to recruit and possibly activate Vps20. Vps20, interacts directly with Snf7/Vps32, the most abundant of the ESCRT-III subunits in yeast. This is thought to trigger the assembly of Snf7/Vps32 into filamentous oligomers that seem to be capped at the growing end by Vps24. Finally, Vps2 associates with the Vps24 cap to mediate the recruitment of the AAA+ ATPase Vps4 that will mediate the disassembly and recycling of the ESCRT components (120). A schematic illustrating the molecular components and interactions between ESCRT subcomplexes is shown in Figure 1.6.

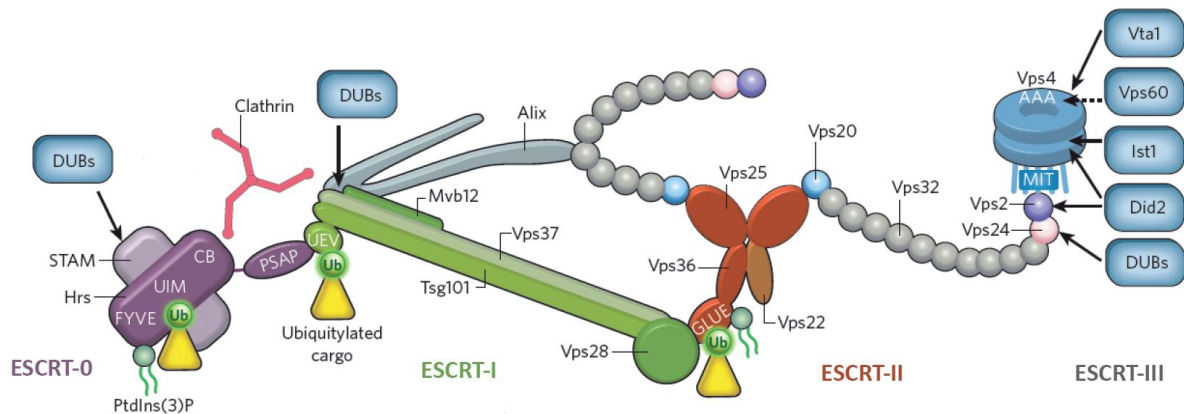


**Figure 1.6 Molecular components of the ESCRT complex.**

The subunits that make up the ESCRT-0, -I, -II, and -III are illustrated. Shown are the mammalian protein names of the subunits but the figure is a combination of data obtained from both yeast and mammalian ESCRTs. ESCRT-0 interacts with deubiquitinating enzymes (DUBs), membrane phospholipids, ubiquitylated cargo that is recognized through its UIM (Ubiquitin-Interacting Motif) and binds clathrin through its CB (Clathrin-box) motif. ESCRT-0 and the ESCRT-I component Tsg101 connect through the PSAP and UEV (Ubiquitin-E2 variant) domains, respectively. The ESCRT-I recognizes ubiquitin and interacts with the accessory protein Alix and DUBs. The Vps28 subunit bridges the ESCRT-I and -II together. The ESCRT-II binds ubiquitin and membrane phospholipids. Its Vps25 subunit recruits and activates the ESCRT-III subunit, Vps20. ESCRT-III subunits are also subject to the activity of DUBs. The ATPase Vps4 interacts with ESCRT-III through its MIT (Microtubule Interacting and Transport) domain. Vps4 activity is regulated by a number of proteins—Vta1, Vps60, Ist1, Did2. Adapted from (120).

#### 1.3.2.1.2.4 Disassembly of the ESCRT-III complex

The role of Vps4 seems to be conserved in all ESCRT-dependent processes, including viral budding, cytokinesis and autophagy. Without Vps4 activity, the entire ESCRT machinery accumulates on membranes and cargo processing is blocked (4, 5, 69). Vps4 is an AAA+ ATPase with a ring-shaped dodecameric cylinder. Binding of Vps4 to ESCRT-III promotes Vps4 assembly into a functional ATPase. Vps4 is thought to act by disassembling ESCRT-III components after membrane scission is complete. ESCRT-III subunits are thought to be pulled into, and through, the ATPase central pore, releasing them from the membrane and back into the cytosol as monomers (69).

### **1.3.2.1.3 ESCRT-mediated viral budding**

HIV-1 and other retroviruses engage components of the ESCRT machinery (see 1.3.2.1.2) to mediate scission of the membrane stalk connecting the nascent virion to the host cell. Access to the ESCRT complex is mediated by the viral L-domains (see 1.3.2.1.1) that either directly or indirectly recruit members of the protein sorting machinery. For instance, HIV-1 enters the ESCRT pathway by binding through its PT/SAP L-domain to the ESCRT-I component Tsg101. The functional relevance of this interaction was confirmed since knockdown of Tsg101 or expression of Vps4 mutants strongly compromised HIV-1 release (49, 96, 144), indicating that HIV-1 particle production is highly dependent on a functional Vps pathway. In addition to its Tsg101-binding site, HIV-1 p6 also contains the auxiliary L-domain LYPX<sub>n</sub>L that binds to the ESCRT-associated protein Alix (ALG-2 linked interacting protein X) (136). Release through this L-domain is inefficient; however, Tsg101-binding site mutants can be efficiently rescued by increasing the cellular expression levels of Alix (142). Importantly, this effect is dependent on an intact Alix binding site in p6. Alix binds to Tsg101 through its C-terminus but although this interaction is dispensable for HIV-1 release, its interaction with the ESCRT-III component CHMP4 is essential. Alix interacts with CHMP4 via its N-terminal Bro1 domain (142). Recently, Alix was shown to associate with the HIV-1 nucleocapsid (NC) through the same domain. This interaction seems to be required for efficient rescue of HIV-1 PTAP mutants (115). In another recent study, the NC-p1 region in HIV-1 Gag was shown to play an inhibitory role in virus release that can be counteracted by the L-domain function of p6 (116). This suggests that—at least in the context of the HIV-1 Gag protein—the primordial purpose of having viral L-domains is precisely to counteract such inhibitory or regulatory sequences present within viral structural proteins, Gag in this case, in order to engage the cellular machinery that will mediate virus release.

Interestingly, although HIV-1 does not possess an L-domain of the PPXY type, it has been shown that overexpression of a specific isoform of the Nedd4 E3 ubiquitin-ligase can enhance release of an HIV-1 clone lacking both known L-domains (22). The ability to enhance release is nevertheless dependent on Tsg101, suggesting that HIV-1 still acts through ESCRT-

I. Moreover, this rescuing activity was also dependent on the ubiquitinating ability of the ligase; however, the target for ubiquitination is so far unknown (22). These examples reflect the advantage of carrying more than one L-domain and the ability of a virus to enter the ESCRT pathway in more than one way.

The functional relevance of the HIV-1 PTAP-ESCRT interaction in the context of HIV-1 assembly and release was recently addressed in a study by Carlson et al. Their findings suggest a revised model for HIV-1 morphogenesis in which Gag assembly at the plasma membrane takes place concomitant –and in kinetic competition—to ESCRT recruitment. In this model, Gag assembly mediates early budding and recruits ESCRT-I and ESCRT-III. ESCRT-III in conjunction with Vps4 would serve to constrict the wide membrane neck of the nascent particle. This early recruitment of the ESCRT would lead to the formation of productive, incomplete gag shells with an average Gag content of 2400 molecules per virion that upon maturation form the cone-shaped capsid shells. In contrast, budding-arrested, unproductive nascent particles have almost complete gag shells and are characterized by a thin membrane stalk connecting them to the infected cell (21).

Equine infectious anemia virus (EIAV) contains a YPDL type of L-domain within its C-terminal p9 domain and it enters the ESCRT pathway through its interaction with Alix (136). This interaction is critical for efficient release of EIAV since Alix knockdown or dominant negative forms of this protein severely compromise particle release. In contrast, EIAV release is resistant to dominant negative forms of Tsg101 or to its depletion (95), indicating that unlike HIV-1, EIAV strongly depends on its L-domain-Alix interaction for efficient budding.

PPXY L-domain-containing viruses depend on the endosomal sorting pathway for efficient release (95). However, unlike the PTAP and YPXL L-domains that directly bind to ESCRT pathway components, PPXY L-domains are not known to directly bind any ESCRT or ESCRT-associated component. Instead, a wealth of studies indicates that they interact with the Nedd4-like family of HECT ubiquitin ligases (93). These ligases are characterized by an amino-terminal C2 domain that provides membrane targeting activity, contain central WW domains, which mediate the interaction with PPXY motifs and a carboxy-terminal HECT domain that contains ubiquitin ligase activity (72). The structural proteins of many PPXY L-domain-containing viruses such as VSV, Ebola, RSV, HTLV-1, and MPMV have been shown to bind to various HECT ubiquitin ligases, including Nedd4, WWP1, WWP2 and ITCH (12, 35,

94). The precise means by which HECT ligases establish a connection to the ESCRT pathway is currently unknown. The ability of this interaction to promote virus release seems to be dependent on a catalytically active HECT domain, suggesting that ubiquitination of a viral or cellular protein could be required for this process. However, the substrate of ubiquitination during viral budding remains undefined (20, 157). Upon VPS4 overexpression, HECT domains have been shown to localize to class E compartments, suggesting that the HECT domains must be recruited to these compartments by ESCRT components or by an as yet unidentified bridging factor. Recent studies indicate that PPXY motif-induced recruitment of HECT ubiquitin ligases results in a ubiquitination reaction that occurs at or near the site of viral budding. Interestingly, the substrate of this ubiquitin modification does not seem to be relevant for the subsequent recruitment of the ubiquitin-binding ESCRT components. Thus, it seems that the mere presence of ubiquitin at the site of budding is sufficient to engage the ESCRT pathway and promote virus budding (157). Figure 1.7 shows a schematic representation of the different entry points into the ESCRT pathway for each type of late domain.

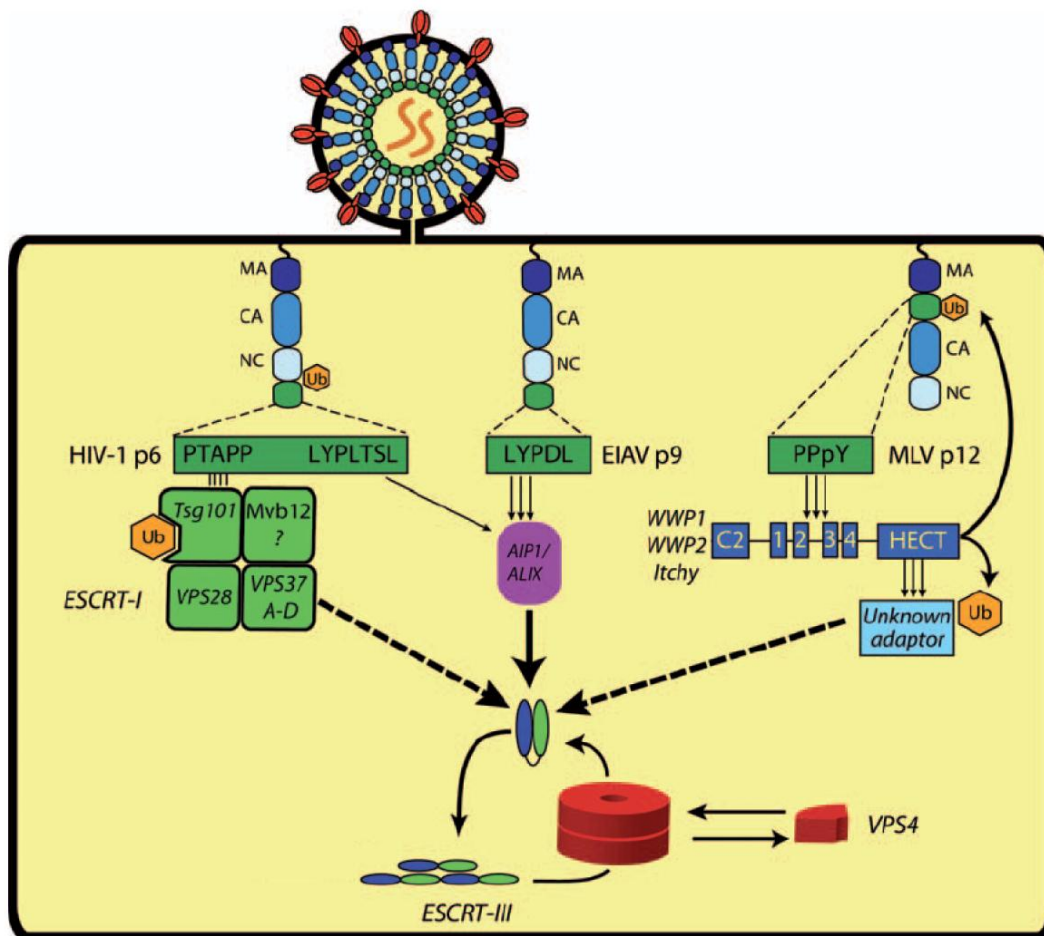


**Figure 1.7** The different ESCRT entry pathways used by the three viral late domains.

The late domains encoded by the three retroviruses HIV-1, EIAV and MLV access the ESCRT machinery differently. The HIV-1 PTAP late domain mediates the direct recruitment of the ESCRT-I component, Tsg101. In contrast, the YPXnL late domain in both HIV-1 and EIAV interacts with the ESCRT-associated protein Alix which in turn can directly interact with the ESCRT-III protein, CHMP4. In the case of PpxY late domains, entry into the ESCRT pathway is thought to be mediated by interaction with E3 ubiquitin ligases of the Nedd4 family. However, the bridging factor between the ligase and the ESCRT machinery has not been clearly defined. Moreover, it is thought that the catalytic activity of the ligase and hence, ubiquitination is necessary for its function in virus release. Although different entry points are used by the different late domains, all pathways seem to depend on an intact ESCRT-III to mediate the final scission step between the nascent virion and the host cell. Subsequent to membrane bud scission, ESCRT-III components are disassembled and recycled back into the cytoplasm by the action of the ATPase Vps4. Modified from (93).

#### 1.4 The Tsg101 UEV-PTAP interaction

Recruitment of the ESCRT machinery is required for the release of nascent HIV-1 particles from the infected host cell. This task is mediated by the recruitment of the cellular ESCRT-I component, Tsg101 (see section 1.3.2.1.2.2) through the HIV-1 PTAP L-domain.

Initial studies that identified Tsg101 as the cellular binding partner of the PTAP L-domain, also determined that the region of protein interaction in Tsg101 corresponds to the first 145 amino acid residues, or N-terminus of the protein (49, 96, 144). The N-terminus of Tsg 101 corresponds to a ubiquitin E2 variant (UEV) domain that shares structural features of classical E2 ubiquitin-conjugating enzymes, but unlike E2 enzymes does not possess catalytic activity for ubiquitin conjugation. Nevertheless, UEVs can still recognize and bind ubiquitin and ubiquitin-modified proteins (42, 118). Indeed, Tsg101 UEV domain contains a separate binding site for ubiquitin that is important for its role in the endosomal sorting pathway (137). Understanding the structural determinants of the p6-Tsg101 interaction has become imperative in the search for novel peptide inhibitors that block virus release (42, 117). Thus, a variety of studies have focused on defining the solution and crystal structures of the Tsg101 UEV domain alone or complexed either to ubiquitin or the HIV-1 p6 PTAP peptide. Early studies by Garrus et al (49) showed that the Tsg101 UEV-p6 interaction fits a 1:1 binding model with an equilibrium dissociation constant ( $K_d$ ) value of 27 +/- 5  $\mu$ M under physiological conditions as determined by surface plasmon resonance (BIAcore) studies (49). Importantly, they could show that Tsg101 UEV bound with similar affinities both full-length HIV-1 p6 and truncated versions that spanned different lengths of p6 but which always included the PTAP motif (49). A follow-up study by Pornillos et al (118), used nuclear magnetic resonance (NMR) spectroscopy to determine the structure of the Tsg101 N-terminal UEV domain and to map the sites of ubiquitin and PTAP binding. Analysis of the Tsg101 UEV domain shows that the UEV fold is in general similar to E2 ubiquitin-conjugating enzymes. This 'E2 fold' consists of four helices packed against one side of a four-stranded anti-parallel  $\beta$ -sheet. The structures are most similar around the central active site. However, the UEV lacks the two C-terminal helices found in all structurally characterized E2 proteins. Significantly, this feature allows the UEV to bind the PTAP-containing peptide. Moreover, Tsg101 contains two N-terminal helices, whereas canonical E2 proteins contain only one. Finally, the first two UEV  $\beta$ -strands form an extended  $\beta$ -hairpin 'tongue' that is important for ubiquitin binding. The sequence and secondary structure of Tsg101 UEV is illustrated in Figure 1.8 (118, 137).

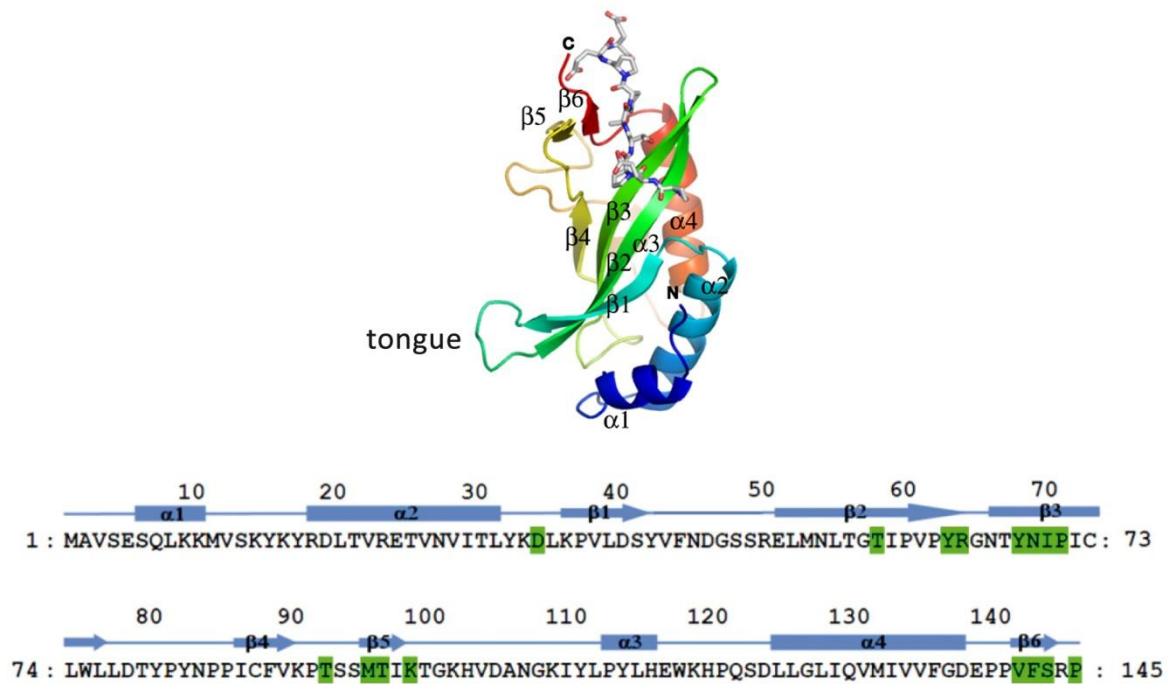


**Figure 1.8 Tsg101 UEV sequence and secondary structure.**

The Tsg101 UEV sequence consists of 145 amino acid residues. The location of beta sheets and alpha helices are shown in the sequence and secondary structure. The position of the beta hairpin tongue is indicated. Residues in green are important for binding to the p6 PTAP peptide. Modified from (71).

NMR chemical shift perturbation experiments were used to map the binding site of the HIV-1 p6 protein on the Tsg101 UEV domain. A nine-residue peptide spanning the p6 PTAP motif was used since it bound Tsg101 UEV with the same affinity as the full-length p6 protein, which under slightly acidic conditions displayed a tighter dissociation constant  $K_d = 4.3 \pm 1.6 \mu\text{M}$  (118). From this study it could be observed that the Tsg101 UEV-PTAP contact surface involves three different structural elements of the UEV: 1) the loop connecting strands 2 and 3; 2) the N-terminal third of the vestigial active-site loop; and 3) the C-terminal residues of the domain (118).

Upon PTAP binding, the binding groove of Tsg101 UEV closes and enwraps the PTAP motif (117). The C-terminal residues become well ordered and the biggest change in the structure comes from rotation of the phenylalanine (Phe) 142 phenyl side chain allowing it to contact the proline (Pro) 10 in PTAP (71). PTAP peptide binding is mediated by extensive intermolecular contacts with the four central residues Pro7-Thr8-Ala9-Pro10 as shown in Figure 1.9.

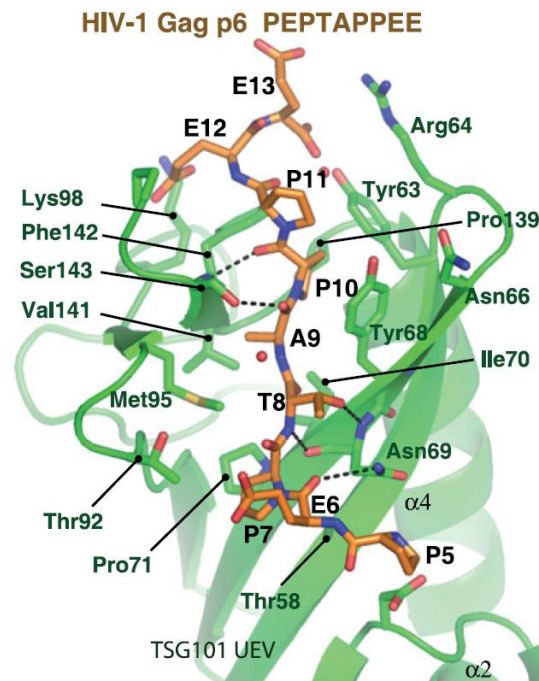


**Figure 1.9 Binding of the HIV-1 PTAP peptide.**

Contacts established between Tsg101 UEV residues and the p6 peptide are shown in the crystal structure of the complex. See text for details. Image was taken from (71).

The combined solution structure analysis by Pornillos et al (117) and crystal structure of the complex from Im et al (71), show that each residue of a p6 nonapeptide  $_5$ PEPTAPPEE $_{13}$  makes significant contacts to the UEV domain, except for Pro5. Glu6 forms a hydrogen bond to the side chain of Asn69 in UEV; however, the energetic contribution of this interaction is minimal. The first residue of the PTAP motif, Pro7 is fitted into a tight shallow pocket formed by the side chains of Thr58, Pro71, Thr92 and by NMR (nuclear magnetic resonance) analysis contact to Met95 is also apparent (71, 117). Pro7 is not as critical for binding as the other residues in the PTAP motif. For instance, a Pro7Ala mutant leads to a 3-fold reduction in affinity (71, 130). X-ray analysis of the complex revealed that the main-chain amide and the side-chain hydroxyl of the PTAP Thr8 residue hydrogen bonds to Asn69 in UEV while the  $\gamma$ -

methyl of Thr8 side-chain points towards solvent and does not establish direct contacts (71). The Ala9 is strictly required at this position; this can be explained by the tight packing around the Ala methyl group formed by the side chains of the UEV residues Ile70, Met95, and Val141 (71). Ala9 forms a hydrogen bond to Ser143 in UEV. The Pro10 is buried deep in a hydrophobic pocket formed by the side chains of Pro139, Tyr63, Tyr68, and Phe142. Like Ala9, Pro10 also forms a hydrogen bond to Ser143 (71, 117). The side chain of Pro11 comes into close contact with the side chain of Tyr68. Glu12 and Glu13 are thought to make marginal contributions to the overall binding affinity (71).

The Tsg101 UEV domain binds to ubiquitin (Ub) as part of its function during endosomal sorting of target proteins into multivesicular bodies (MVBs) followed by their degradation in the lysosome. The UEV domain can bind to ubiquitin at the same time as it binds to a PTAP peptide, although the 1:1 interaction between UEV and Ub is much weaker ( $K_d \sim 500 \mu\text{M}$ ) (49) and induces only minor conformational changes (109). The site of ubiquitin recognition in UEV has been described in detail (118, 137). The crystal structure of the UEV-Ub complex shows that Ub forms a five-stranded mixed  $\beta$ -sheet packed against a helix as in the unbound form (137). UEV recognizes Ub through the  $\beta$ -tongue formed by strands 1 and 2 and also uses residues from the loop that follows strand 4 as shown in Figure 1.10.

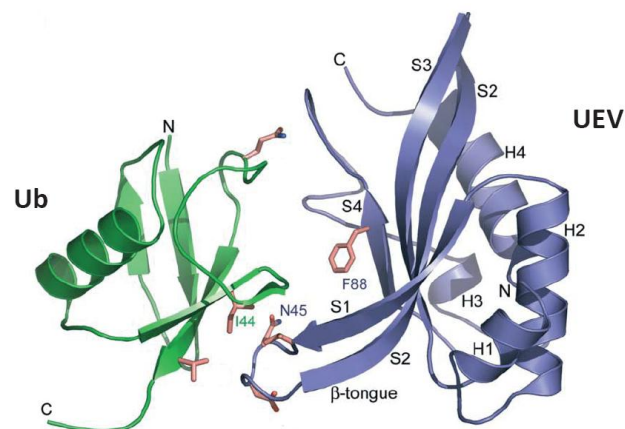


**Figure 1.10 Structure of the complex between the Tsg101 UEV Domain and Ub.**

The main binding determinants in UEV are the  $\beta$ -tongue formed from strands 1 and 2, as well as residues within the loop that follows strand 4. Ub binding to UEV includes the Ile44 hydrophobic patch in Ub. Image was modified from (137).

Mutation of residues within the  $\beta$ -tongue reduces Ub binding (118) and can impair physiological processes, such as the downregulation of the EGF receptor (137). The elongated interface buries Ub Ile44 and surrounding residues, which comprise the Ile44 hydrophobic patch of Ub that has functional roles in endocytosis, proteasomal degradation and HIV release (137). Residues in the loop between strand 4 and strand 5 of Ub also form part of the UEV-Ub interface (137). Moreover, x-ray analysis of the complex indicates that UEV could in principle bind to polyubiquitin since Lys48 and Lys63 residues, as well as the C terminus of Ub are accessible and not buried at the UEV interface (137).

As mentioned above, UEV can in principle bind to Ub and a PTAP peptide simultaneously as depicted in Figure 1.11.

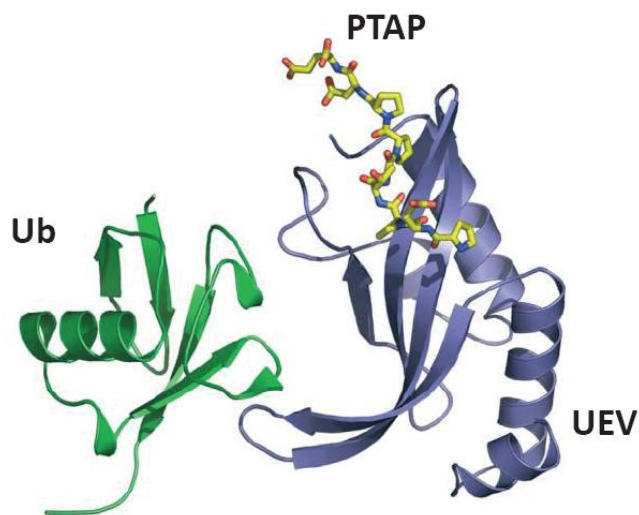


**Figure 1.11 Tsg101 UEV can simultaneously bind a PTAP peptide and Ub.**

The Tsg101 UEV domain uses different interfaces to recognize and bind to both Ub and a PTAP peptide. Adapted from (137).

This coupled interaction might be relevant in the context of HIV-1 budding since fusion of a Ub moiety to the C-terminus of HIV-1 p6 increased the affinity of Tsg101 UEV binding about 10-fold, resulting in an average  $K_d$  value of 2.3  $\mu$ M. This finding suggests that Tsg101 could bind ubiquitinated Gag molecules more tightly *in vivo* (49). A role for ubiquitin in retrovirus budding is not without precedent. It is known that retrovirus particles of avian leukosis virus ALV, HIV, SIV and MLV contain free ubiquitin. Moreover, cumulative mutation of lysine residues in HIV-1 Gag and proteasome inhibition impede virus budding, presumably because it depletes intracellular ubiquitin pools (93). In addition, fusion of a Ub moiety to the C-terminus of retroviral Gag proteins can bypass the need for a L-domain or can even

have a synergistic effect in the presence of a L-domain (157). The strongest evidence supporting a role of ubiquitination in virus egress is provided by the fact that PPXY L-domains recruit ubiquitin ligases of the Nedd4 family and that virus release is dependent on the catalytic activity of the ligase (93, 157). The relevant target for ubiquitination, however, is not known. It is possible that ubiquitination of a cellular protein, perhaps related to the class E Vps pathway or the endocytic machinery is the functional target of ubiquitination. On the other hand, it is plausible that the sole presence of ubiquitin at the site of budding, irrespective of the target, might be necessary and sufficient to engage components of the ESCRT machinery (157).

## ***1.5 Phosphorylation as a posttranslational modification usurped by HIV-1***

### **1.5.1 Kinase structure and levels of substrate specificity**

Phosphorylation is a versatile posttranslational modification used to orchestrate multiple and diverse cell signaling events. For instance, phosphorylation is involved in controlling cell division, differentiation, motility, and metabolism. Protein kinases are the effectors of phosphorylation and constitute one of the largest families of genes in eukaryotes, making up about 2 % of the genome (140). Moreover, it is estimated that 30 % of all cellular proteins are phosphorylated on at least one residue. This would mean that a typical kinase must recognize between one and a few hundred true phosphorylation site in a background of around 700,000 potentially phosphorylatable residues. Even the most promiscuous kinases can select their targets from among this big pool of substrates. Although the cell can tolerate some off-target phosphorylation, it is of utmost importance to identify the proper target. Thus, phosphorylation seems to be an overwhelming task for kinases. Hence, multiple mechanisms have evolved that convey accurate specificity to the reaction, starting with the kinase itself (140).

There are more than 500 protein kinases and more than 140 protein phosphatases in eukaryotes (66). Most eukaryotic kinases are structurally similar, exhibiting a high degree of flexibility and large rotational freedom about their lobes. This allows for the binding of

substrates, cofactors, autoinhibitory domains or interacting proteins (15). Typical kinases have a conserved catalytic domain of about 250 amino acids in length that consists of an N-terminal lobe of  $\beta$ -sheets and a C-terminal lobe of  $\alpha$ -helices. ATP-Mg<sup>2+</sup> binds in a cleft between the two lobes, making many contacts to the N-terminal lobe and burying the adenosine in a hydrophobic pocket with the phosphate backbone pointing outwards towards the solution as depicted in Figure 1.12 (8).

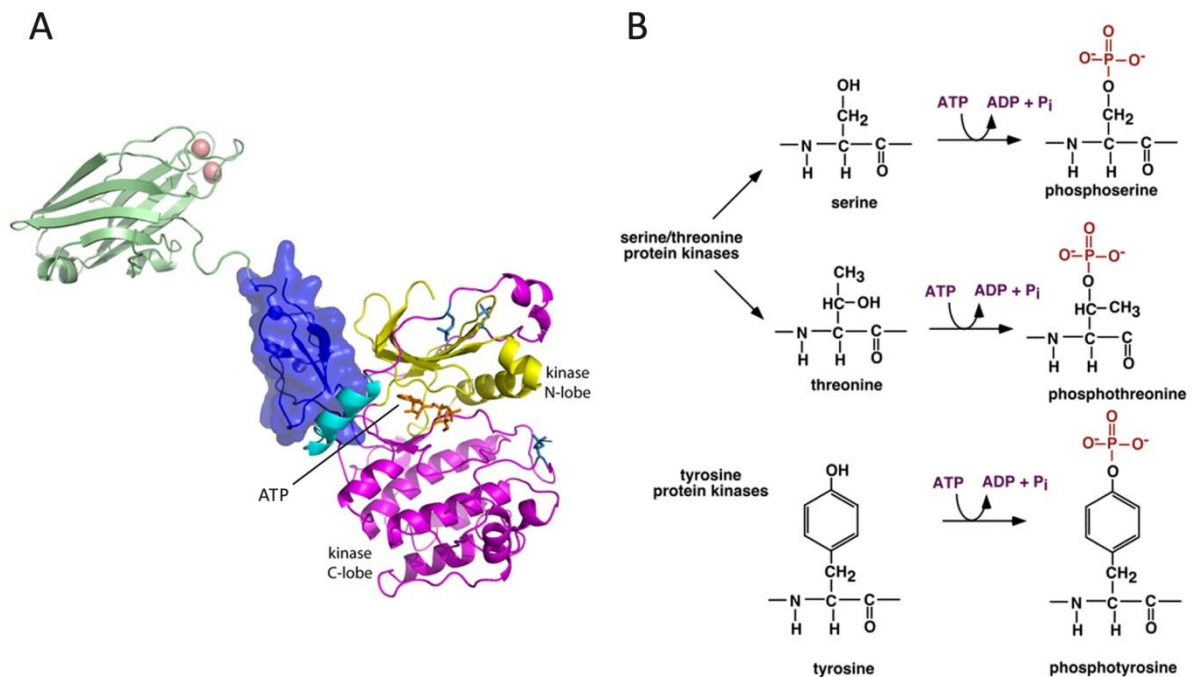


**Figure 1.12 Protein kinase structure with ATP and amino acid phosphorylation reaction.**

A) Crystal structure of the cyclin-dependent kinase-2 (CDK2) illustrates the common structural fold shared by many kinases that consists of two lobes: an N-terminal lobe (in yellow) made up of beta-sheets and C-terminal lobe (in purple) made up of alpha-helices. ATP is bound in between two lobes. Adapted from (90). B) Phosphorylation of hydroxyl groups by serine/threonine and tyrosine kinases (from online lectures by Hartmut Luecke, University of California, Irvine <http://bass.bio.uci.edu/~hudel>).

The protein substrate binds along the cleft and a set of conserved residues within the kinase catalytic domain catalyze the transfer of the terminal  $\gamma$ -phosphate of ATP to the hydroxyl of the Ser, Thr or Tyr residue of the substrate. Although all typical kinases share this common structure, they differ in terms of the charge and hydrophobicity of surface residues. Importantly, these differences contribute to kinase specificity (140).

As mentioned above, in order to prevent promiscuous activity, phosphorylation is subject to different levels of regulation that help achieve target specificity. The first level of substrate specificity is achieved by the kinase active site. The structure of the catalytic

domain helps discriminate between Ser/Thr and Tyr kinases. The catalytic cleft of Ser/Thr kinases is not as deep as that of Tyr kinases, since Ser/Thr residues have smaller side groups unlike Tyr residues. This feature also contributes to the specificity of phosphatases. The specificity contributed by the catalytic cleft depth is not absolute and there are instances when Ser/Thr kinases can phosphorylate Tyr residues; the opposite reaction is not as common. A second level of specificity is imparted by consensus sequences: the sequence of amino acids N- and C-terminal to the substrate phosphosite (P-site). In the majority of cases, the kinase active site will interact with the four amino acids on either side of the P-site. Some kinases prefer to phosphorylate a residue having basic neighbors; others prefer to have a Pro near to the P-site (103). However, the presence of a consensus phosphorylation site in a protein does not guarantee that the protein is a substrate *in vivo* and authentic phosphorylation sites do not always conform to the consensus. The basis for the interaction with these consensus sequences involves charge, hydrogen bonding potential or hydrophobic interactions (140). In addition, protein folding brings distant residues together, thus, the three-dimensional structure can determine whether a protein kinase can recognize a residue as a substrate (103). Another level of specificity is conveyed by the presence of docking motifs on the substrate that are recognized by interaction domains present in the kinase. This greatly increases the affinity of kinases. Some of the best well-known docking motifs occur in MAPK substrates. These can occur as D or DEF domains, which conform to a specific pattern of residues. The D domains are commonly 50-100 residues away from the P-site, while the DEF domains are found 10 amino acid residues downstream of the phosphorylation site. Docking motifs or interaction domains are also found within kinases and consist of SH2 (src-homology-2), SH3 (src-homology-3), and PH (pleckstrin homology) domains (to name just a few) in Tyr kinases. In Ser/Thr kinases, the interaction domain is usually part of the kinase domain and thus do not offer as much flexibility as Tyr kinases in this respect. The cellular localization of a kinase also imparts an important degree of specificity to the interaction since it limits the kinase to interact only with those substrates present within the same compartment. Scaffolding proteins play a critical role in preventing crosstalk between kinases that are involved in multiple pathways, thus making a very important contribution to substrate specificity (10). Many substrates require multiple phosphorylation events before being activated; this is actually an advantage to off-target

phosphorylation, which can occur despite all the described modes to achieve specificity. Thus, kinetic proofreading by phosphatases can help ensure that only the correct residues are phosphorylated before an effect takes place (140).

### 1.5.2 Phosphorylation of HIV-1 proteins

Protein kinase activity has been detected within purified particles of many enveloped viruses including retroviruses, herpesviruses, poxviruses and orthomyxoviruses. In many cases, these virion-associated protein kinases or VAPKs play important roles in viral infectivity, uncoating, transcription and replication (65). It has been shown that kinases are incorporated into HIV-1 particles. One is the activated form of the ERK2/MAPK, the other is the catalytic subunit of PKA (c-PKA), while the other is an unidentified 53 kDa protein kinase (24, 25).

#### *Capsid*

The capsid (CA) protein of HIV-1 was initially reported to be phosphorylated at Ser residues (97, 143) later identified as Ser109, Ser149 and Ser178; however, other additional residues in CA seem to be phosphorylated. It was shown that mutation of these three residues does not affect virus assembly or budding but instead seems to interfere with the virus uncoating process, thus preventing the reverse transcription process. It was further hypothesized that CA phosphorylation may generate repulsive forces that lead to core destabilization and particle uncoating (26). A follow-up study suggested that the CA is phosphorylated by c-PKA (25). More recently, the effect of these mutants designed to mimick a constitutive phosphorylated state was studied in the context of *in vitro* CA assembly and was also tested *in vivo*. The mutations were found to inhibit CA assembly *in vitro* and resulted in aberrant HIV-1 virions *in vivo*, thus providing support to the idea that CA phosphorylation serves to disassemble the CA early after entry promoting the uncoating process (17).

#### *Matrix*

The matrix (MA) protein of HIV-1 has been reported to be primarily phosphorylated on Tyr prior to or during virus assembly, while in virions and in isolated pre-integration complex (PIC) from infected cells, it seems to be phosphorylated exclusively on Ser residues

(39). Further study of Ser mutants within MA revealed that they were important for virus infectivity. This observation led to the hypothesis that phosphorylation of MA at these multiple Ser residues might disrupt the overall charge balance on MA, disrupting electrostatic interactions between MA and the plasma membrane. According to this model, cellular kinases specifically incorporated into the virion phosphorylate MA at an early postentry step, releasing it from the lipid bilayer and making it available to associate with the PIC (18). Previously, MA protein phosphorylation had been implicated in its targeting to the plasma membrane; however, it was shown that MA mutations that mimic phosphorylation have no effect on its ability to associate with membranes (125).

### *Accessory proteins*

In addition, the HIV-1 accessory proteins Vpu, Nef, Rev, Vif, Tat and Vpr have been reported to be phosphorylated. The cytoplasmic domain of Vpu is phosphorylated by casein kinase II (CKII) and this phosphorylation is necessary for the degradation of CD4 in the endoplasmic reticulum. Nef is phosphorylated by the protein kinase C and this phosphorylation leads to increased downregulation of CD4 from the cell surface. Rev phosphorylation by CKII and MAPK was reported to enhance its binding efficiency to RNA. Phosphorylation of Vif seems to be important for HIV-1 replication. Tat phosphorylation by CDKII and the dsRNA-dependent serine/threonine protein kinase (PKR) was shown to be important for HIV-1 transcription (2, 38).

### 1.5.3 HIV-1 p6 as the major phosphoprotein in virus particles

The C-terminus of the structural HIV-1 Gag protein corresponds to the p6 domain. Besides containing L-domain activity critical for mediating virus release, it is also subject to various posttranslational modifications, such as ubiquitination, sumoylation and phosphorylation. In a study conducted by Müller et al (101), p6 was identified as the major phosphoprotein in HIV-1 virions; it was estimated that at most 5 % of p6 molecules are phosphorylated at multiple Ser, Thr and Tyr residues as determined by phosphoamino acid analysis. Moreover, *in vitro* kinase studies revealed that p6 can be phosphorylated by virion-associated kinases, most likely ERK2. The functional relevance of p6 phosphorylation was subsequently addressed by Hemonnot et al (60); their study suggests that phosphorylation of a single residue in p6—Thr23— by the ERK2 kinase is required for efficient virus release. Moreover, they found that p6 Thr23 mutant virions display an aberrant morphology and are less infectious. However, ERK2 does not seem to be solely responsible for p6 phosphorylation and they suggest that additional cellular kinases are likely involved in this process.

## Goal of the study

The HIV-1 p6 protein establishes various interactions with cellular and viral proteins and plays a critical role in HIV-1 particle release. Moreover, p6 was identified in our group to exist as the major phosphoprotein within HIV-1 particles. p6 is made up of 52 amino acid residues, out of which 13 are potential phosphorylation sites. The phosphorylation state and potential function of this modification has not been examined in detail. Thus, the overall aim of this study was to analyze the functional consequences of potential phosphorylation site mutants in p6 and to identify actual sites of phosphorylation. The first step was to select p6 residues that were strongly predicted to be phosphorylated and that were highly conserved among different HIV-1 subtypes by using phosphorylation prediction programs and p6 sequence alignments of different HIV-1 subtypes. Mutants of selected residues were analyzed for potential effects in virus release, maturation and replication. This analysis was combined with mass spectrometry, a powerful analytic tool, to identify actual phosphoresidues in p6. Investigating and understanding the relevance of p6 phosphorylation might contribute to uncover potential targets for anti-viral therapy and pave the way towards effective drugs against cellular activities that support viral replication.

## 2 Materials and Methods

### 2.1 Materials and instruments

Material	Manufacturer
Acrylamide	Rotiphorese Gel, Roth, Karlsruhe, Germany
BioCAD Sprint Perfusion Chromatography System	Applied Biosystems Deutschland GmbH, Darmstadt, Germany
Dialysis tubing	Spectra/Por® 3 (MWCO 3.5 kDa/MWCO 0.1-0.5 Kda) Sartorius AG, Göttingen, Germany
DNA gel extraction kit	Nucleospin® Extraction II, Macherey-Nagel, Düren, Germany
Blotting paper	3MM Chr, Whatman, Dassel, Germany
Dulbecco's Modified Eagle's Medium (DMEM) high glucose	Gibco/Invitrogen, Karlsruhe, Germany
ELISA plates	Maxisorb, Nunc, Wiesbaden, Germany
Epon 812	Carl-Roth GmbH, Karlsruhe, Germany
FCS	Biowest, Nuaille, France
FugeneHD	Roche, Basel, Switzerland
Infrared scanner	Odyssey, LI-COR Inc., Lincoln, NE, USA
Interleukin-2	Biomol, Hamburg, Germany
ITC200	MicroCal LLC, Northampton, MA
Kanamycin	Roth, Karlsruhe, Germany
Microfuge® tube	Beckman Coulter, Krefeld, Germany
Microtip-sonifier	Sonifier 250, Branson, CT, USA
Mircoplate reader	MR5000, Dynatech, Enbrach, Switzerland
Nitrocellulose membrane	Protran, Schleicher & Schüll/Whatman, Dassel, Germany
Ni <sup>2+</sup> NTA sepharose	GE Healthcare Europe GmbH, Munich, Germany
NuPAGE Bis-Tris 4-12 % gel	Invitrogen GmbH, Darmstadt, Germany
OptiPrep™	Axis Shield, Oslo, Norway
Phosphatase inhibitor cocktail Set V, 50X	Calbiochem/Merck, Darmstadt, Germany
Phytohemagglutinin	Sigma-Aldrich, Steinheim, Germany
Plasmid purification kit	NucleoBond MaxiPrep Kit, Macherey-Nagel, Düren, Germany
Prepacked Superdex 200 16/60	GE Healthcare Europe GmbH, Munich, Germany
RPMI1640	Gibco/Invitrogen, Karlsruhe, Germany
Ultracentrifuge	Optima XL-70, Beckman Coulter, Fullerton, CA, USA
SDS-PAGE electrophoresis chamber	Minigel-Twin, Biometra, Göttingen
Semi-Dry Blotter	Fastblot B44, Biometra, Göttingen
Spectrophotometer	DU 640, Beckman Coulter, Fullerton, CA, USA
Tabletop ultracentrifuge	TL-100, Beckman Coulter, Fullerton, CA, USA
Transmission electron microscope EM10	Zeiss, Germany

## 2.2 Buffers and reagents

Name	Concentrations	Recipe
4x separating gel buffer	1.5 M Tris-HCl pH 8.8	90.8 g Tris ad 500 ml H <sub>2</sub> O
4x stacking gel buffer	0.5 M Tris-HCl pH 6.8	30.3 g Tris ad 500 ml H <sub>2</sub> O
30% acrylamide (200:1)		1.5 g N,N'-Methylen-bis-acrylamid, 1000 ml 30% Rotiphorese Gel A
30% acrylamide for stacking gels	29% acrylamide 1% bisacrylamide	
5x protein sample buffer	200 mM Tris/HCl pH 8.8 10% Sucrose 5 mM EDTA 0.1% Bromphenol Blue 4% SDS 2% β-MeEtOH	before usage, add 10 ml 20% SDS 1 ml β-MeEtOH to 50 ml sample buffer; <i>store at 4°C</i>
Western blot blocking buffer	5% milkpowder in TBST	
Separating gel (2 minigels; 10 ml)	17% acrylamide (200:1) 375 mM Tris-HCl pH 8.8 0.1% SDS 0.1% APS 0.0014% TEMED	5.8 ml acrylamide 200:1 2.5 ml 4x separating gel buffer 50 μl 20% SDS 1.8 ml H <sub>2</sub> O <i>for polymerization add</i> 100 μl 10% APS; 14 μl TEMED
stacking gel (2 minigels; 4 ml)	3% acrylamide 125 mM Tris-HCl pH 6.0 0.1% SDS 0.06% APS 0.3% TEMED	400 μl 30% acrylamide 500 μl 4x stacking gel buffer 20 μl 20% SDS 3.0 ml H <sub>2</sub> O <i>for polymerization add</i> 24 μl 10% APS; 12 μl TEMED
10x TBST (1000 ml)	200 mM 1M Tris 150 mM NaCl 0.5% Tween	200 ml 1 M Tris pH 7.5 87.66 g NaCl 5 ml Tween
1x Western blot transfer buffer (1000 ml)	48 mM Tris 39 mM Glycine 0.375% SDS 20% methanol	5.82 g Tris 2.93 g Glycine 0.375 g SDS 200 ml methanol
50x TAE buffer (1000 ml)	2 M Tris-acetate 50 mM EDTA	242 g Tris 57 ml acetic acid

## Materials and Methods

		100 ml 0.5 M EDTA pH 8.0
10x SDS-PAGE electrophoresis buffer (1000 ml)	250 mM Tris 1.92 M glycine 1% SDS	30.29 g TRIS 144.13 g Glycine 10 g SDS
10x PBS (1000 ml)	1.37 M NaCl 27 mM KCl 80 mM Na <sub>2</sub> HPO <sub>4</sub> 18 mM KH <sub>2</sub> PO <sub>4</sub>	80 g NaCl 2 g KCl 14.4 g Na <sub>2</sub> HPO <sub>4</sub> ·2H <sub>2</sub> O 2.4 g KH <sub>2</sub> PO <sub>4</sub>
2x HeBS transfection buffer (1000 ml)	280 mM NaCl 50 mM HEPES 1.5 mM Na <sub>2</sub> HPO <sub>4</sub> pH 7.05-7.12	16.4 g NaCl 11.9 g HEPES 0.267 g Na <sub>2</sub> HPO <sub>4</sub> ·H <sub>2</sub> O filter sterilize through 0.45 μm pore size filters; store at 4°C
2x CaCl <sub>2</sub> transfection buffer (1000 ml)	250 mM CaCl <sub>2</sub>	36.8 g CaCl <sub>2</sub> ·2H <sub>2</sub> O; filter sterilize through 0.45 μm pore size filters; store at -20°C
LB medium (1000 ml)	1 % peptone 0.5 % yeast extract 171 mM NaCl	10 g tryptone 5 g yeast extract 5 g NaCl 0.5 ml 10 N NaOH pH 7.0
LB agar	13 % agar in LB medium	1 l LB medium 13 g agar
Fixative for thin section-EM (6 ml)	2.5 % glutaraldehyde 0.2 M NaCacodylate	600 μl glutaraldehyde 3 ml NaCacodylate 2.4 ml H <sub>2</sub> O
Silver stain fixative	50 % methanol 12 % CH <sub>3</sub> COOH 500 μl formaldehyde	500 ml 120ml 500 μl
200x NaN <sub>3</sub> stock solution	10 % NaN <sub>3</sub> in PBS	5 g NaN <sub>3</sub> in 50 ml PBS
10x DNA loading buffer (10 ml)	50 % sucrose 10 mM EDTA 2 % bromphenol blue 2 % orange G	5 g sucrose 200 μl 0.5 M EDTA 0.2 g bromphenol blue 0.2 g orange G

### 2.3 Primers

Name	Sequence (5' → 3')	Used to clone
alphahuENaCfw	GCGCGGATCCATGGAGGGGAACAAGCTGG	ENAC $\alpha$ human
alphahuENaCrv	GCGCGAATTCGGGCCCCCAGAGGAC	ENAC $\alpha$ human
FL_ANXA1BamHI_rev	GCGCGGATCCCCGTTTCCTCCACAAAGAGCC	Annexin 1 human
FL_ANXA1NheI_fw	GCGCGCTAGCATGGCAATGGTATCAGAATTC	Annexin 1 human
FL_ANXA1stop_rev	GCGCGGATCCTTAGTTTCCTCCACAAAGAGC	Annexin 1 human
FLhuANXA1-BamHI-rev	CAAACGGGATCCGTCTTGTG	FRB-Annexin 1
FLhuANXA1-PstI-forw	CGACTGCAGAGTGTGAAATC	Annexin 1 human
HAUb-CterAvrII-fw	GCGCCCTAGGATGGCTAGCTACCCTTATG	HA-Ubiquitin-FRB
HAUb-CterAvrII-rv	GCGCCCTAGGTCAGCGGTTTAACTTAAGC	FRB-HA-Ubiquitin
HAUb-CterSpeI-rv	GCGCACTAGTTCAGCGGTTTAACTTAAGC	FRB-HA-Ubiquitin
HAUb-NterXbaI-fw	GCGCTCTAGAATGGCTAGCTACCCTTATG	HA-Ubiquitin-FRB
huANXA1_1_forw	CAATCCATCCTCGGATGTC	Annexin 1 human
huANXA1_1_rev	CAGCACGAAGTTCATCAGC	Annexin 1 human
huANXA1_2_forw	AGCAGGCCTGGTTTATTG	Annexin 1 human
huANXA1_2_rev	CTGGAGTTTTTAGCAGAGC	Annexin 1 human
huANXA1_siRNA1	CACGUUUACGUCUGUCCCCTT	Annexin 1 siRNA
huANXA1_siRNA2	UAAGGGCUUUCUUAAGUGUTT	Annexin 1 siRNA
huANXA1_siRNA3	CAGCGACAUCCAGGAUGGATT	Annexin 1 siRNA
huANXA1CterSpeI-rv	GCGCACTAGTGTTCCTCCACAAAGAGCC	FRB-Annexin 1
huANXA1NterXbaI-fw	GCGCTCTAGAATGGCAATGGTATCAGAATTC	Annexin 1-FRB
ITCHBamHI-rv	GCGCGGATCCTTACTCTTGTCCAAATCCTTC	FRB-Itch
ITCHCterHECTrev	GCGCACTAGTCTCTTGTCCAAATCCTTCTG	FRB-Itch HECT
ITCHCter-SpeI-rv	GCGCACTAGTCTCTTGTCCAAATCCTTC	FRB-Itch
MLVGag(Basyuk)-rv	GCGCGAATTCGTCATCTAGGGTCAGGAG	MLV gag
ITCHHECTNotI-fw	GCGCGCGGCCGCATGAGCTTCAGTCCCCAAG	Itch HECT domain
ITCHNotI-fw	GCGCGCGGCCGCATGTCTGACAGTGGATCAC	Itch Ub ligase
ITCHNterHECTfw	GCGCTCTAGAATGAGCTTCAGTCCCCAAG	Itch HECT-FRB
ITCHNter-NheI-fw	GCGCGCTAGCATGTCTGACAGTGGATCA CAAC	Itch-FRB

Nedd4LCterHECTrev	GCGCACTAGTATCCACCCCTTCAAATCC	FRB-Nedd4L HECT
Nedd4LCter-SpeI-rv	GCGCACTAGTATCCACCCCTTCAAATCC	FRB-Nedd4L
Nedd4LDC2CterSpeI-rv	GCGCACTAGTATCCACCCCTTCAAATCCTT	FRB-Nedd4LdelC2HECT
Nedd4LDC2NterXbaI-fw	GCGCTCTAGAATGGAGCGACCCTATACATT	Nedd4LdelC2HECT-FRB
NEDD4LHECTNotI-fw	GCGCGCGGCCGCATGTCCGTGAAAAGACCAG	Nedd4L HECT
NEDD4LMfeI-rv	GCGCCAATTGTTAATCCACCCCTTCAAATCC	Nedd4L
NEDD4LNotI-fw	GCGCGCGGCCGCATGGCGACCGGGCTCG	Nedd4L
Nedd4LNterHECTfw	GCGCTCTAGAATGTCCGTGAAAAGACCAG	Nedd4L HECT-FRB
Nedd4LNter-XbaI-fw	GCGCTCTAGAATGGCGACCGGGCTCGGGGAG	Nedd4L-FRB
NterApaI-fw	GCGCGGGCCCCTAGGAAAAAGGGCTGTTGG	pNL4-3
pECFP-N1_fw	AGTACATGACCTTATGGGAC	sequencing
pNL43-Mlul(2)-fw	GCGCTTTCTTCAGAGCAGACGCGTGCCAACAGCC	pNL4-3
pNL43-Mlul(2)-rv	GCGCGGCTGTTGGCACGCGTCTGCTCTGAAGAAA	pNL4-3
pNL43-Mlul(3)-fw	GCGCCAGAGCAGACGCGTGCCAACAG	pNL4-3
pNL43-Mlul(3)-rv	GCGCCTGTTGGCACGCGTCTGCTCTG	pNL4-3
pNL43-Mlul-fw	GCGCCTCAGAGCAGACGCGTGCC	pNL4-3
pNL43-Mlul-rv	GCGCGGCTGTTGGCACGCGTCTGC	pNL4-3
pNL43-rv	GCGCACTCAGGAATCCAGGTGGC	sequencing
S40N(2)-fw	GCGCCCTATCGATAAGGAACTGTATCCTTTAGCTA ACCTCAGATC	pNL4-3-uncoupled
S40N(2)-fw	GCGCCCTTTAGCTAATCTCAGATCAC	pNL4-3-uncoupled
S40N(2)-rv	GCGCGATCTGAGGTTAGCTAAAGGATACAGTTCCT TATCGATAGG	pNL4-3-uncoupled
S40N(2)-rv	GCGCGTGATCTGAGATTAGCTAAAGG	pNL4-3-uncoupled
S51N(2)-fw	GCGCGACCCCTCGAATCAAGCCAATTTTTTAGGGT AGATC	pNL4-3-uncoupled
S51N(2)-rv	GCGCGATCTACCCTAAAAAATTGGCTTGATTCGAG GGGTC	pNL4-3-uncoupled
S51N-fw	GCGCGACCCCTCGAATCAAGCCAAT	pNL4-3-uncoupled
S51N-rv	GCGCATTGGCTTGATTCGAGGGGTC	pNL4-3-uncoupled
Ser14Ala-fw	GCGCAGAAGAGGCCTCAGGTTTG	pNL4-3
Ser14Ala-rv	GCGCAAACCTGAAGGCCTCTTCTG	pNL4-3
Ser14Asp-fw	GCGCAGAAGAGGACTCAGGTTTG	pNL4-3
Ser14Asp-rv	GCGCAAACCTGAAGTCCTCTTCTG	pNL4-3

Ser25Ala-fw	GCGCCAACCTCCCGCTCAGAAGCAG	pNL4-3
Ser25Ala-rv	GCGCCTGCTTCTGAGCGGGAGTTG	pNL4-3
Ser25Asp-fw	GCGCCAACCTCCCGATCAGAAGCAG	pNL4-3
Ser25Asp-rv	GCGCCTGCTTCTGATCGGGAGTTG	pNL4-3
Thr8Asn-fw	GCGCAGAGCCAAATGCCCCACC	pNL4-3
Thr8Asn-rv	GCGCGGTGGGGCATTGGCTCT	pNL4-3
Thr8Gln-fw	GCGCAGAGCCACAAGCCCCACC	pNL4-3
Thr8Gln-rv	GCGCGGTGGGGCTTGTGGCTCT	pNL4-3
Thr8Glu-fw	GCGCAGAGCCAGAAGCCCCACC	pNL4-3
Thr8Glu-rv	GCGCGGTGGGGCTTCTGGCTCT	pNL4-3
Tsg101UEV-fw	GCGCCTAGTAACGGCCGCCAGTG	Tsg101UEV
Tsg101UEV-rv	GCGCCGGCCGCCAGTGTGATGG	Tsg101UEV
Ub-CterSpel-fw	GCGCTCTAGAATGCAGATCTTCGTGAAGAC	FRB-Ubiquitin
Ub-CterSpel-rv	GCGCACTAGTGCGGTTTAACTTAAGCTTGG	FRB-Ubiquitin
unc-seqBcl-rv	GCGCGCTTTATGTCCGCAGATTTCTATGAGTAT	sequencing
unc-seqSP2fw	GCGCTTTTGGCTGAAGCAATGAGCCAAG	sequencing
WWP1Cter-AvrII-rv	GCGCCCTAGGTTCTTGTCCAAATCCCTC	FRB-WWP1
WWP1CterHECTrev	GCGCACTAGTTTCTTGTCCAAATCCCTCTGT	FRB-WWP1HECT
WWP1EcoRI-rv	GCGCGAATTCTCATTCTTGTCCAAATCCC	WWP1 ligase
WWP1HECTNotI-fw	GCGCGCGGCCCGCATGGCATTAAAACCCTATGAC	WWP1 HECT
WWP1NotI-fw	GCGCGCGGCCCGCATGGCCACTGCTTCACC	WWP1 ligase
WWP1NterHECTfw	GCGCTCTAGAATGGCATTAAAACCCTATGAC	WWP1HECT-FRB
WWP1Nter-NheI-fw	GCGCGCTAGCATGGCCACTGCTTCACCAAGG	WWP1-FRB
WWP2CterHECTrev	GCGCACTAGTCTCCTGTCCAAAGCCCTC	FRB-WWP2HECT
WWP2Cter-Spel-rv	GCGCACTAGTCTCCTGTCCAAAGCCCTC	FRB-WWP2
WWP2EcoRI-rv	GCGCGAATTCTTACTCCTGTCCAAAGCCC	WWP2 ligase
WWP2HECTNotI-fw	GCGCGCGGCCCGCATGAAACCCTATGACCTGC	WWP2 HECT
WWP2NotI-fw	GCGCGCGGCCCGCATGGCATCTGCCAGCTCTA	WWP2 ligase
WWP2NterHECTfw	GCGCTCTAGAATGAAACCCTATGACCTGC	WWP2 HECT-FRB
WWP2Nter-XbaI-fw	GCGCTCTAGAATGGCATCTGCCAGCTCTAGC	WWP2-FRB

## 2.4 Plasmids

Name	Description	Reference
Uncoupled FL	pNL4-3 uncoupled backbone, contains point mutants of all Ser, Thr and Tyr in p6, except for Thr8	This work
Uncoupled Nter	pNL4-3 uncoupled backbone, contains point mutants of N-terminal Ser and Thr residues in p6	This work
Uncoupled Cter	pNL4-3 uncoupled backbone, contains point mutants of C-terminal Ser and Thr residues in p6	This work
pET11c-Tsg101UEV	Tsg101UEV domain cloned for protein expression	This work
pHIVGagWT-FKBP	pcDNA3 backbone, HIV WT Gag tagged with FKBP	S. Jäger
pHIVGagΔp6-FKBP	pcDNA3 backbone, HIV GagΔp6 tagged with FKBP	S. Jäger
Tsg101-FRB	pC <sub>4</sub> -RHE backbone, FRB tagged Tsg101	S. Jäger
FRB-Ub	pC <sub>4</sub> -RHE backbone, FRB tagged Ub	Appendix A
FRB-Itch	pC <sub>4</sub> -RHE backbone, FRB tagged Itch	Appendix A
FRB-WWP1	pC <sub>4</sub> -RHE backbone, FRB tagged WWP1	Appendix A
FRB-WWP2	pC <sub>4</sub> -RHE backbone, FRB tagged WWP2	Appendix A
Nedd4L-FRB	pC <sub>4</sub> -RHE backbone, FRB tagged Nedd4L	Appendix A
pNL4-3	Subviral plasmid	(1)
pNL4-3-MluI	Subviral plasmid; contains MluI silent restriction site	This work
pNL4-3 uncoupled	pNL4-3 backbone, uncoupled <i>gag</i> and <i>pol</i> reading frames	This work and (89)
pNL4-3 p6T8D	pNL4-3 backbone, contains a single point mutation in p6 Thr8	This work
pNL4-3 p6S14A	pNL4-3 backbone, contains a single point mutation in p6 S14	This work
pNL4-3 p6S14D	pNL4-3 backbone, contains a single point mutation in p6 S14	This work
pNL4-3 p6S25A	pNL4-3 backbone, contains a single point mutation in p6 S25	This work
pNL4-3 p6S25D	pNL4-3 backbone, contains a single point mutation in p6 S25	This work
pNL4-3 p6T8N	pNL4-3 backbone, contains a single point mutation in	This work

	p6 Thr8	
pNL4-3 p6T8E	pNL4-3 backbone, contains a single point mutation in p6 Thr8	This work
pNL4-3 p6T8Q	pNL4-3 backbone, contains a single point mutation in p6 Thr8	This work

## 2.5 Cell lines

Name	Origin/features	Reference
293T	human embryonic kidney fibroblast , transduced with SV40 large T antigen	(134)
C8166	human umbilical blood lymphocytes, infected with defective HTLV-I	(128)
HeLa	human cervix carcinoma	(129)
MT-4	human T-cells isolated from a patient with adult T-cell leukemia, HTLV-I transformed	(99)
TZM-bl	HeLa derived, harboring a Tat-inducible $\beta$ -galactosidase and luciferase reporter	(148)

## 2.6 Antibodies

Antibody for WB	Source	Application	Dilution
IRDye <sup>TM</sup> 800CW anti-mouse-700	Rockland	WB	1:20,000
IRDye <sup>TM</sup> 800CW anti-mouse-800	Rockland	WB	1:20,000
IRDye <sup>TM</sup> 800CW anti-rabbit-700	Rockland	WB	1:20,000
IRDye <sup>TM</sup> 800CW anti-rabbit-800	Rockland	WB	1:20,000
IRDye <sup>TM</sup> 800CW anti-rat-800	Rockland	WB	1:20,000
Mouse anti-Tsg101 (4A10)	GeneTex, Inc	WB	1:100
Mouse anti-Ub (P4D1)	Covance	WB	1:2000
Rabbit anti-HIV CA	Kräusslich lab	WB	1:5000
Rabbit anti-Nedd4L	Wes Sundquist	WB	1:300
Rabbit anti-RSV CA	Volker Vogt	WB	1:10,000
Rat anti-HA high affinity	Roche	WB	1:500
Sheep anti-HIV CA	Kräusslich lab	WB	1:5000

## ***2.7 Molecular Biological methods***

### **2.7.1 Transformation and plasmid amplification**

Chemically competent bacteria Stbl2, DH5 $\alpha$  or BL21 (DE3) were transformed using the heat-shock procedure with plasmid DNA (1  $\mu$ g). Bacteria were thawed on ice; DNA was added into the cells and incubated for 15 min on ice, heated for 4 min at 37°C and then cooled on ice for 2 min. The transformed bacteria were then incubated for 30min-1 h at 37°C in 800  $\mu$ l antibiotic-free LB medium; they were then streaked out on an LB plate containing the appropriate antibiotic. Plates were incubated overnight at 37°C and single colonies were used to inoculate LB medium for mini (2.5 ml) or maxi (250 ml) plasmid preparations the following day.

For preparative purification of plasmid DNA the NucleoBond<sup>®</sup> maxiprep kit (Macherey-Nagel) was used. Pellets of purified plasmids were dissolved in 10 mM Tris-HCl pH 8.0. Concentration and purity of the plasmid preparations were assessed by measuring extinctions at 260 nm and 280 nm in a UV spectrophotometer (Beckman Coulter).

For analytical mini-preparation of plasmid DNA, the NucleoBond<sup>®</sup> Buffer Set-I was used (Macherey-Nagel). 2.5 ml overnight bacteria culture were pelleted for 5 min at 2000 xg (5000 rpm) and resuspended in 250  $\mu$ l S1 buffer. Bacteria were lysed for 3-5 min through addition of 150  $\mu$ l S2 buffer and the reaction was stopped by neutralization with 250  $\mu$ l S3 buffer. Afterwards, cell debris was pelleted for 10 min at 17,000 xg (15,000 rpm) at 4°C and discarded. The DNA in the supernatant was precipitated by addition of 600  $\mu$ l 100% isopropanol, pelleted for 10 min at 17,000 xg at 4°C, washed once with 70% ethanol at room temperature and finally dissolved in 50  $\mu$ l water or 10 mM Tris-EDTA pH 7.0 buffer. Minipreparations from newly cloned plasmids were tested by restriction digest as well as transfection of 293T cells by calcium phosphate transfection (2  $\mu$ l miniprep-plasmid per well of a 12 well-plate).

### 2.7.2 DNA sequencing

Sequencing of plasmids was performed by GATC Biotech (Konstanz, Germany) and data were analyzed using BioEdit (Tom Hall, Carlsbad, USA) or Vector NTI<sup>®</sup> (Invitrogen) software.

### 2.7.3 Polymerase chain reaction (PCR)

Polymerase chain reaction allows the specific enzymatic amplification of DNA fragments located between two oligonucleotide primers complementary to the 5'- and 3'-regions of the desired fragment. Primers were designed so that typically 12-18 nucleotides at the 3'-end of the primer were complementary to the template. At the 5'-end of the primer, restriction sites were introduced when necessary.

For preparative amplification of DNA segments by PCR, the following recipe was used:

5.0 µl	10x Pfu-buffer
0.3 – 1.0µl *	Pfu polymerase
2.0 µl	fw-Primer (10 pmol/µl = 10 µM)
2.0 µl	rev-Primer (10 pmol/µl)
3.0 µl	2.5 mM dNTPs
0.2 µg	DNA template
36.8 µl	H <sub>2</sub> O

\* the amount of Pfu polymerase used depends on the length of the expected DNA product

Exponential amplification of the template during PCR is achieved by repeated cycles of amplification, during which the template is denatured, the primers are annealed to the template or PCR product already present, and elongated by the polymerase. The following temperature cycling protocol was used for PCR:

step	temperature	duration
1: denaturation	94°C	5 min
2: denaturation	94°C	1 min
3: annealing	55°C	30 sec
4: elongation	72°C	30 sec – 4 min*
repeat steps (2-4) 25-30x		
5: elongation	72°C	10 min

\* depending on product length (~0.5 kb/min for Pfu polymerase)

5 µl of the reaction was analyzed by DNA gel electrophoresis afterwards.

### 2.7.4 Restriction digest and ligation

All enzymes and buffers for DNA cloning were from Fermentas or NEB Biolabs and used as instructed. For a control restriction digest, 1 µg plasmid was incubated with 2 U restriction enzyme in a volume of 20 µl at the recommended temperature for 1-2 hrs and 10 µl of the samples were analyzed by DNA gel electrophoresis to check size of the resulting DNA fragments.

For further subcloning of the digested DNA, 2 µl plasmid or 40 µl gel-purified PCR product was digested with 20 U restriction enzyme in a volume of 50 µl for 2 hrs. Before ligation, vectors were dephosphorylated to avoid religation. For this, 1.5 U calf intestine alkaline phosphatase (CIAP) were incubated with the DNA for 30 min at 37°C. Ligation was performed using 3 µg vector, an estimated 5 molar excess of insert and 1 U T4 DNA ligase in 1x ligase buffer in a total volume of 30 µl for 2 hrs at room temperature. The samples were subsequently transformed into a 50 µl aliquot of competent bacteria.

### 2.7.5 DNA electrophoresis

Depending on the size of the DNA fragment to be purified, 0.5–2 % agarose in TAE buffer was dissolved by heating, ethidiumbromide was added 1:20,000 and the gel was poured into the gel tray. DNA samples were mixed with DNA loading buffer, loaded onto the

gel and resolved for 20-40 min at 90 V. Bands of DNA were visualized with UV light of 312 nm and compared to a DNA standard run on the same gel.

For purification of DNA fragments from an agarose gel, the desired DNA band was excised from the gel illuminated with UV light of lower wavelength (366 nm) to avoid UV damage and purified using a DNA gel extraction kit (Macherey-Nagel).

### **2.7.6 FRB and FKBP expression plasmids**

To generate expression plasmids for FRB fusion proteins with an HA-tag at the C-terminus, coding sequences of the respective protein were PCR-amplified with primers adding an 5'-XbaI and an 3'-SpeI restriction site. Using the cloning strategy proposed in the kit's manual, which is based on the compatibility of the cohesive ends of XbaI and SpeI sites, the PCR product was cloned either into the XbaI or SpeI site of the pC<sub>4</sub>-R<sub>H</sub>E vector so that the FRB gene is fused either N-terminally or C-terminally.

### **2.7.7 Generation of p6 single point mutants**

The p6 Ser residues at positions 14 and 25 were selected and mutated to either an alanine or an aspartate (S14A, S14D, S25A, and S25D). The single point mutants were generated by oligonucleotide-directed mutagenesis using the appropriate primers and confirmed by sequencing. Fragments carrying the particular p6 point mutation were cloned back into the full-length infectious molecular clone, pNL4-3.

### **2.7.8 Generation of an infectious pNL4-3 clone containing uncoupled gag-pol frames and p6 mutant derivatives**

We generated an NL4-3 provirus with uncoupled gag and pol frames based on the strategy used by Leiherer et al (89). In brief, we introduced an *MluI* silent restriction site in the NL4-3 proviral clone at nucleotide position 1356 with respect to Gag ATG. The ApaI-MluI fragment (nucleotide position 1217-1356 with respect to Gag ATG) was replaced with a synthetically produced fragment (GENEART AG, Regensburg, Germany) thereby destroying the original slippery site UUUUUUA at position 1296 and the 3' stem-loop structure by point

mutations to abrogate frameshifting. In its place, the complete functional frameshift signal, including the slippery site and stem-loop was introduced 5' to the Gag stop codon. In the resulting provirus, the gag and pol genes were extended by 15 and 210 nucleotides, respectively, compared to those of the parent NL4-3 provirus clone. We introduced a *Clal* silent restriction site into this new uncoupled gag-pol construct and derivatives of this construct were generated by synthetically produced fragments (GENEART AG, Regensburg, Germany), which carried mutations in predicted phosphorylated residues of p6 at either of 3 different regions: N-terminus, C-terminus, or the entire p6. These fragments were then cloned back into the uncoupled gag-pol construct by making use of 3 restriction sites: *XmaI*, *Clal* and *MluI*. Predicted Ser and Thr residues in p6 were mutated into Asn, while the single Tyr in the p6 amino acid sequence was changed into a Phe. The change to these two amino acids was selected since these are thought to better maintain the proper folding of the protein (104).

## ***2.8 Biochemical Methods***

### **2.8.1 SDS-Polyacrylamide Gel Electrophoresis (SDS-PAGE) and Western Blot**

Protein samples for SDS-PAGE were boiled in 1x sample buffer and stored at -20°C. For analysis by SDS-PAGE samples were applied on a freshly prepared 12.5 % cross-linking polyacrylamide gel and the electrophoresis was performed at 200 V for 1 h or longer. The gel was then semi-dry blotted onto a nitrocellulose membrane between three sheets of whatman-paper on top and bottom, everything soaked in Western blot transfer buffer for 1 h (400 V, 240 mA, 10 W for two 6 x 9 cm blots). The membrane was subsequently blocked for 1 h at RT in 5 % skim milk/TBST and after 3 x 5 min washing incubated with the first antibody 1 h at RT or overnight at 4°C. All primary antibodies used for Western blotting were diluted in 1 % BSA/TBST/0.05 % NaN<sub>3</sub>, stored at 4°C. The blot was then washed 3 x 5 min with TBST and incubated with the secondary antibody for 30 min at RT.

For quantitative detection of immunoreactive bands, membranes were incubated with fluorescence-dye-coupled secondary antibodies (Rockland, diluted 1:20 000 in PBST/1 % BSA) for 30 min at RT, then washed 3 x 5 min followed by 1x PBS 10 min. After washing,

the blot was scanned on a digital infrared scanner (LI-COR Inc.). Signals were evaluated with Odyssey application software 2.1 (LI-COR Inc.).

### **2.8.2 Silver staining**

The integrity and purity of OptiPrep-purified virus preparations was confirmed by silver staining of virus proteins. 2.5 µl samples from sucrose pellet and OptiPrep virus pellets were analyzed and virus proteins separated by SDS-PAGE. All silver stain solutions must be prepared fresh. Subsequently, the gel was incubated while shaking for 1h RT with 100 ml per gel silver stain fixation buffer. The gel washed 3 x 10 min with 100 ml 50 % EtOH/ 50 % (solution I) Millipore H<sub>2</sub>O, followed by 3 x 20 min washes with Millipore H<sub>2</sub>O. The gel was then transferred into solution II (100ml H<sub>2</sub>O+150 ml solution A: 430 mg sodium thiosulfate in 5 ml H<sub>2</sub>O) and incubated for 1 min while shaking. The gel is subsequently washed 3 x 20 sec with Millipore H<sub>2</sub>O and solution III is added (0.2 g AgNO<sub>3</sub>+75 ml formaldehyde in 100 ml H<sub>2</sub>O) and the gel is incubated for 20 min at RT. Finally, the gel is developed in solution IV (6 g sodium carbonate+5 µl solution A+50 µl formaldehyde in 100 ml H<sub>2</sub>O). The gel is developed for 5-10 min. For storage at 4°C, wash once with water and change into fixation buffer.

### **2.8.3 Enzyme-Linked Immunosorbent Assay (p24-ELISA)**

The in-house p24-ELISA for detection of HIV-1 CA-protein in samples was used to determine virus concentration of p24 equivalents.

Maxisorb 96-well plates (Nunc, Wiesbaden, Germany) were coated with monoclonal mouse-antibody raised against p24 (CA) (183-H12-5C) o/n at RT in a moist chamber and then blocked with 10 % FCS/PBST for 2 h in a moist chamber. Virus dilutions in PBST were added to the single wells and a titration of purified CA-protein was applied as a standard. Samples were incubated o/n at RT in a moist chamber. After washing with PBST, the plate was incubated 1h at 37 °C with a rabbit-antiserum raised against CA protein, followed by another washing step. Finally, the samples were incubation with horseradish peroxidase-coupled secondary antibody raised in goat against rabbit IgG for 1 h at 37 °C. After washing with PBST and H<sub>2</sub>O, the amount of bound antibody was visualized by addition of the chromogenic substrate tetramethyl benzidine (TMB) for 5 min. The labeling reaction was stopped by the

addition of 0.5 M sulfuric acid and the absorbance of the reaction product quantified in a spectrofluorimetric plate-reader at 405 nm wavelength.

#### 2.8.4 Tsg101 UEV domain purification

A his-tagged version of the 145aa Tsg101 UEV domain (GI: 21465898) was custom synthesized into the pCR2.1 vector (MWG Eurofins) via *NdeI* and *BamHI*; gene was subcloned into the pET-11c vector and expressed in *Escherichia coli* BL21 codon plus cells. Briefly, 250 ml LB medium with ampicillin was inoculated with a colony of cells and incubated overnight at 37°C. 50 ml of overnight culture were added to each of 4 flasks containing 1 l LB medium and grown at 37°C in an orbital shaker (160 rpm). Once the optical density of the culture reached a value of 0.8 at 600 nm, protein expression was induced with 100 µM IPTG. After 3 h of growth, cells were harvested by centrifugation and the pellet was resuspended in 1x PBS pH 8.0. The cells were broken by sonication (Branson microtip sonifier 250) for 3 x 2 min at 50 % intensity while cooling on ice and ultracentrifuged for 20 min at 15,000 rpm (rotor JA-20, Beckman Coulter). The cleared supernatant was loaded onto a Ni<sup>2+</sup> NTA sepharose (GE Healthcare) column, eluted and dialyzed against either 50 mM Tris pH 8.0, 150mM NaCl for crystallization or against 1x PBS pH 8.0, 150 mM NaCl for isothermal titration calorimetry experiments. The protein was concentrated and the his-tag was then removed by overnight incubation with TEV protease. The untagged protein was then purified by gel filtration using a Superdex 200 16/60 (GE Healthcare) column. All chromatographic purifications were performed using a BioCAD Sprint Perfusion chromatography system (Applera Dtlid. GmbH). Protein was concentrated to 43mg/ml using Vivaspin concentrators (3 or 10 kDa cut-off, Vivascience) and dialysis was performed in SpectraPor dialysis tubing (Spectra/Por® 3 (MWCO 3.5 kDa/MWCO 0.1-0.5 Kda) Roth, Karlsruhe, Germany). Protein concentration was determined spectroscopically by absorbance measurements at 280nm, using an extinction coefficient of  $25\,900\text{ M}^{-1}\text{ cm}^{-1}$  and a molecular weight of 16.61 kDa. The protein sample was either used for isothermal titration calorimetry or sent for crystallization trials to the group of Dr. Winfried Weissenhorn at the EMBL in Grénoble.

### 2.8.5 Peptides

Peptides, PEPNAPPEE, PEPTAPPEE, PEPAAPPEE, PEPSAPPEE, were obtained as lyophilized salts of trifluoroacetic acid (Peptide Specialty Laboratories, Heidelberg, Germany) and resuspended in 1x PBS pH 8.0, 150 mM NaCl for isothermal titration calorimetry. Additionally, part of PEPNAPPEE peptide was resuspended in 50 mM Tris pH 8.0, 150 mM NaCl) for crystallization. Peptides were shock-frozen in liquid nitrogen and stored at -80°C. The peptide concentration was estimated by infrared spectroscopy by Prof. Matthias Mayer (ZMBH, Heidelberg University).

### 2.8.6 Phosphopeptide mass spectrometry analysis

The samples that were delivered for MS analysis consisted of Optiprep gradient-purified HIV-1 particles derived from 293T cells 48 h after transfection. Virions collected from the supernatant were immediately treated with a phosphatase inhibitor cocktail (Calbiochem), adding fresh inhibitors after each successive purification step. The virus pellet was resuspended in 50 µl 1x PBS and the quality of the samples was assayed by silver gel staining and the virus concentration was determined by p24 ELISA. A virus capsid amount equivalent to 1 µg of p6 protein, were loaded onto a NuPAGE Bis-Tris 4-12 % gel (Invitrogen) (initially provided by Xabier Contreras, BZH). The gel was run at 150 V. p6-containing bands were identified by simultaneously running a small virus sample, which was analyzed by Western blotting. Four different bands were cut and excised corresponding to p6 as part of the Gag precursor protein, as a cleavage intermediate or in its free, cleaved form. The protein-containing bands were sent for analysis and successively digested with trypsin, peptides extracted and further analyzed by liquid chromatography-tandem mass spectrometry (LC-MS/MS) on an LTQ Orbitrap velos mass analyzer. Remaining samples from each band were pooled and phosphopeptides enriched by metal oxide affinity chromatography using titanium dioxide (TiO<sub>2</sub>-MOAC). The eluate of each sample was again analyzed via LC-MS/MS. Data was analyzed using the MASCOT search algorithm and identified phospho-peptide MS/MS spectra were manually validated.

### **2.8.7 Isothermal Titration Calorimetry (ITC)**

To determine binding affinity of peptides (PEPNAPPEE, PEPTAPPEE, PEPAAPPEE, PEPSAPPEE) to Tsg101 UEV isothermal titration calorimetry was used. Purified TSG101 UEV domain was dialyzed against 1x PBS pH 8.0, 150 mM NaCl buffer overnight at 4°C. Peptides were dissolved in the same buffer. The day of the experiment, protein and peptide aliquots were quick-thawed at 37°C. Protein concentration was determined spectroscopically by absorbance measurements at 280nm, using an extinction coefficient of 25 900  $M^{-1} cm^{-1}$  and a molecular weight of 16.61 kDa. Protein and peptides were diluted to the appropriate concentration. The samples were then degassed by applying vacuum for about 5 min. All ITC experiments were carried out at 25°C on an ITC200 instrument (MicroCal LLC, Northampton, MA). The sample cell contained 0.2 ml of 25  $\mu$ M Tsg101 UEV protein and the peptides (500  $\mu$ M-2 mM) were added in 18 injections of 1.5  $\mu$ l each. The data were processed using Origin software (MicroCal). The binding constant ( $K_d$ ) was fitted as a one-site model.

## **2.9 Cell Biological Methods**

### **2.9.1 Cell culture**

Adherent cell lines 293T and HeLa were cultured in Dulbecco's Modified Eagle's Medium (DMEM) high glucose, supplemented with 10 % FCS, 100 U/ml penicillin, 100  $\mu$ g streptomycin and 20 mM HEPES buffer at 37°C, 5 % CO<sub>2</sub>. Suspension cells MT-4 and C8166 were cultured in RPMI 1640, supplemented with 10 % FCS, 100 U/ml penicillin, 100  $\mu$ g streptomycin and 20 mM HEPES buffer at 37°C, 5 % CO<sub>2</sub>. Freshly isolated primary blood mononuclear cells (PBMCs) were cultured in RPMI 1640.

## 2.9.2 Transfection of cells

Cells were seeded app. 24 h before transfection with one of the following methods:

### *Polyethylenimine (PEI)-method*

Polyethylenimine is a cationic polymer that forms positively charged complexes with DNA that can then enter the cell. For this method, DNA was diluted in DMEM without any supplements and 3 times the amount ( $\mu\text{g}$ ) of DNA was added in volume of polyethylenimine (1 mg/ml in  $\text{H}_2\text{O}$ ), mixed well and incubated for at least 30 min at RT. The mixture was subsequently added dropwise to the cells.

### *Calcium phosphate precipitation method*

DNA was added and mixed into 0.25 M  $\text{CaCl}_2$ . The mixture was then slowly pipetted into the same volume of 2x HeBS buffer while vortexing, incubated for 30 min at RT and then slowly added to the cells. The medium was exchanged 6 h post transfection.

### *FuGene method*

Two times the amount of DNA to be transfected of FuGene6 reagent was added in volume to DMEM without any supplement and incubated for 5 min at RT. Then, DNA was added and incubated for further 15 min before adding the mixture to the cells.

## 2.9.3 RNA interference

siRNAs were purchased from MWG Biotech (Eberseberg, Germany) as standard desalted 21mer duplexes and stored as 100  $\mu\text{M}$  solution. The target sequence used for a Tsg101 specific siRNA molecule is published in (49). For RNAi-mediated silencing of a target protein, 293T cells grown at low confluency (app. 30 %) were transfected with the siRNA applying the calcium phosphate transfection protocol. For one well of a 6 well plate, 100

pmol siRNA was transfected in 500  $\mu$ l total transfection mixture. Approximately 24 h later, expression plasmids were cotransfected with a second dose of either 40 pmol or 80 pmol siRNA. About 24 h later, cell lysates and supernatants were collected and knockdown efficiency was evaluated by quantitative Western blotting.

#### **2.9.4 Analysis of heterodimerizer-mediated Gag-FKBP release**

For the small molecule-induced interaction of retroviral Gag proteins with cellular factors the ARGENT™ Regulated Heterodimerization Kit was used. This kit is based on the natural macrolide rapamycin that can bind both to the FKBP (FK506 binding protein) and the FRAP (FKBP-rapamycin associated protein) protein at the same time. The ARIAD kit provides a cell permeable and chemically optimized derivative of rapamycin called AP21967 (“heterodimerizer”): two proteins of interest can be joined together through AP21967 when one is fused to FKBP and the other to FRB. The heterodimerizer AP21967 was stored as a 1 mM stock solution in 100 % ethanol at -20°C and added 1:20,000 to the cell culture medium. To analyze release of Gag-FKBP induced by recruitment of a cotransfected FRB-fusion protein, 293T cells seeded in 12 well plates were transfected with 30  $\mu$ l CaCl<sub>2</sub>, 30  $\mu$ l 2x HeBS, 0.6  $\mu$ g pGag-FKBP plasmid and variable amounts of FRB-tagged plasmid. 6 hrs after transfection, the medium was changed with 1 ml medium containing 50  $\mu$ M AP21967. 30-32 h post transfection, cells were dissolved in 150  $\mu$ l protein sample buffer, while the supernatant was collected, cleared by low speed centrifugation and pelleted through a sucrose cushion to concentrate Gag particles. After centrifugation the supernatant was carefully sucked off and the pellet was dissolved in 30  $\mu$ l sample buffer. 5  $\mu$ l of the pelleted supernatant and the cell lysate were analyzed by quantitative Western blotting. Gels of cell lysates and particles were blotted on the same membrane to minimize deviations from different blotting efficiencies. The efficiency of Gag release was calculated as a ratio of Gag in the supernatant to total Gag and expressed relative to a positive control (mostly pTSG101-FRB), which was set to 1.0.

### **2.9.5 Isolation of human peripheral blood mononuclear cells (PBMCs)**

Peripheral blood mononuclear cells (PBMC) were purified from buffy coats of HIV-negative blood donors, grown in supplemented RPMI 1640 (10 % FCS, Na pyruvate, Pen/Strep, MEM non-essential amino acids, all used 1:100)=R10+. About 35 ml of each buffy was poured into a T75 cm<sup>2</sup> flask and filled up to 70 ml with PBS. The mixture was poured over a 15 ml Ficoll gradient at RT and centrifuged 40 min at 2000 rpm, RT without acceleration/deceleration. White blood cells from each donor were subsequently isolated, pooled and centrifuged 10 min 2500 rpm. 3 ml ACK lysis buffer was added to each pellet to lyse erythrocytes, pellet was gently resuspended and incubated for 10-15 min RT, then filled up to 50 ml with PBS. This was followed by centrifugation at 2500 rpm for 10 min. The pellets were finally resuspended in 150 ml fresh RPMI (R10+) and immediately stimulated by the addition of 10 ng/ml IL-2 and 2 µg/ml PHA. PBMC pooled from three donors each were used for infection.

### **2.9.6 Thin-section electron microscopy of cell samples**

HeLa cells were fixed at 48 hrs post transfection with 2.5 % Glutaraldehyde in 0.1 M Cacodylate buffer, pH 7.2. After 1 h at RT the cells were washed with 0.1 M Cacodylate buffer, pH 7.2 and post-fixed with 2 % OsO<sub>4</sub> in 0.1 M Cacodylate buffer, pH 7.2 for 30 min at 4°C. OsO<sub>4</sub> was washed away with excess of water and cells were dehydrated with ethanol (a graded series of 40, 50, 60 and 70 % ethanol at RT). Afterwards the cells were incubated with 6 % uranyl acetate in 70 % ethanol for 2 h in dark at 4°C and further dehydrated with a graded series of 80, 90 and 100 % ethanol. To release the cells from the plastic dish propylene oxide was used and collected cells were embedded in epoxy resin EPON 812. EPON was polymerized at 60°C for one day and sectioned to 50 nm slices using ultramicrotome (Ultracut, UCT (Leica), diamond knife (Diatome)). Sections containing cells were picked up on electron microscopic grids (100 mesh) covered with film of formvar and carbon. Grids with sections were stained for 2 min with 2 % lead citrate and examined in a transmission electron microscope EM10 (Zeiss).

Viral particles were counted using systematic uniform random sampling and classified into three groups: mature, immature and budding particles.

## **2.10 *Virological methods***

### **2.10.1 Virus propagation and purification by OptiPrep gradient**

293T cells were seeded at  $3 \times 10^6$  in 10 cm-dishes 24 h prior to transfection with the calcium phosphate transfection method. 10  $\mu$ g pNL4-3 were transfected per dish. Supernatants were harvested app. 40-48 h post transfection and cleared by brief centrifugation at 1500 rpm for 5 min at 4°C and subsequently filtered through 0.45  $\mu$ m filter. Approximately 33 ml of supernatant were layered onto a 6 ml sucrose cushion (20 % sucrose (w/v) in PBS) and pelleted in the ultracentrifuge using an SW32 rotor at 24,000 rpm for 2 h at 4°C. The pellet was resuspended in 50  $\mu$ l of buffer (PBS, 20 mM HEPES, 10 % FCS) and added to a layered OptiPrep gradient from 35 % (bottom layer) to 6 % (top layer) in an SW60 rotor and centrifuged at 32,000 rpm for 1h 30 min. The virus band was collected and resuspended in approximately 4 ml PBS and centrifuged at 44,000 rpm for 45 min using an SW60 rotor. Pellets were incubated for 30 min on ice and subsequently resuspended in 50  $\mu$ l PBS. Aliquots of the virus were stored at -80°C.

### **2.10.2 Analysis of HIV-1 particle release**

293T cells or HeLa cells were seeded at  $3.5\text{-}5 \times 10^5$  and transfected by calcium phosphate precipitation or FuGene 6 with the appropriate pNL4-3-derived plasmid. 30-48 h after transfection, cell lysates and supernatants were collected. For quantitative analysis of infectious HIV-1 particles in the cell culture supernatant by Western blotting or ELISA, 2.5 ml culture supernatant were centrifuged for 5 min at 100 xg (1500 rpm) or filtered through a 0.45  $\mu$ m pore-sized filter. 1.4 ml of the cleared supernatant was layered on 100  $\mu$ l 20 % sucrose/PBS in a 1.5 ml-Microfuge® tube (Beckman) and centrifuged for 1h at 124,000 xg (45,000 rpm, TLA-45 rotor). Pellets were subsequently resuspended in 50-140  $\mu$ l SDS sample buffer or PBS. Cell lysates were collected in 500  $\mu$ l SDS sample buffer. All samples were stored at -80°C.

### **2.10.3 Infectivity assay**

TZM-b1 cells were seeded in 96-well plates at  $5 \times 10^3$  cells/well in 100  $\mu$ l. After 24 h they were infected with 100  $\mu$ l of supernatant harvested from transfected 293T cells (HIV-1 was produced by transfection with the plasmid pNL4-3) and serial 3 fold dilutions were performed in DMEM. Cells were incubated for 48 h at 37°C. Supernatant was removed and cells were lysed with 50  $\mu$ l of Steady-Glo<sup>®</sup> reagent in 50  $\mu$ l DMEM (Steady-Glo<sup>®</sup> Luciferase Assay System, Promega, Mannheim, Germany) for 30 min at RT. 80  $\mu$ l of cell lysate was transferred to a white 96-well plate and luminescence was measured in a plate luminometer.

### **2.10.4 Replication kinetics of HIV-1 and p6 mutant derivatives**

HIV-1 was produced by transfection of 293T cells with the plasmid pNL4-3, pNL4-3-uncoupled or corresponding mutant variant of either parental plasmid. The amount of p24 in the supernatant was determined by ELISA and 5 ng of virus p24 was used to infect  $1 \times 10^5$  C8166 cells or PBMCs in 200  $\mu$ l fresh RPMI (supplemented R10+ for PBMCs) per well (96-well plate, V-bottom). 95  $\mu$ l of supernatant were collected every 2 days and inactivated with 5  $\mu$ l of 5 % Triton X-100, leading to a final concentration of 0.25 % of Triton X-100.

### 3 Results

#### *3.1 Identification and selection of predicted and conserved phosphorylated residues in the p6<sup>Gag</sup> domain of HIV-1*

In higher eukaryotes, protein phosphorylation involves serine, threonine and tyrosine residues. The p6<sup>Gag</sup> domain of HIV-1 consists of 52 amino acid residues, of which 13 could in principle be phosphorylated. However, protein phosphorylation results from the recognition of specific amino acid sequences or motifs by a particular kinase. This is the principle behind phosphorylation prediction programs that are widely available on the internet, such as NetPhos/NetPhosK, GPS (group-based prediction system) and DISPHOS (disorder enhanced phosphorylation sites predictor). Such programs mainly rely on sequence-based prediction algorithms, designed to identify common prevalent features of amino acid sequences surrounding Ser, Thr and Tyr residues. These short sequences or motifs are then compared to existing databases of phosphorylated proteins. Some of these programs have the additional feature of assigning a kinase to a predicted residue. Thus, to assess the number of predicted phosphorylation sites in p6<sup>Gag</sup> I made use of the 3 prediction programs mentioned above and used high threshold values for identification of phospho sites and kinases, in order to reduce the number of false positives. Table 3.1 compares results obtained with the 3 different prediction programs, showing only those residues that obtained the highest prediction scores.

p6: <sub>1</sub> LQSRPEPTAPPEESFRFGEE**TTTP**SQKQEPIDKELYPLASLRSLFGSDPSSQ<sub>52</sub>

Predicted residue	DISPHOS	NetPhos(K)	GPS	Predicted kinase
Serine	3	3	N.P.	PKC
	14	14	14	CKI, ILK
	25	25	25	DNAPK, ATM
	40	40	N.P.	PKC
	43	43	N.P.	CKI
	47	47	N.P.	GSK3

	50	N.P.	N.P.	U.D.
	51	51	N.P.	CKII, DNAPK, ATM
<b>Threonine</b>	8	8	N.P.	GSK3
	N.P.	21	N.P.	GSK3, GRK, PLK
	22	N.P.	N.P.	GRK
	23	23	23	p38MAPK, CDK, MTOR
<b>Tyrosine</b>	N.P.	36	36	BTK

**Table 3.1 Predicted phosphorylated residues in the p6<sup>Gag</sup> domain of HIV-1.**

Shown above the table is the 52 amino acid sequence of HIV-1 p6. Potential phosphorylation sites are highlighted in green. This marking does not reflect the residues that were highly predicted to be phosphorylated by the programs. Three different prediction programs were used to obtain putative phosphorylated residues in the p6<sup>Gag</sup> domain of HIV-1. The table compares the residues obtained as a result of the analysis of the p6 sequence with the respective program: NetPhos combined with NetPhosK, DISPHOS or GPS. The predicted kinase(s) responsible for phosphorylation of the particular residue is indicated when available. NP indicates a residue that was either not predicted to be phosphorylated or had a prediction value under the threshold and was therefore not included. NP= not predicted, UD= undetermined.

p6<sup>Gag</sup> consensus sequences derived from different HIV-1 subtypes were aligned in order to identify residues that are highly conserved among these strains as shown in Table 3.2. Results from this analysis, as well as data obtained from the phosphorylation prediction programs was combined to select p6 residues that displayed both a high degree of conservation among HIV-1 subtypes and a high prediction score for phosphorylation.

	..3...8...14.....21.....36....40.43.....51.
pNL43.p6.	LQSRPEPTAPPEESFRFGEE <b>TTTP</b> SQKQEPIDKELY <b>P-LASLRSLFGSDPSSQ-</b>
CON_OF_CONS	.....A...G...I.P-.P...K.....-...K...N..L..X
CONSENSUS_A1	P.....A.I.GM...I. <b>S</b> -PP...QK.R.QD.P.V..K...N..L..X
CONSENSUS_A2	P... <b>T</b> .....A.NL.M...I. <b>S</b> -.L...LK <b>TR</b> .P.NPAI..K...N..L..X
CONSENSUS_B	.....-.....N...X
CONSENSUS_C	..N.....A.....-...P-AP...K.R.---P. <b>T</b> ..K.....L..X
CONSENSUS_D	.....A...G...I.P-...QK.....- <b>T</b> ..K...N..L..X
CONSENSUS_F1	.....A...G.R...I.P-.P...QK.EG...P...K...N..X---
CONSENSUS_G	..N.....A...G...IAP-.P...QKE.....-...K.....X---
CONSENSUS_H	.....A...G...M.P-.P...LK...-P.....N..L..X
CONSENSUS_K	.....A...G...I.P-.PR.. <b>TK</b> ...QG.P. <b>T</b> ..K...N..L..X

**Table 3.2 Sequence alignment of p6 consensus sequences derived from different HIV-1 subtypes.**

Dots indicate conserved residues among the sequences. If a residue is not conserved it is indicated as it occurs within a particular sequence. Ser, Thr and Tyr residues are highlighted in red. The consensus sequences for subtypes A, B, C, D, F, G, H, and K were compared to the reference sequence derived from the HIV-1 clone NL4-3. Sequences were obtained and aligned using the Los Alamos HIV sequence compendium and HIV sequence alignment feature (86).

To assess the functional role of the potentially phosphorylated residues in the HIV-1 replication cycle, we introduced specific point mutations into the p6 sequence. The p6 residues, Ser14 and Ser25 were chosen for further study and were thus mutated either to an alanine or an aspartate (S14A, S14D, S25A, and S25D). Importantly, aspartate was chosen based on the premise that such a residue contains the negative charge and bulkiness that would resemble a phosphorylated residue. In addition, an initial set of p6 mutants of the Thr residue within the highly conserved PT<sub>8</sub>AP motif (T8A, T8I, T8D) and of the Thr residue at position 23 (T23A, T23D, T23I) that had been previously generated by B. Müller were also included in this study. The Thr23 mutants had been previously tested by B. Müller and no detrimental effect was observed on virus particle release or infectivity. However, a later study by Hemmonot et al indicated that a p6 Thr23 mutant was strongly impaired in release (60). Therefore, we decided to include and retest the effects of this mutant. The p6 mutants were generated by oligonucleotide-directed mutagenesis and confirmed by sequencing. Fragments carrying the particular p6 point mutation were cloned back into the full-length infectious molecular clone, pNL4-3. Of note is that due to the fact that the virus *gag*- and *pol*-reading frames overlap, introducing changes into the *gag* sequence may result in amino acid changes in the Gag-Pol polyprotein precursor. Indeed, in most instances (T8A, T8D, S14A, S14D, S25A, S25D, T23A, and T23D) it was not possible to mutate the p6 residue without affecting the *pol* frame sequence. However, it has been reported that mutation of the central region of the *pol* frame, corresponding to residues <sub>21</sub>threonine-glutamine<sub>61</sub> and to residues <sub>5</sub>proline-aspartate<sub>32</sub> in the p6<sup>Gag</sup> domain, has no deleterious effect on virus protein expression and stability, assembly, release or productive infection of T cell lines (13, 111).

### 3.2 Effect of p6 mutants in HIV-1 release and viral protein processing

The effect of the proviral p6 mutants T8, S14, S25, and T23 in virus production and viral protein processing was tested by transient transfection of 293T cells and compared to wt NL4-3. Shown in Figure 3.1 are the western blots of cell associated viral products and released virus particles.

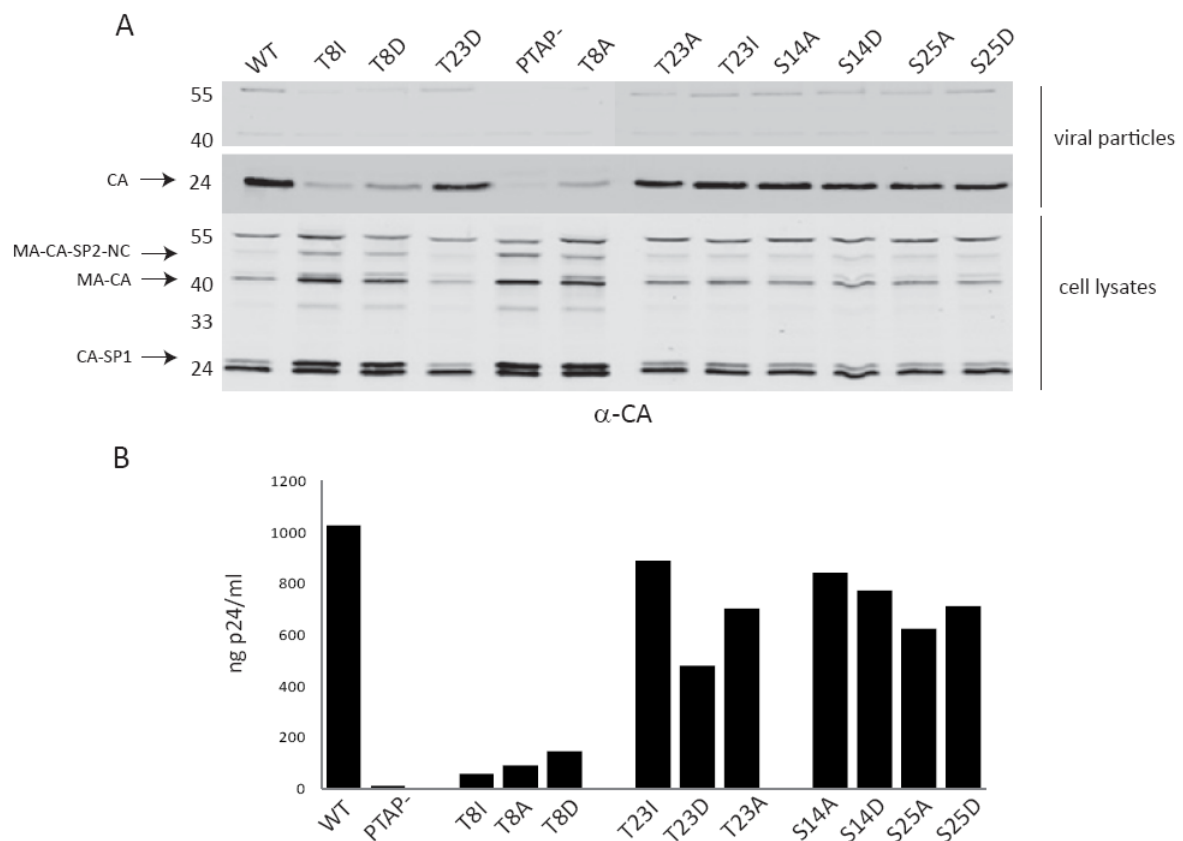


**Figure 3.1 Effect of p6 mutants in virus production and Gag protein processing.**

Western blot analysis of 293T cells transfected with the proviral HIV-1 clones harboring a point mutation within the p6<sup>Gag</sup> sequence. (A) Virus supernatants and cell lysates were collected 48 h posttransfection (pt) and virus supernatants were layered and pelleted over a 20 % sucrose cushion. The amount of released virus can be visualized as the 24 kDa capsid (CA) band (indicated by an arrow), representing mature virions. Gag processing products are shown in the cell lysate samples and Gag processing intermediates are indicated by arrows. The PTAP- construct was used as a negative control for release. (B) The levels of virus p24 (CA) were determined for each viral construct by quantitative Western blotting using a preset CA standard. Membranes were probed against CA-specific antibody. Positions of molecular mass standards are shown with numbers in kDa at the left.

It is evident that the amount of virus produced by the Ser14, Ser25 and Thr23 mutants is not affected and is comparable to that of the wt while it is clear that, as expected, the Thr8 mutants are strongly impaired in release. Moreover, the cell associated viral products show a Gag processing pattern is identical to the wt in the case of the Ser and Thr23 mutants. In contrast, the T8 mutants accumulate intermediate Gag processing products as indicated by the arrows in the blot. The PTAP- construct has the PTAP motif in p6 exchanged for a LIRL sequence; consequently, its budding efficiency is strongly inhibited. This construct served as a negative control for these experiments. The efficiency with which virions were released was determined by quantitative western blot analysis of virus sucrose pellets and compared to a p24 capsid (CA) standard to obtain ng amounts of released virus. The graph in Fig 3.1 B shows that similar amounts of p24 CA are obtained for the Ser and T23 mutants relative to the wt, while the amount of virus released by the T8 mutants and by the PTAP- construct is highly impaired as previously shown (36, 64). However, the T8D mutant had a less pronounced effect on release as compared to the other T8 mutants as shown in Figure 3.2.

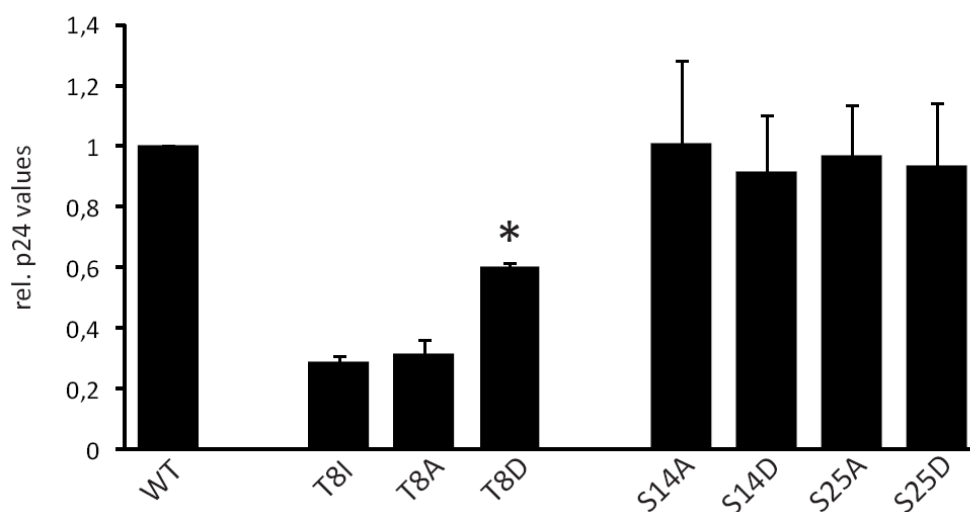


**Figure 3.2 Comparison of the levels of HIV-1 produced by the T8 mutants.**

Comparison of virus p24 levels released by the p6 T8 mutant virions show that the p6 T8D mutant (indicated by an asterisk) has less pronounced effect on release in comparison to the other T8 mutants. Relative values of p24 CA are shown. Error bars represent the standard deviation of four independent experiments.

Taken together, these findings imply that neither the T23 nor the S14 and S25 residues, individually, are required for efficient particle release, suggesting that phosphorylation of the single residues is not required for this late viral step. Moreover, the T8D mutant shows a slightly enhanced effect on release that might be attributable to

putative phosphorylation of this residue. Instead, it is plausible that the aspartate at this position partially satisfies structural requirements to mediate interaction with its cellular partner, Tsg101. Therefore, this mutant requires further analysis.

### 3.3 Infectivity and replication capacity of HIV-1 p6 mutants

To determine whether the p6 mutants are impaired in viral processes other than budding, the capacity of these viruses to undergo single-round infection was assayed.

Supernatants of 293T cell-derived mutant viruses were titrated onto TZM-bl reporter cells containing  $\beta$ -galactosidase and luciferase reporter genes under the control of a long terminal repeat (LTR) promoter. Luciferase activity of the reporter cells was measured 48h post infection (pi). Figure 3.3 displays the relative infectivity of all the p6 mutants in comparison to the WT. Since it was clear to us--from this study and previous studies--that

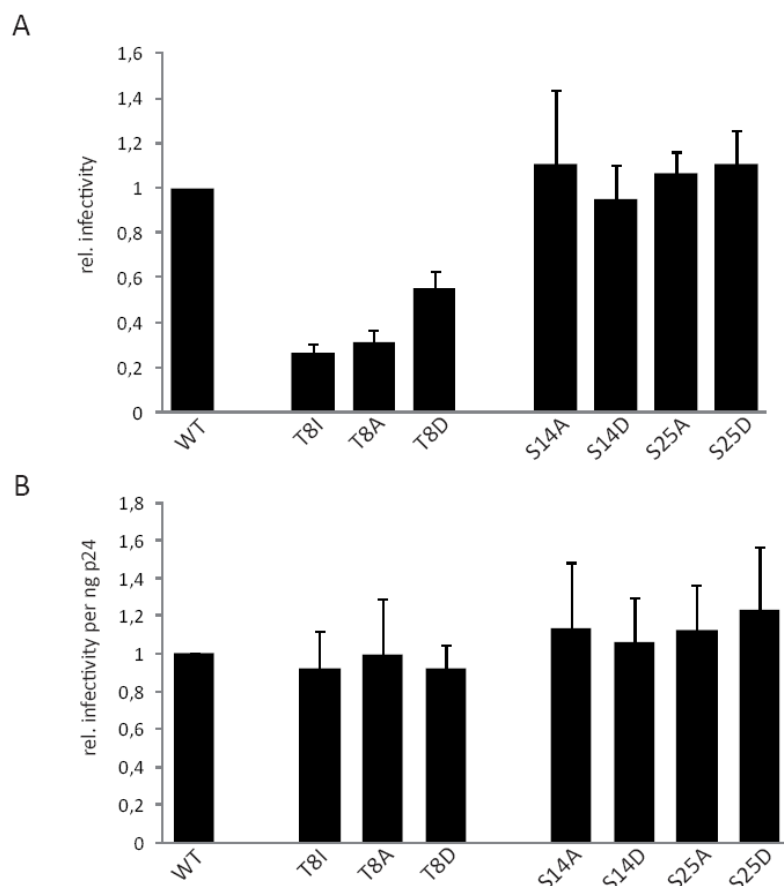


**Figure 3.3 Single-round infectivity of HIV-1 p6 mutants.**

Virus supernatants derived from transfected 293T cells were titrated onto the HeLa reporter cell line, TZMbl. Cells were lysed 48h pi and luciferase activity was measured as relative light units. (A) The graph displays infectivity values of each mutant relative to the wt levels. (B) The infectivity values were normalized to the ng

amount of virus CA (values ranged between 2800 ng p24/ml to 750 ng p24/ml) present per mutant. Error bars represent the standard deviation from three independent experiments, each done in triplicate.

the T23 p6 mutant does not play a role in the replication cycle of the virus, we decided to discontinue experiments with this mutant. As it can be observed, the infectivity values for the Ser mutants are not affected and levels similar to the wt are obtained. In contrast, the T8 mutants are strongly impaired; however, when the infectivity values are normalized to the amount of virus CA (p24) found in the supernatant per mutant, no obvious differences are apparent. Because this assay does not allow one to observe more subtle differences in replication over an extended period of time, a viral replication kinetics assay was carried out in two different cell types: C8166, a CD4<sup>+</sup> lymphocytic cell line and on primary lymphocytes isolated from 3 different donors. Briefly, sucrose-purified virus particles produced from transfected 293T cells were used to infect C8166 cells with a defined concentration (5 ng p24 per well) and supernatants were monitored for p24 release every second day for a total period of 13 days. Primary lymphocytes were infected with 5ng of virus collected from the supernatants of transfected 293T cells. Virus supernatants were collected every 2 days for a total period of 15 days and assayed for p24 levels by ELISA (enzyme-linked-immunosorbent assay). In Figure 3.4, the amount of virus released into the supernatant is plotted over time for wt, T8, S14 and S25 p6 mutants. Figure 3.4 A and B shows that the Ser14 and Ser25 mutants display kinetics almost identical to those of the wt throughout the course of infection. In contrast to the p6 T8A and T8I mutants that are replication defective and display delayed kinetics relative to the wt, the T8D mutant achieves slightly better replication levels at early time points (Figure 3.4 C).

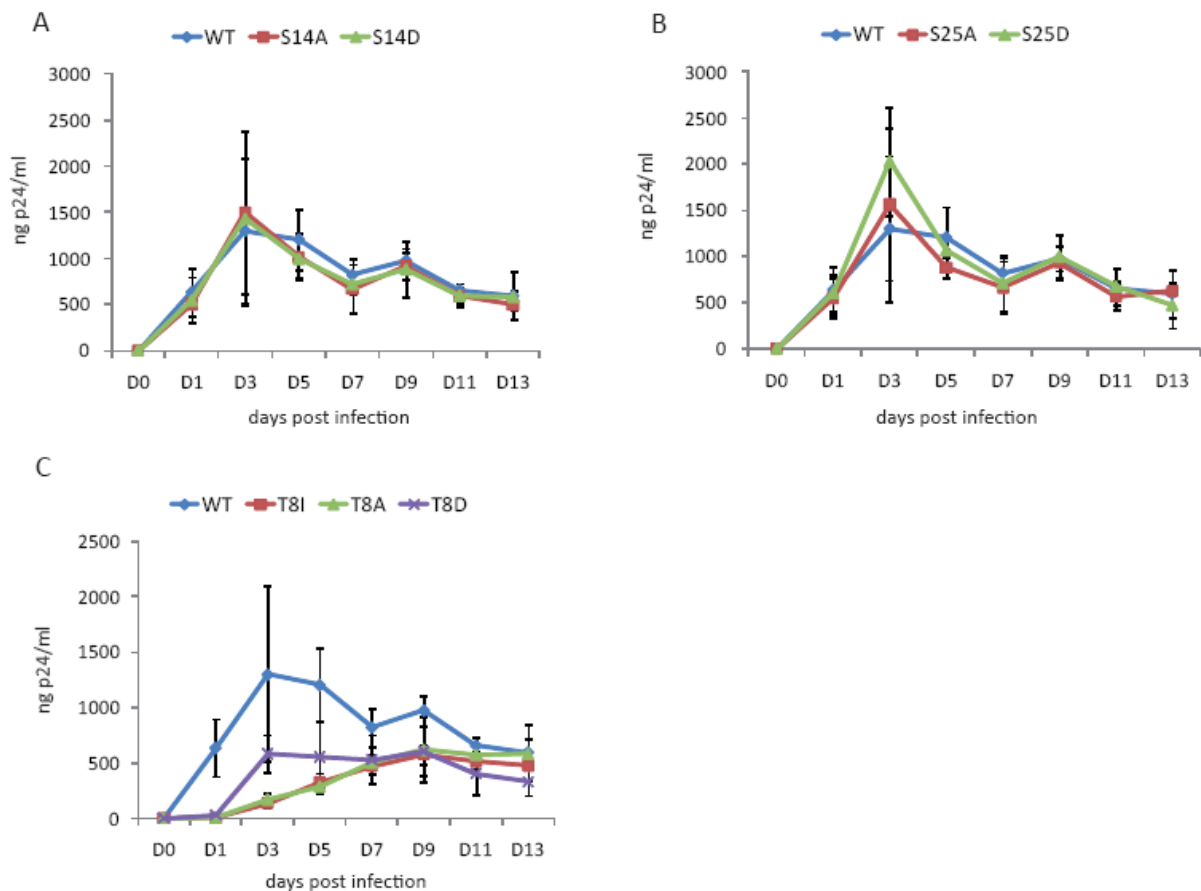


**Figure 3.4 Replication kinetics of HIV-1 p6 mutants.**

C8166 cells were infected with 5ng of wt or the corresponding p6 mutant. Virus supernatant was collected every 2 days for a period of 13 days and assayed for p24 levels by ELISA. (A) and (B) Both S14 and S25 mutants replicate equally efficient relative to the wt virus. (A) All T8 mutants display delayed kinetics in comparison to the wt; however, the T8D mutant shows a slightly enhanced replication capacity at early timepoints. Error bars show the standard deviation of 3 independent experiments done in triplicates.

Overall, these results indicate that phosphorylation of the p6 Ser14 and Ser25 mutants is not likely to play a role in virus infectivity in C8166 cells. On the other hand, the p6 T8D mutant has a slightly better replication capacity than the T8A and T8I mutants, again suggesting that the negative charge and bulkiness of the aspartate at this position provides some gain of function capability to this mutant. This could indirectly hint at a role for phosphorylation of this residue.

The replication capacity of the different viruses was also assayed in a more relevant cell system. Therefore, I infected primary lymphocytes combined from 3 different donors with wt HIV-1 and the T8 p6 mutants. Additionally, the T23 p6 mutant was included in this assay to completely exclude a possible role of this residue in the replication efficiency of HIV-

1 while the S14 and S25 mutants were excluded from this study since all previous experiments suggested against these residues being involved in the replication cycle of the virus. A PTAP- mutant and an efavirenz (a reverse-transcriptase inhibitor)-treated wt HIV-1 sample served as negative controls. Results from this analysis are shown in Figure 3.5.

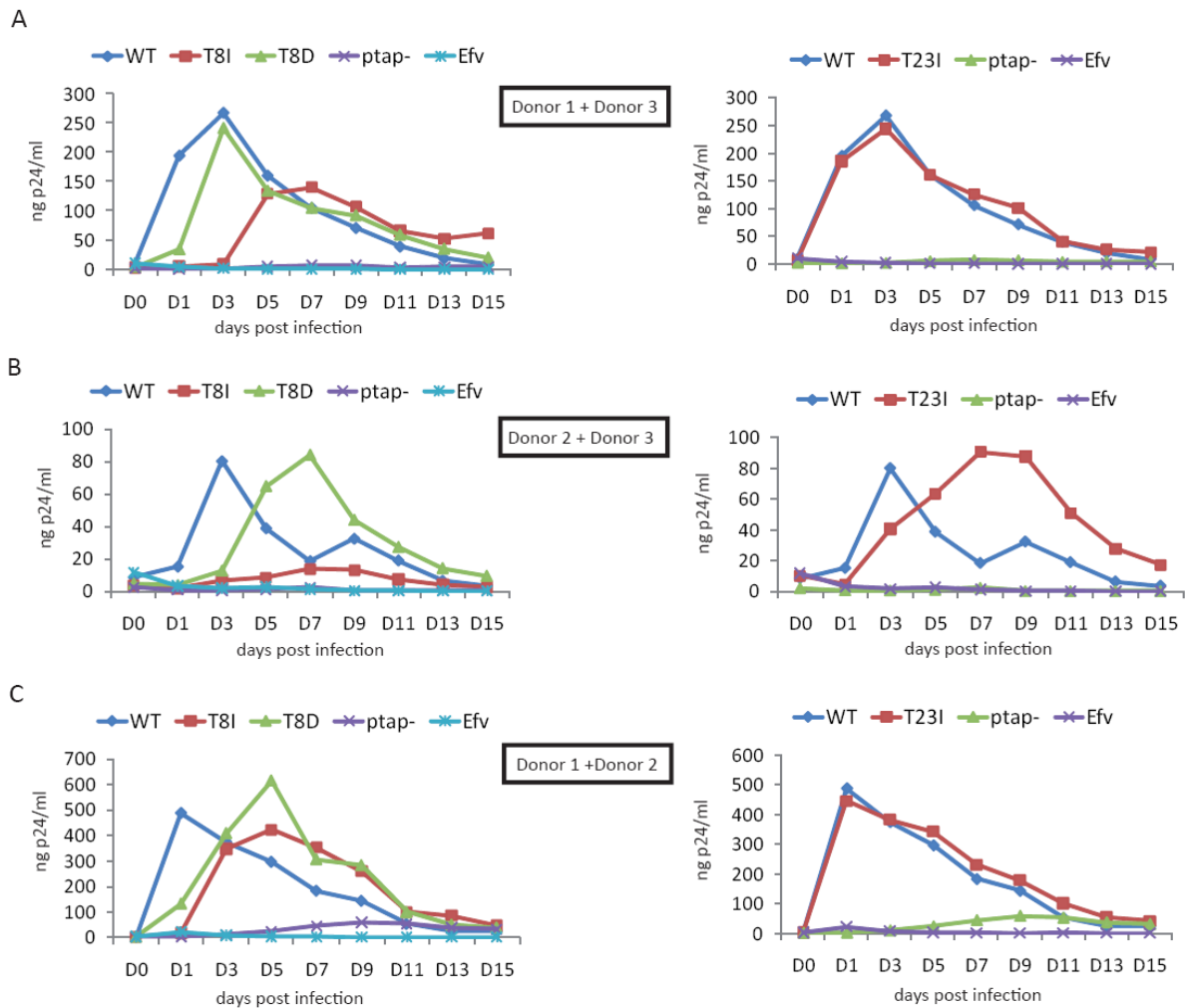


**Figure 3.5 Replication kinetics of HIV-1 p6 mutants in primary lymphocytes.**

Peripheral blood mononuclear cells (PBMCs) were isolated from 3 different donors, combined among each other and infected with 5 ng of HIV-1 wt or the corresponding p6 mutant virus. Virus supernatants were collected every 2 days for a total period of 15 days and assayed for p24 levels by ELISA. The graphs show the replication curves obtained from infected donor 1+3 (A), donor 2+3 (B) or donor 1+2 (C) primary lymphocytes. In all cases it is observed that the Thr23 p6 mutant is not affected in its replication capacity, while all Thr8 mutants display delayed kinetics.

The behavior of the mutants was comparable in all donors and it can be observed that in all cases, the T23 mutant replicates in a similar manner to the wt. The T8 mutants display delayed replication kinetics, also in the case of the T8D mutant which in only one case peaks at the same day and close to level of the wt. Importantly, the T8I mutant never reaches the virus production levels that are reached by the wt or the T8D mutant at later days,

suggesting still that the T8I mutant has a replicative disadvantage that can be partially overcome by the T8D mutant.

### 3.4 Analysis of a p6 T8E mutant

Due to its negative charge and increased side chain bulkiness relative to an aspartate, a glutamate residue (E), might in principle, better resemble an amino acid modified with a phosphate group. Expecting to obtain a stronger phenotype which would corroborate our observations with the T8D mutant, two new p6 mutants were prepared, one containing a T8E point mutation and as an additional negative control, one containing a T8N point mutation. Contrary to our expectations, the T8E mutant did not show an increased effect on virus release as depicted in Figure 3.6.

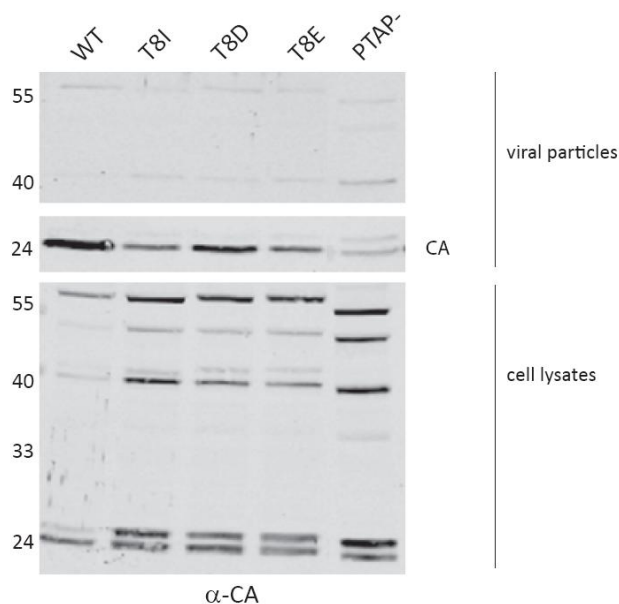


**Figure 3.6 Effect of a p6 T8E mutant on HIV-1 release and gag processing.**

Western blot analysis of wt and p6 mutant viruses derived from 293T transfected cells. Cell- and particle-associated virus products were harvested 30h pt. Particles released into the cell supernatants were pelleted over a 20% sucrose cushion and all samples were probed against virus-specific CA antibody. The blot shows that the amount of viral particles obtained from the p6 T8E mutant is not enhanced relative to the T8D mutant. Accumulation of Gag processing intermediates are observed at about the 40kDa and below the 55kDa bands for the T8 mutants. Positions of molecular mass markers in kDa are shown at the left and the mature virus band is indicated at the right.

This observation was confirmed in repeated experiments. On the other hand, the T8N p6 mutant, to our surprise, showed wt levels of released virus in repeated experiments, as well as a wt-like gag processing pattern as illustrated in Figure 3.7. The western blot shows that the highest levels of virus release can be obtained with either the wt construct or the p6 T8N mutant. Moreover, out of all the p6 mutants, the T8N mutant most closely resembles the cell-associated Gag processing pattern of the wt virus Figure 3.7 A. The enhanced effect in release by the p6 T8N mutant was corroborated in multiple experiments as depicted in Figure 3.7 B, which compares the relative p24 values among some of the p6 mutants to the wt virus.

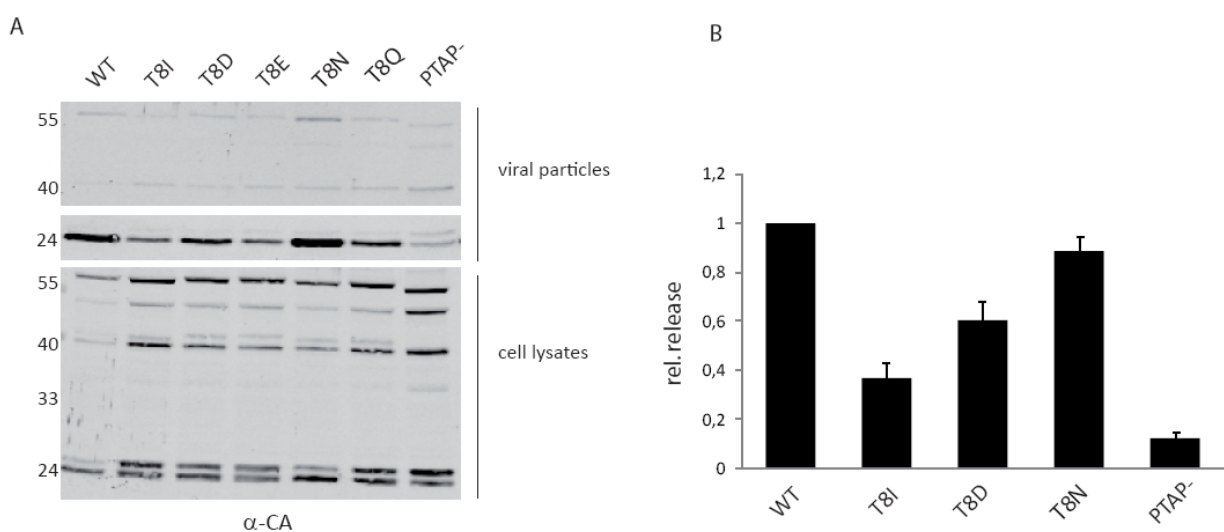


**Figure 3.7 Effect of the HIV-1 p6 T8N and T8Q mutants on virus release and Gag processing.**

Western blot analysis of wt and p6 mutant viruses derived from 293T transfected cells. Cell lysates and virus supernatants were harvested 30h pt. Virus particles were purified over a sucrose cushion and all samples were probed against virus CA antibody. (A) The amount of viral particles obtained from the p6 T8N mutant is comparable to that of the wt. Although, both the T8E and T8Q mutants are slightly more efficient in release than the PTAP- control, they do not achieve the levels obtained with the T8N mutant. (B) Graph represents the quantitative WB analysis of p24 CA bands obtained from each virus relative to the wt. The T8N mutant achieves the highest levels of virus release in comparison to all other p6 mutants. Error bars show standard error of the mean from nine independent experiments. Positions of molecular mass markers in kDa are shown at the left.

Overall, these results argue against an involvement of PTAP phosphorylation in its virus budding activity and open the door to further exploration and characterization of the p6 T8N mutant and its role in HIV-1 release.

### 3.5 Comprehensive analysis of predicted phosphorylation sites in HIV-1 p6

In order to study the relevance of p6 phosphorylation in HIV-1's life cycle, it is necessary to examine the effect of p6 mutations in each one of its predicted phosphorylated residues. It is possible that only a combination of point mutations at different residues is needed to observe an effect in virus release and/or replication capacity. However, this type of analysis is hindered first of all, by the fact that generating combinations of point mutants throughout the whole p6 sequence is rather time-consuming and second and most important of all, by the fact that the *gag* and *pol* reading frames of the virus overlap. A frameshift signal located at the spacer peptide 1 sequence in *gag* (the amino terminus of the p6\* transframe sequence in *gag-pol*) normally causes the ribosome to slip back every 1 out of 20 translation events, resulting in the synthesis of the *pol* products as depicted in Figure 3.8. Therefore, it is not possible to make extensive mutations in p6 without seriously compromising the integrity of the *pol* sequence and its products.

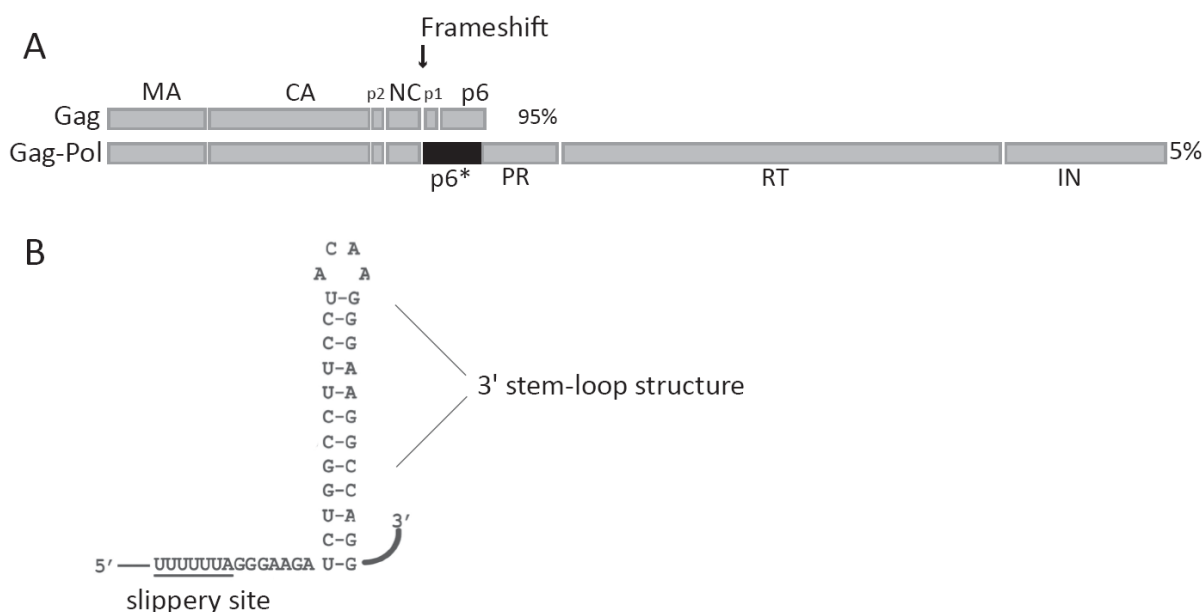


**Figure 3.8. The HIV-1 frameshift determinants.**

(A) *Pol* is in a different reading frame than *gag*, thus a ribosomal frameshifting event ensures the synthesis of the *pol* products at a strict ratio of 20:1 Gag to Gag-Pol molecules. The arrow indicates the position of the frameshift signal in *gag*. (B) The frameshift event is promoted by both a heptanucleotide slippery site sequence and a 3' stem-loop structure present at the amino terminus of the p6\* sequence. MA = matrix, CA = capsid, p2

= space peptide 2, NC = nucleocapsid, p1 = spacer peptide 1, p6\* = p6 transframe, PR = protease, RT = reverse transcriptase, IN = integrase.

### 3.5.1 Uncoupling the overlapping *gag* and *pol* reading frames

Recently, Leiherer et al published a study in which they uncouple the *gag* and *pol* reading frames of HIV-1 to examine the role of the p6\* protein in viral replication (89). p6\* is located at the amino terminus of the Pol moiety within the Gag-Pol precursor and is thought to play a role in the activation of the viral PR. The strategy used by Leiherer et al is based on the destruction of the original slippery site and 3' stem-loop structure by point mutations (without altering the p1 sequence) to abrogate the frameshift signal. The complete functional frameshift signal, including the slippery site and stem-loop was introduced at the 5' end of the Gag stop codon. In the resulting provirus, the *gag* and *pol* genes are extended by 15 and 210 nucleotides, respectively, compared to those of the parent NL4-3 provirus. A schematic of the strategy used by Leiherer et al is depicted in Figure 3.9.

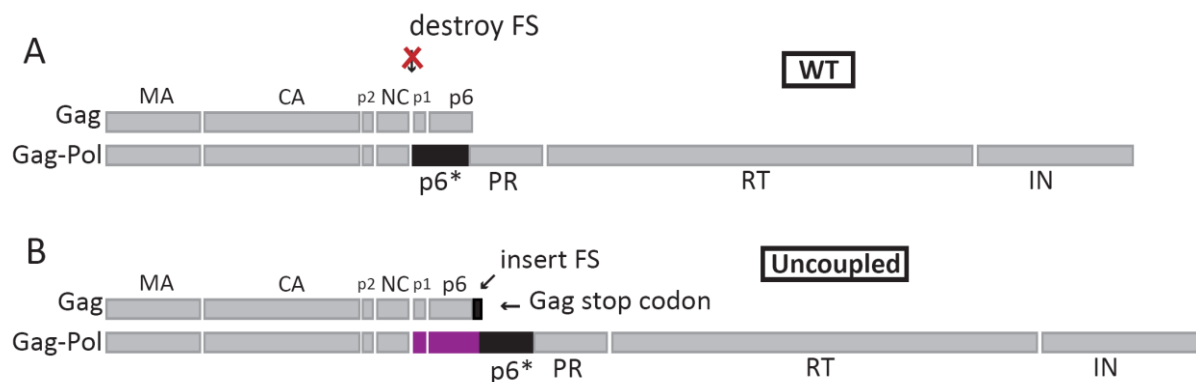


**Figure 3.9 Schematic of the strategy used to uncouple the HIV-1 *gag*- and *pol*-reading frames.**

(A) The wt provirus's Gag and Gag-Pol products translated in the presence of the original frameshift. In order to uncouple the overlapping reading frames, the frameshift signal at the amino terminus of the p6\* TF is abrogated by point mutations that do not change the p1 sequence. (B) An artificial frameshift site is inserted at the 3' end of the *gag* gene, indicated by the arrow, resulting in the synthesis of a Gag-Pol polyprotein with p6\* TF directly fused to p6<sup>Gag</sup> highlighted in magenta. Insertion of the frameshift signal also results in a *gag* reading frame extended by 5 residues and terminated by insertion of a stop codon highlighted by the arrow. FS = frameshift signal, MA = matrix, CA = capsid, p2 = space peptide 2, NC = nucleocapsid, p1 = spacer peptide 1, p6\* = p6 transframe, PR = protease, RT = reverse transcriptase, IN = integrase.

We made use of this strategy to address more extensively the role of p6 phosphorylation in the replication cycle of HIV-1. Therefore, a 363 base pair gene fragment harboring an abrogated frameshift signal and designed to contain the new slippery-site and

stem-loop at the end of the Gag codon was synthetically produced and cloned into the NL4-3 proviral clone.

### 3.5.2 Effect of frameshift displacement on virus maturation and particle production

Because the new 'uncoupled' proviral construct was significantly modified in order to separate the *gag* and *pol* reading frames, it was necessary to determine to what extent viral protein synthesis and particle production could have been affected by the corresponding mutations. For this purpose, 293T cells were transiently transfected with the WT and uncoupled construct and released virus particles and cell-associated viral products were collected 30h pt. Cell lysates and purified virus particles were subjected to Western blot analysis using a CA-directed antibody. As shown in Figure 3.10, both the parental NL4-3 WT virus and the uncoupled viral construct produced comparable amounts of mature virus particles as well as Gag-derived products in the cell lysates. The extension of the p6<sup>Gag</sup> carboxyl terminus by five amino acids (0.5 kDa) was nicely reflected by a slight shift of the uncoupled-specific 55 kDa Gag precursor.

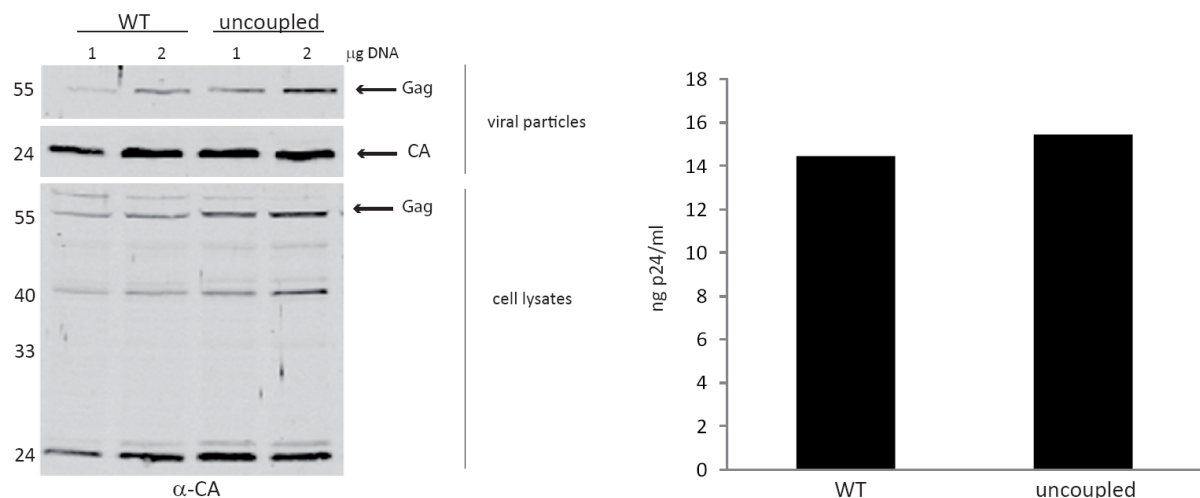


**Figure 3.10 Influence of frameshift displacement on virus maturation and release.**

293T cells were transiently transfected with the indicated viral plasmids. For analysis of virus composition, particles released into cell supernatants were harvested 30h pt and sedimented through a 20% sucrose cushion. Left, viral proteins were separated by SDS-PAGE and analyzed by Western blotting using a CA-specific antibody. Viruses containing the frameshift displacement (uncoupled) are released to comparable levels as the parental WT virus. In addition, cell-associated Gag products exhibit a similar processing pattern that is slightly shifted in the uncoupled construct due to the extension of the *gag* and *gag-pol* genes. Positions of molecular mass markers are shown at the left, and the arrow at the right indicates virus-specific protein bands. Right, the

amount of virus particles produced by the WT and uncoupled constructs was determined by quantitative WB of the CA band intensities derived from (A) and compared against a standard amount of p24 CA. Results are shown for the viruses transfected with 2  $\mu$ g of DNA as depicted in (A).

Together, these observations strongly argue for the functionality of the displaced frameshift signal in the uncoupled provirus and suggest that virus production, packaging and maturation of the precursor proteins are equally efficient in WT and uncoupled viruses.

### 3.5.3 Effect of frameshift displacement on virus infectivity

To evaluate whether the uncoupled virus was capable of infecting cultured cells, WT and uncoupled particles released from transfected 293T cells were used to infect TZM-bl indicator cells. Luciferase activity was measured 48h pi. As shown in Figure 3.11, the infectivity of uncoupled particles was slightly decreased to approximately 80% of the WT infectivity.

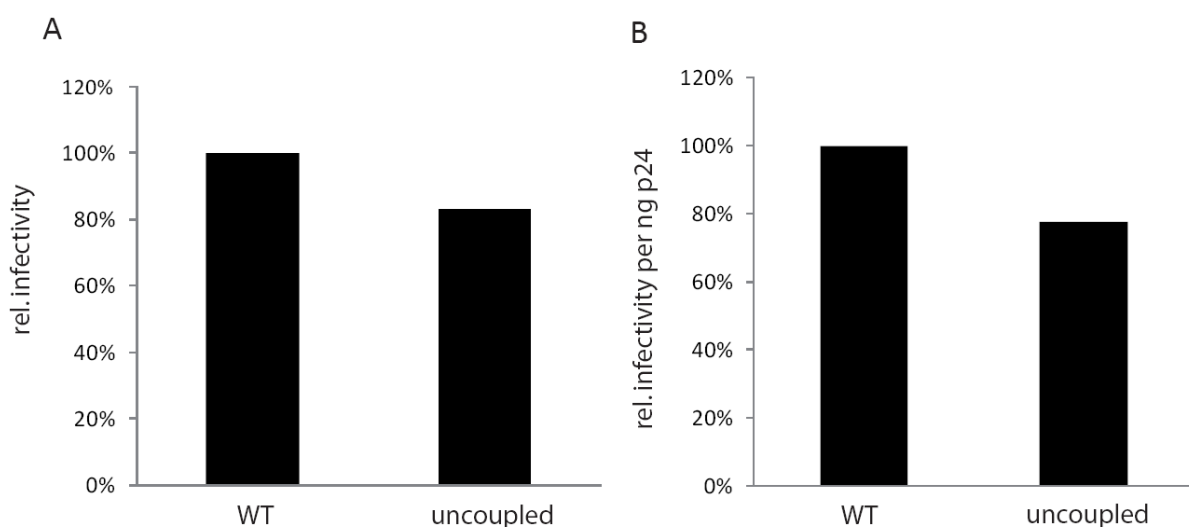


**Figure 3.11 Analysis of frameshift displacement on virus infectivity.**

To evaluate viral infectivity, WT and uncoupled virus supernatants produced from transfected 293T cells were used to infect the CD4+ TZM-bl reporter cell line. (A) At 48h pi, luciferase activity was measured and values obtained were related to the WT infection (100%). The uncoupled virus is slightly less infectious than the WT virus. (B) Infectivity values were normalized for CA content by quantitative WB using a CA standard.

The reduced infectivity of the uncoupled virus might be due to compromised frameshifting or to the rearranged protein domains. In sum, these data are in agreement with the study by Leiherer et al (89) and show that the NL4-3 derivative uncoupled is an infectious virus mutant representing an excellent tool to perform extensive mutations in p6.



To assess the impact of the extensive p6 mutations on virus production and processing of viral precursor proteins, 293T cells were transiently transfected with the (parental NL4-3) WT, uncoupled (WT) and uncoupled mutants. Virus particles released were harvested 30h pt, and the protein content of both virus particles and cell-associated viral products were analyzed by Western blotting. As observed in Figure 3.13, no obvious defect in viral protein processing in any of the mutants could be seen.

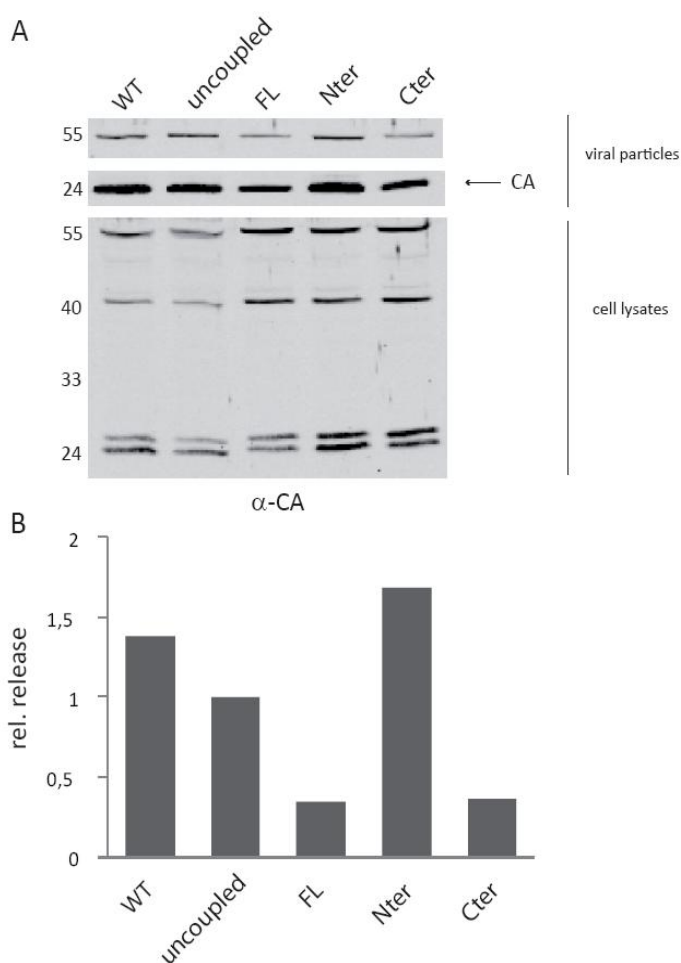


**Figure 3.13. Characterization of virus maturation and production by the uncoupled p6 mutant viruses.**

293T cells were transiently transfected with the corresponding proviruses. (A) Cell lysates and virus supernatants were harvested 30 h pt and virus particles were isolated through a 20 % sucrose cushion. Particle- and cell-associated proteins were separated by SDS-PAGE and analyzed by Western blotting using a CA-specific antibody. The FL and Cter viruses are compromised in release with no apparent accumulation of processing intermediates. Positions of molecular mass markers in kDa are shown at the left, and the arrow at the right indicates the mature virus CA band. Vertical lines on the right indicate the position of the Western blots containing either the released virion bands or the cell-associated virus protein bands. (B) To determine the amount of virus that was released by each virus, the intensity of the mature virus CA band shown in (A) was quantitated by Western blotting using a preset CA standard. The release efficiency of each virus relative to the uncoupled virus is shown.

Interestingly, we observed a pronounced decrease in the amount of virus that was released by the FL and Cter mutants, while the Nter mutant was released to a level greater than the WT construct. None of the mutant viral particles seemed to display an aberrant accumulation of the processing intermediate p25 which would otherwise suggest a defect in particle morphology. These results suggest that predicted phosphorylated residues within the C-terminal region of p6 may be involved in some aspect of virus budding. The effect observed with the Nter mutant could suggest that phosphorylation within this region might

serve to negatively regulate virus release. However, further attempts to corroborate this data have proven difficult to achieve. The effect, in particular that of the FL and Cter mutants, has been rather variable suggesting at times that potential phosphorylation of p6 does not play a role in virus release (data not shown). Different transfection reagents, plasmid DNA amounts and cell systems were tested to assess their effect in the stability of the phenotypes observed; however, no conclusive result was so far obtained. The integrity of the mutants as well as the presence of the proper point mutations was corroborated several times. Thus, future analysis of these mutants should be able to define their role, if any, in the HIV-1 replication cycle.

### ***3.6 p6 phosphopeptide analysis by Mass Spectrometry***

Mass spectrometry (MS) has become an invaluable tool in the identification of unknown compounds and in the elucidation of the structural and chemical properties of molecules. Moreover, it has also been a fundamental technique for virology; for instance, it has been used to identify viral capsid proteins, detect viral mutants, measure intact viruses and to characterize posttranslational modifications (139). Indeed, advances in MS have quickly evolved so that nowadays ample numbers of *in vivo* phosphorylation sites can be detected and quantified in a relatively short period of time (56). Protein phosphorylation events are detected by increases in amino acid residue mass of +80 Da, which report the addition of metaphosphoric acid (HPO<sub>3</sub>). Sites of phosphorylation can be identified from mass shifts in fragment ions generated by gas-phase (MS/MS) of phosphopeptides (151).

Because MS provides a strong and reliable basis to identify protein residues that are phosphorylated, we decided to analyze the phosphorylation status of HIV-1 p6 using this powerful technique. For this purpose, we initially established a collaboration with the core facility for MS at the Zentrum für Molekular Biologie Heidelberg (ZMBH) headed by Dr. Thomas Ruppert. The samples that were delivered for analysis consisted of Optiprep gradient-purified HIV-1 particles derived from 293T cells. Virions collected from the supernatant were immediately treated with a phosphatase inhibitor cocktail, adding fresh inhibitors after each successive purification step. A virus capsid amount equivalent to 1 µg of p6 protein was loaded on a 17.5 % Tris-Tricine gel and bands corresponding to p6 and full-

length precursor Pr55 Gag protein—shown in Figure 3.14—were in-gel digested with trypsin for further analysis.

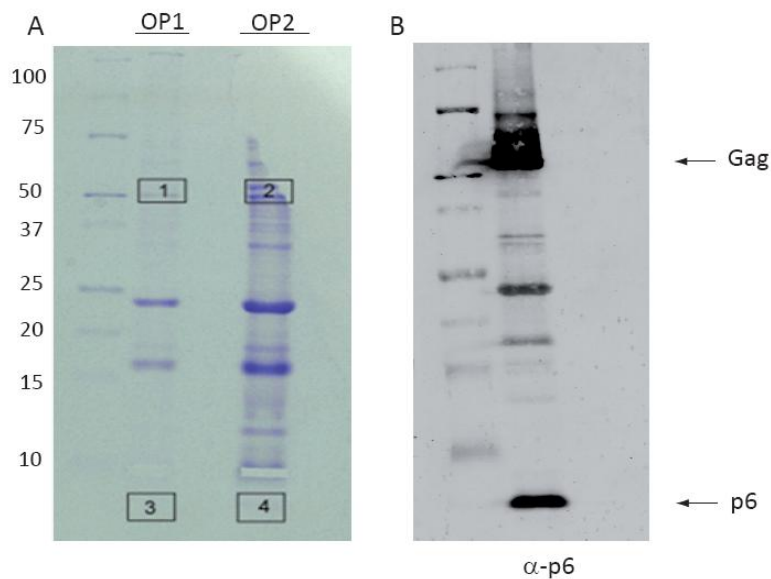


**Figure 3.14. Selection of virus protein bands for mass spectrometry analysis.**

NL4-3 derived virus from transfected 293T cells were harvested 48 h pt in the presence of a phosphatase inhibitor cocktail and purified by Optiprep-gradient. (A) A virus p6 protein amount of 1  $\mu\text{g}$  was loaded from two independent virus preparations (OP1 and OP2) onto a 17.5 % Tris-Tricine gel and analyzed by SDS-PAGE. Protein bands were visualized by coomassie staining. Two protein bands (bands 1 and 2) that corresponded to the full-length Pr55 Gag precursor protein and the free, cleaved form of the p6 protein (bands 3 and 4) were cut out from each virus preparation for further analysis. Positions of molecular mass markers in kDa are shown at the left. (B) Concomitant analysis of virus proteins by Western blot. A virus p6 amount of 0,5  $\mu\text{g}$  was loaded and analyzed by SDS-PAGE as in (A). Subsequently, virus proteins were transferred onto a nitrocellulose membrane and the membrane was probed against p6-specific antibody. Corresponding band proteins in the blot are indicated by an arrow.

The samples were analyzed by liquid chromatography-tandem mass spectrometry (LC-MS/MS). In tandem MS, a phosphopeptide mixture is separated by capillary liquid chromatography. The eluate is introduced into the mass spectrometer via a process that generates multiply protonated gas-phase peptide cations. The mass-to-charge ratio ( $m/z$ ) and intensity of the peptide precursors are recorded and then those with a high  $m/z$  value (most abundant peptide cations) are selected for sequencing by tandem MS. The phosphorylated peptide generates a series of fragment ions that differ in mass by a single amino acid, allowing the identification of the peptide primary sequence and position of the phosphoryl modification (56). Results from the MS analysis are shown in Figure 3.15.

A

Viral protein	Sequences	Modifications	Cellular proteins
<b>MA</b>	K.TLRAEQASQEVK.N K.EALDKIEEEQNK.S R.FAVNPGLLLETSEGCR.Q R.QILGQLQPSLQTGSEELR.S	—	EF-1 alpha Ezrin Radixin Hsp70 Ubiquitin Alanyl t-RNA synthetase
<b>CA</b>	R.AEQASQEVK.N R.MYSPTSILDIR.Q R.VLAEAMSQVTNPATIMIQQ.G R.TLNAWVK.V	Oxidation Oxidation	
<b>p6</b>	R.SLFGSDPSSQ.- R.FGEETTPSQK.Q	—	
<b>RT</b>	K.IATESIVIWGK.I K.ALVEICTEMEK.E K.GSPAIFQCMTK.I K.IGPENPYNTPVFAIK.K K.ALTEVVPLTEEALELAENR.E K.YTAFTIPSINNETPGIR.Y	Oxidation Oxidation	
<b>IN</b>	R.IVDIIATDIQTK.E	—	

B

Viral protein	Sequences	Modifications	Cellular proteins
<b>MA</b>	K.TLRAEQASQEVK.N K.EALDKIEEEQNK.S R.ASVLSGGELDKWEK.I R.FAVNPGLLETSEGCR.Q R.QILGQLQPSLQTGSEELR.S K.AQQAAADTGNNSQVSNYPI	Deamidated Deamidated Oxidation	Ezrin Radixin Moesin Ubiquitin Hsp70 EF-1 alpha Annexin A2 Annexin A11 Tsg101 Vps4B
<b>CA</b>	R.TLNAWVK.V R.WIILGLNK.I R.AEQASQEVK.N R.MYSPTSILDIR.Q K.ETINEEAAEWDR.L R.VLAEAMSQVTNPATIMIQQ.G K.ALGPATLEEMMTACQVGG.A	Oxidation  Oxidation Oxidation	
<b>p6</b>	R.SLFGSDPSSQ.- K.ELYPLASLR.S R.FGEETTTPSQK.Q K.QEPIDKELYPLASLR.S	—	
<b>RT</b>	K.FKLPIQK.E K.QLTEAVQK.I K.DLIAELQK.Q K.IATESIVIWGK.T K.ALVEICTEMEK.E K.GSPAIFQCSMTK.I R.YQYNVLPQGWK.G K.IGPENPYNTPVFAIK.K K.YTAFTIPSINNETPGIR.Y K.GAHTNDVKQLTEAVQK.I K.ALTEVVPLTEEALELAENR.E	Oxidation Oxidation  Deamidated Deamidated	
<b>IN</b>	R.IVDIIATDIQTK.E	—	

C

Viral protein	Sequences	Modifications
<b>p6</b>	R.FGEETTTPSQK.Q	—

D

Viral protein	Sequences	Modifications
<b>p6</b>	R.FGEETTTPSQK.Q	—

**Figure 3.15 List of peptides obtained from the mass spectrometry analysis of HIV-1 proteins.**

A list of the viral peptide sequences identified from the indicated viral proteins are shown in the tables A, B, C, D. Occurrence of posttranslational modifications is indicated when present and are listed next to the particular peptide sequence where the modification was observed. In addition to virus-derived peptides, sequences corresponding to cellular proteins were also identified and are listed on the rightmost columns of (A) and (B). (A) Results derived from analysis of band 1 (see Figure 3.14); (B) results derived from analysis of band 2; (C) results derived from analysis of band 3 and (D) results derived from analysis of band 4.

Peptide sequences corresponding to the viral proteins CA, MA, p6, IN and RT could be identified from the bands 1 and 2 (Figure 3.14), which correspond to the gel area that includes the Gag precursor protein. The RT is made up of two subunits with a molecular weight of 66 and 51 kDa each and thus it is no surprise that it comes up in the analysis of this band. Less clear is the reason why IN came up on the analysis since it has a molecular weight of 32 kDa. Not only were viral proteins identified, but the MS revealed the presence of multiple cellular proteins that seem to be incorporated into the virions. The actin-binding proteins ezrin, radixin and moesin were found in both virus preparations. Ubiquitin, which has been previously reported to occur in retroviral particles, was also detected. Moreover, the ESCRT and ESCRT-associated proteins Tsg101 and Vps4 and the membrane-binding annexin proteins could be identified in one of the preparations. Finally, the elongation factor 1 alpha (EF-1 alpha) known to be incorporated into virus particles and the alanyl t-RNA synthetase were also identified in the virus particles. Several of these proteins have been previously seen in other biochemical analyses by different groups (28, 108). The only posttranslational modifications detected in this analysis were oxidation of MA and CA protein peptides and oxidation and deamidation of RT peptides; thus, no phosphorylation-specific modification was observed for p6 or for any other viral protein although there is biochemical evidence that indicates that both the MA and CA proteins are phosphorylated (18, 26, 39, 75). Nevertheless, results do not seem to be conclusive for two main reasons: 1) no p6-derived peptides containing the PTAP motif could be identified in the analysis and so far there is no obvious explanation for this; 2) as mentioned above, although there is data indicating that both the MA and CA proteins are phosphorylated, none of the identified MA or CA peptides were found to be phosphorylated. Nevertheless, it cannot be excluded that treatment with the phosphatase inhibitors was inefficient and did not prevent the removal of phosphate groups from phosphorylated viral proteins. Another possibility is simply due to

the transient nature of phosphorylation events and it is possible that these events were not caught fast enough to preserve them for the analysis. Moreover, phosphopeptides exist at low stoichiometric amounts, thus although the p6 protein has been identified as the major phosphoprotein in HIV-1 virions, only about 5% of the protein is phosphorylated (101) and it plausible that the number or amount of signals emitted from phosphorylated p6 protein peptides are not enough to be detected. In addition, phosphopeptides might be otherwise suppressed during ionization of the sample. Conveniently, this latter limitation may be overcome by phosphopeptide enrichment of the sample (56). Phosphopeptide enrichment relies on metal-based affinity approaches. Some of the most frequently used methods include immobilized metal affinity chromatography (IMAC), metal oxide affinity chromatography (MOAC), and strong cation exchange (SCX). In IMAC, positively charged metal ions, such as Fe (III) or Ga (III) are chelated onto a solid phase resin and presented for interaction with negatively charged phosphoryl groups. MOAC uses titania or zirconia as the metal oxide chromatography modifier. Titanium dioxide (TiO<sub>2</sub>) is commonly used to capture phosphopeptides. SCX works essentially on the same principle and differs in the way that phosphopeptides are eluted from the column (56).

We sought to initiate a new collaboration with Dr. Albert Sickmann and Dr. René Zahedi at the Institute for Analytical Sciences (ISAS) in Dortmund, Germany. Dr. Sickmann's group specializes in identifying protein posttranslational modifications and thus has ample experience in performing this type of analysis. For this purpose, new optiprep gradient-purified HIV-1 virions were prepared from transfected 293T cells. Virus supernatants were treated with a phosphatase inhibitor cocktail immediately after harvesting and during subsequent purification steps. A virus CA amount equivalent to about 1 µg of p6 was loaded from each of two independent preparations onto a 4-12 % NuPAGE Bis-tris gradient gel and virus proteins were separated by electrophoresis. At the same time, 0.8 µg of CA protein from one of the virus preparations was loaded as a control for subsequent Western blot analysis of p6-containing viral products as shown in Figure 3.16. Four different bands were analyzed for each virus preparation. The bands corresponded to the Pr55 Gag precursor protein, cleaved p6 and the other two bands were meant to include intermediate processing products or putative phosphorylated p6 products. Phosphorylated proteins can exhibit a shift in their electrophoretic mobility. Thus, we thought it plausible that the bands observed

above the 6 kDa band of free p6 could derive from hyperphosphorylated p6 forms. The boxed areas in the blot indicate the p6-containing bands that were cut out for the MS analysis.

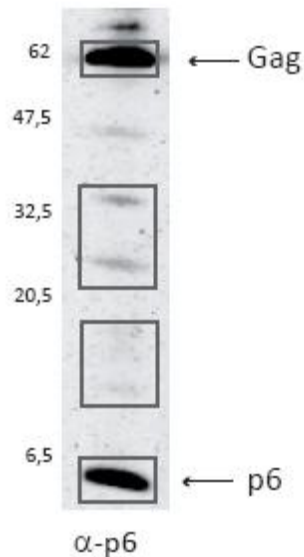


**Figure 3.16 Western blot analysis of HIV-1-derived p6 products.**

NL4-3 derived virus from transfected 293T cells was harvested 48 h pt in the presence of a phosphatase inhibitor cocktail and purified by Optiprep-gradient. A virus CA amount equivalent to 1  $\mu\text{g}$  of p6 from each virus preparation was loaded onto a 4-12% Bis-Tris gradient gel and virus proteins were separated by electrophoresis (not shown). A virus CA amount equivalent to 0.2  $\mu\text{g}$  of p6 was simultaneously run and analyzed further by Western blot. The membrane was probed against p6-specific antibody. Boxed areas indicate the four virus bands that were selected for MS analysis. Virus bands pertaining to the Gag precursor protein and to free p6 are indicated by arrows. Positions of molecular mass markers in kDa are shown at the left.

Each of the virus bands was cut and in-gel digested with trypsin. Peptides were then extracted and analyzed by nano-LC-MS/MS on an LTQ (linear ion trap) Orbitrap mass analyzer. Nano-LC allows for high-resolution nano-scale flow separation that is coupled to a hybrid mass spectrometer, the LTQ Orbitrap. This mass spectrometer combines two ion traps that result in a high sensitivity and accuracy for detection and identification of small molecules in the sub-femtomole range. The viral peptides that were identified in this analysis are shown in Figure 3.17. Importantly, peptides from all of Gag were identified. This included peptides derived from the C-terminal p6 domain.



**Figure 3.17 Mass spectrometry analysis of p6 posttranslational modifications.**

At the left, schematic of the Gag protein and precursor protein domains: MA, CA, NC, p6. The two white spaces in between the NC denote the two spacer peptides SP2 and SP1 from left to right of the Gag protein. At the right are shown the sequences for the respective protein domains and highlighted in orange are peptide sequences identified in the MS analysis. Peptides from every domain in Gag were identified.

In total, four virus bands were analyzed for each optiprep virus preparation (OP1 and OP2). Phosphopeptide analysis of OP1 identified two phosphorylations: one in the cleaved form of the MA protein at the Ser residue in position 6 and one in the cleaved form of p6 at the Ser residue in position 40. Phosphopeptide analysis of OP2 detected multiple phosphorylation within the Gag precursor protein. The Ser6 phosphorylation in MA (the positions of the phosphoresidues is given in the context of each Gag-derived protein) was detected as well as three phosphorylations in the p6 domain, namely Ser40, Ser51 and Thr22/23. From the analysis it was not possible to distinguish between the closely spaced Thr signals, hence both Thr22 and Thr23 are considered as potentially phosphorylated residues. In addition, the Ser40 in free p6 was again detected in the second virus preparation (OP2), as well as cleaved MA which was observed to harbor two other phosphoresidues at

positions Ser9 and Tyr132 in addition to the Ser6. A schematic of the phosphorylations identified in the analysis is shown in Figure 3.18.

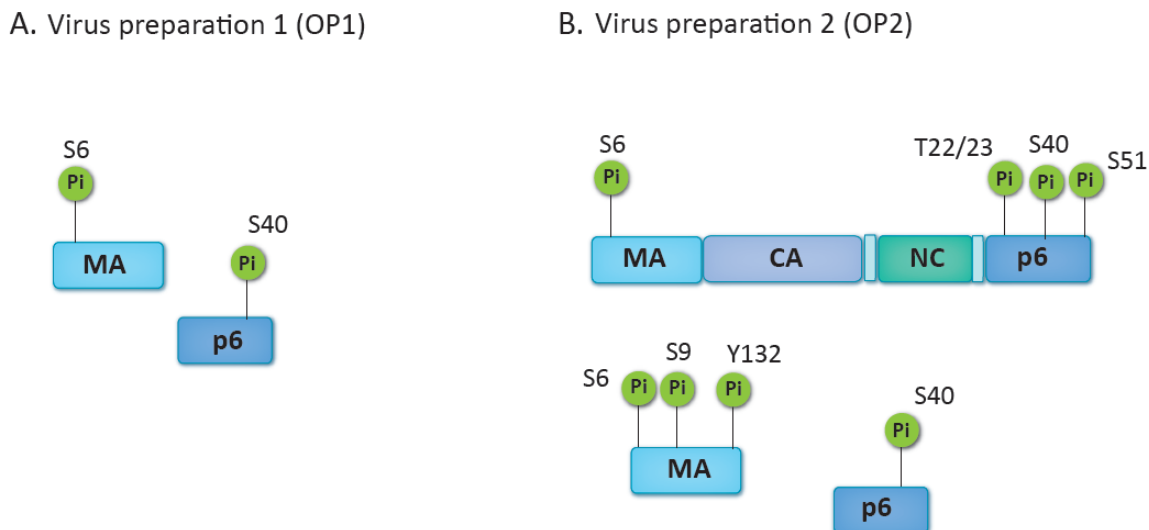


**Figure 3.18 Schematic of identified phosphoresidues in HIV-1 proteins by MS analysis.**

MS analysis was carried out by nano-LC tandem MS coupled to a LTQ Orbitrap mass spectrometer. Four different p6-positive bands were analyzed from each of two independent optiprep-gradient virus preparations. (A) Phosphorylations identified in the first virus preparation (OP1) were those of the cleaved MA protein and the cleaved form of p6. (B) Phosphorylations detected in the second virus preparation (OP2) include the gag precursor protein as well as the cleaved forms of MA and p6. The position of the phosphorylated residue is given in the context of each Gag-derived protein.

However, since it is plausible that phosphopeptides are suppressed during ionization and because phosphopeptides exist at a low stoichiometric abundance, we wanted to maximize the efficiency with which phosphopeptides could be detected. Thus, phosphopeptides in the virus samples were enriched by MOAC as described above, using titanium dioxide (TiO<sub>2</sub>) as the metal oxide chromatography modifier. Phosphopeptide enrichment of each virus preparation was followed by LC-MS/MS analysis. Overall, this analysis not only confirmed most of the phosphoresidues that were initially identified, but it also detected additional phosphoresidues in p6<sup>Gag</sup>, either as part of processing intermediates or in the free form of p6. Moreover, phosphorylation of the cleaved CA protein was also detected. In addition to the previously identified p6<sup>Gag</sup> phosphoresidues Ser40, Ser51, Thr22/23 and Ser6 in the MA precursor, a new phosphoresidue in p6<sup>Gag</sup> was detected at Ser43. NC-SP1-p6 processing intermediates were identified and carried phosphoresidues within p6 at two positions: Thr21 and Thr22/23. The cleaved form of the CA protein was

found to be phosphorylated at two positions: Ser146 and Thr148/Ser149. Finally, two new phosphoresidues were detected in free p6: Ser51 and Thr22/23. Again, the close spacing between the Thr residues in the case of p6 or Thr and Ser residues in the case of CA did not allow to discriminate which Thr residue—T22 or T23— or Thr/Ser—T148 or S149—is actually phosphorylated. A schematic of the phosphorylations identified in each virus preparation after phosphopeptide enrichment is shown in Figure 3.19.

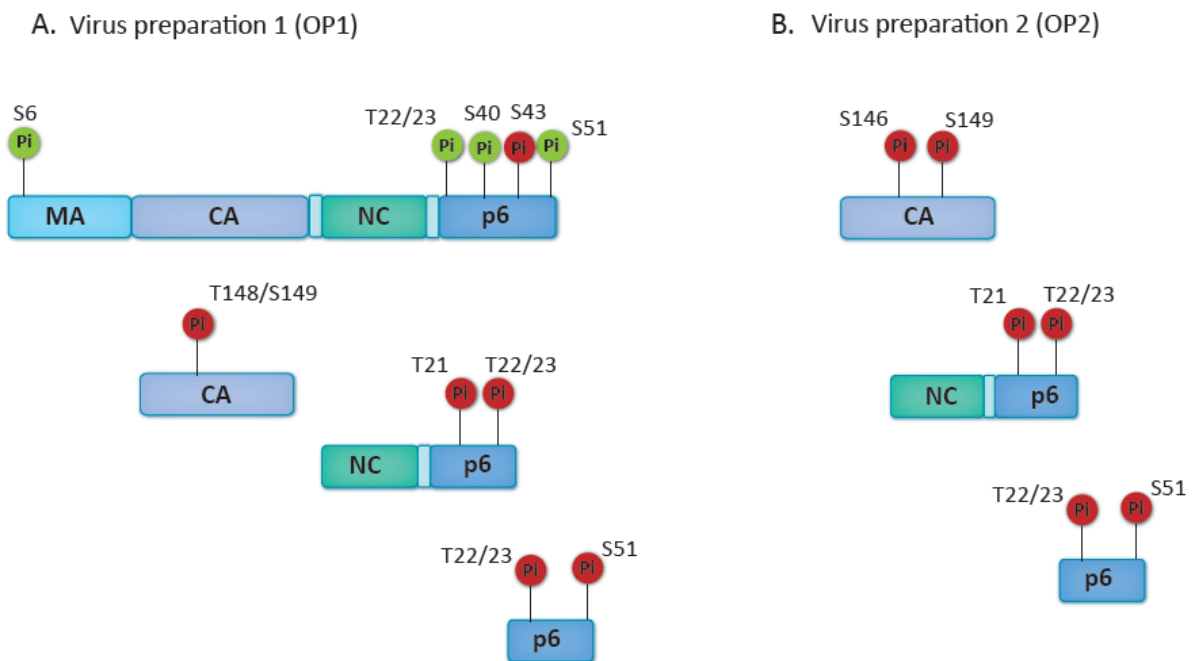


**Figure 3.19 Phosphopeptide enrichment analysis of p6 phosphorylation.**

The positions of the phosphorylated residues are given relative to the individual Gag-derived proteins. Newly detected phosphoresidues after phosphopeptide enrichment are highlighted in red; in green are residues that were also identified after phosphopeptide enrichment but which had been previously observed in the first analysis (Figure 3.18). (A) Phosphopeptide enrichment confirmed the presence of phosphoresidues that were observed during the first analysis (Figure 3.18). Moreover, it revealed another phosphoresidue in p6<sup>Gag</sup>, namely S43. In addition, the free form of p6 was observed to be phosphorylated at two positions while an NC-SP1-p6 processing intermediate was identified and carried two phosphoresidues. A phosphorylation within the CA was found to occur either at T148 or S149. (B) New phosphoresidues were identified in virus prep 2 (OP2): two residues within the CA, two within the NC-SP1-p6 processing intermediate and two more within free p6.

Overall, MS analysis and phosphopeptide enrichment were successfully applied towards the identification of phosphorylated p6 residues in HIV-1. Importantly, all identified phosphoresidues had high scores for phosphorylation and were manually validated. Taken together, the analyses suggest that p6 undergoes phosphorylation at multiple residues that are possibly acquired prior to proteolytic processing of the Gag precursor. The only exception seems to be the phosphorylation of T21, which according to the data probably

occurs after the first processing step catalyzed by the viral protease that separates MACASP2 from NCSP1p6 and is then lost, since free p6 was not found to contain the phosphorylated form of this residue. A third analysis was conducted in HIV-1<sub>NL4-3</sub> viruses derived from 293T cells. This analysis confirmed phosphorylations in p6<sup>Gag</sup> at T22/23 (positions of phosphorylated residues are given relative to the Gag-derived protein in all cases) and in MA at S6. A processing intermediate containing MACA was identified and it contained a phosphoresidue within CA at T148/S149. This phosphoresidue was also found in free CA.

These observations led us to question whether the p6 phosphorylation pattern might vary in viruses produced from different cell lines. Therefore, MT-4 cells were infected by HIV-1<sub>NL4-3</sub> coculture and 48 h after infection virus was collected and purified by Optiprep gradient. Importantly, the virus supernatant was treated with a phosphatase inhibitor cocktail immediately after harvesting and in every subsequent step throughout the purification procedure. Two independent virus purifications were prepared from MT-4 cells and a virus CA amount equivalent to 1.5 µg of p6 from each preparation was loaded onto a 4-12 % Bis-tris gel. Virus proteins were separated and analyzed by electrophoresis. Additionally, a virus amount equivalent to 0.5 µg p6 was loaded on the same gel for Western blot analysis to identify p6-containing protein bands. Four p6-positive protein bands (Figure 3.20) were cut, in-gel digested with trypsin, phosphopeptides enriched and analyzed by MS.

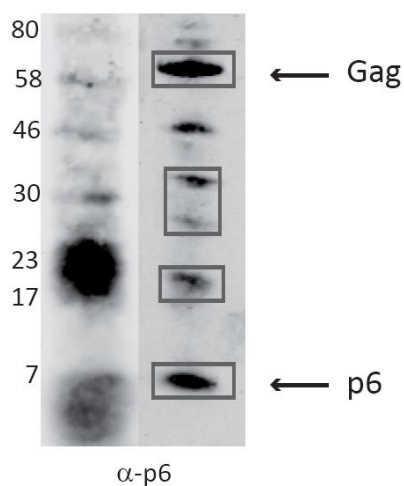


**Figure 3.20 Western blot analysis of HIV-1-derived p6 products.**

NL4-3 derived virus from infected MT-4 cells was harvested 48 h pi in the presence of a phosphatase inhibitor cocktail and purified by Optiprep-gradient. A virus CA amount equivalent to 1.5 µg of p6 from each virus preparation was loaded onto a 4-12% Bis-Tris gradient gel and virus proteins were separated by electrophoresis (not shown). A virus CA amount equivalent to 0.5 µg of p6 was simultaneously run and analyzed further by Western blot. The membrane was probed against p6-specific antibody. Boxed areas indicate the four virus bands that were selected for MS analysis. Virus bands pertaining to the Gag precursor protein and to free p6 are indicated by arrows. Positions of molecular mass markers in kDa are shown at the left.

The MS analysis of MT-4 cell-derived HIV-1 virions identified phosphoresidues in p6 as part of the Gag precursor protein, as an NCSP1p6 processing intermediate or in its cleaved form. p6<sup>Gag</sup> residues S40 and T22/23 (position of the residues are given relative to the Gag-derived

protein) were observed to be phosphorylated in one of the two virus preparations. The processing intermediate NCSP1p6 contained the p6 phosphoresidues T22/23 and S51 in both virus preparations. Finally, the free form of p6 is phosphorylated at S40 and S50/51. Other HIV-1 proteins found to contain phosphoresidues were the MA protein at S6 and S9 and CA at T148/S149 or S149 only. Table 3.3 lists the p6 phosphoresidues detected from 293T cell- and MT-4 cell-derived HIV-1.

HIV-1 protein /processing intermediate	293T cells	MT-4 cells
Gag	T22/23 S40 S43 S51	T22/23 S40
NCSP1p6	T21 T22/23	T22/23 S51
p6	T22/23 S40 S51	S40 S50/51

**Table 3.3 Comparison of p6 phosphoresidues identified from 293T cell and MT-4 cell virus preparations.** Shown is a list of p6 phosphoresidues detected in HIV-1 derived either from 293T or MT-4 cells. The position of the p6 phosphoresidues is given relative to the p6 protein.

Overall, three independent 293T cell-derived virus preparations were analyzed while two independent MT-4 cell-derived HIV-1 preparations were subjected to MS analysis. Thus, the analyses indicate that p6 is indeed subject to posttranslational modification and is hence phosphorylated at multiple residues. Moreover, the combined data suggests that the p6 phosphorylation pattern is cell-type dependent. However, to confirm this assumption it would first be necessary to analyze one more independent HIV-1 preparations from MT-4 cells. Concomitantly, the analysis of the MT-4 derived virus bands could be repeated and extended to ensure that only those phosphoresidues listed in Table 3.3 occur.

### ***3.7 Effect of a p6 T8N mutant in the HIV-1 replication cycle***

Mutations within the critical PTAP motif are detrimental for HIV-1 release. By EM, such budding mutant virions remain connected to the host plasma membrane through a membrane stalk (53). The PTAP motif can also exist as PSAP; however, there is no indication of any other residue occurring at this position. As shown in section 3.4 we unexpectedly

observed that a p6 T8N mutant can efficiently rescue HIV-1 release. Therefore, we became interested in characterizing this mutant's properties. We were especially interested in understanding why this mutant does not occur in nature when it seems to function efficiently as a late domain. It is plausible that although the Asn at this position enables the virus to bud, this residue may be detrimental to the virus at another step during its replication cycle. Thus, we tested this mutant's ability for single-round infection. For this purpose, supernatants from transfected 293T cells were used to infect TZM-bl reporter cells. 48 h pi, the cells were lysed and luciferase activity was recorded as a measure of virus activity. Figure 3.21 A shows that the single-round infectivity of the p6 T8N mutant is not significantly compromised and is comparable to that of the WT virus. This is also obvious when infectivity values are normalized to CA content as shown in Figure 3.21 B.

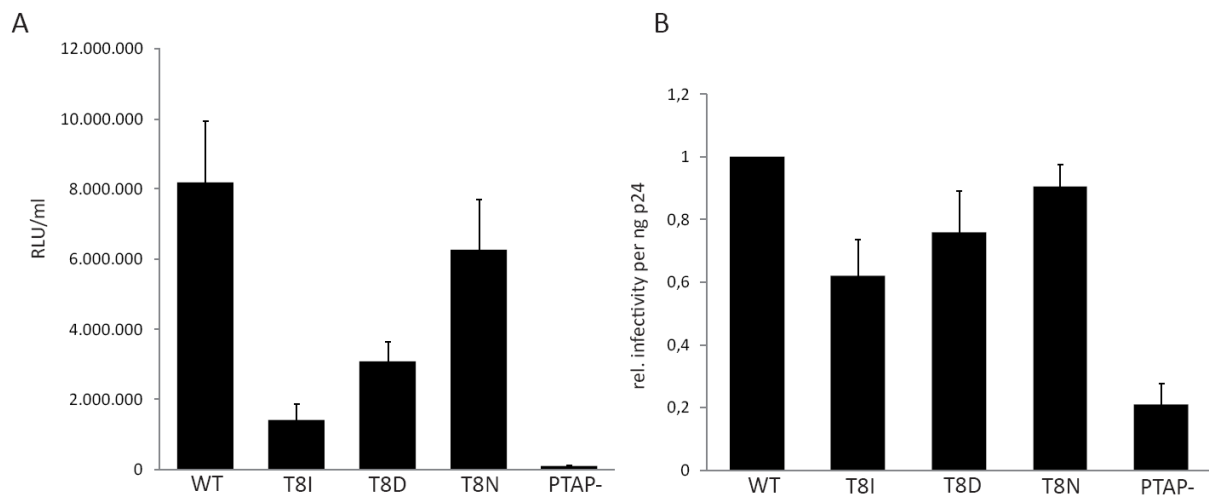


**Figure 3.21 Effect of the p6 T8N mutant in viral infectivity.**

An Asn residue within the critical p6 PTAP motif does not affect virus single-round infectivity. 293T cells were transfected with the indicated proviruses and the virus supernatant was harvested 48 h pi and titrated onto the indicator TZM-bl cell line. Cells were lysed 48 h pi and luciferase activity was measured as relative light units (RLU). (A) Infectivity levels as RLU are given for each p6 mutant. (B) Infectivity values normalized to virus p24 content for each p6 mutant are shown relative to the WT.

These observations indicate that the p6 T8N mutant is infectious and thus, this does not explain why this mutant does not occur in nature. In order to assess whether the p6 T8N mutant is capable of sustaining a spreading infection, I infected PBMCs from 3 different donors with CA-normalized amounts of WT and p6 mutant virus particles, and viral replication was monitored by quantification of CA amounts in culture supernatants over a period of 15 days. However, this assay awaits analysis. We have so far assumed that the p6 T8N mutant supports HIV-1 release by the same means that wildtype p6 does: by recruiting

Tsg101 to sites of virus budding. Thus, in order to confirm that the p6 T8N mutant behaves in a manner similar to wildtype p6, I conducted siRNA experiments involving Tsg101. Briefly, 293T cells were transfected with 100 pmol of siRNA against Tsg101. About 24 h later, a second transfection was done with either 40 pmol or 80 pmol siRNA against Tsg101. At the same time, the cells were transiently transfected with wildtype NL4-3 virus or with the p6 T8N mutant provirus. Released virus particles and cell-associated viral products were collected 40 h post-transfection. Cell lysates and purified virus particles were subjected to Western blot analysis to detect the efficiency of the Tsg101 knockdown and to detect levels of virus released. As shown in Figure 3.22 A, cellular levels of Tsg101 remaining after siRNA treatment were almost undetectable and cells treated with a scrambled version of the RNA were not affected in Tsg101 expression. Concomitant transfection with proviral DNA revealed that as expected, WT release is strongly inhibited in the absence of Tsg101. Importantly, the same was true for the p6 T8N mutant virus. The amount of virus p24 released into the medium was further quantified and is shown in Figure 3.22 B. Taken together these observations suggest that the ability of the p6 T8N mutant to support HIV-1 release depends on the availability of intracellular Tsg101 pools from which Tsg101 might be recruited to sites of p6 T8N virus budding.

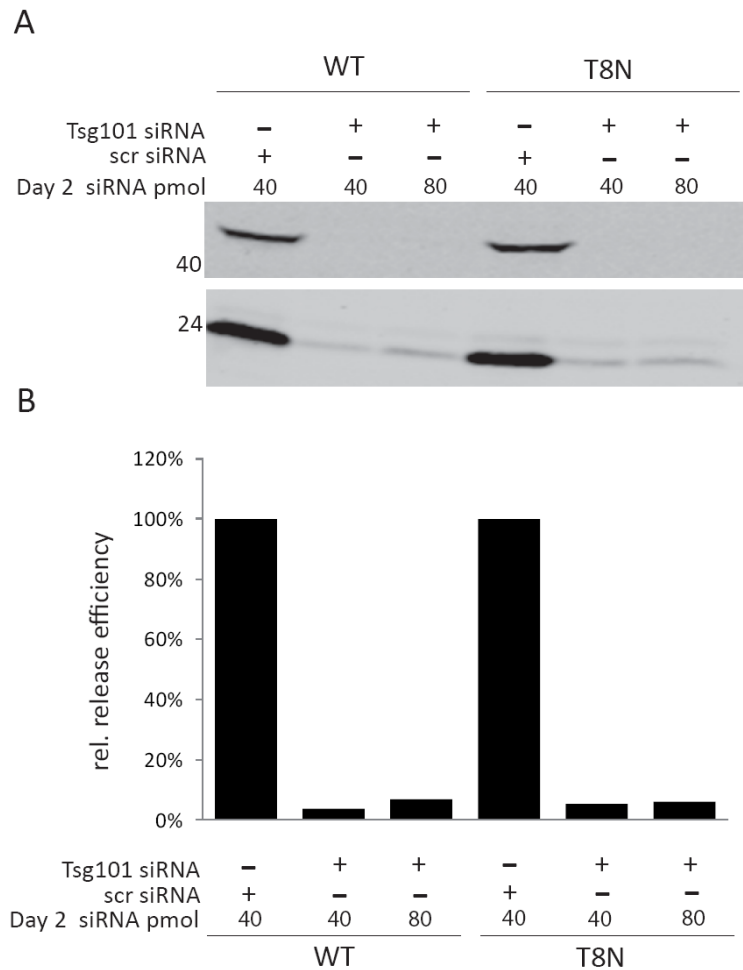


**Figure 3.22 Effect of Tsg101 knockdown on the release efficiency of the p6 T8N mutant virus.**

(A) Upper panel: Anti-Tsg101 western blot showing depletion of Tsg101 protein from 293T cells. Cells were transfected on day 1 with 100 pmol of Tsg101 siRNA or with a scrambled (scr) siRNA as indicated. About 24 h later, cells were transfected with either 40 pmol or with 80 pmol of Tsg101 siRNA or 40 pmol scr siRNA. Lower panel: Anti-CA antibody showing that depletion of Tsg101 inhibits virus release. Cells transfected with siRNA were also cotransfected with WT virus or with p6 T8N virus. About 40 h after the initial transfection, supernatants and cell lysates were collected and virus particles were pelleted over a 20 % sucrose cushion. (B) Levels of virus CA released into the medium were determined by quantitative WB and are shown relative to the WT virus treated with scr siRNA.

### 3.7.1 Morphology of p6 T8N mutant virion analyzed by electron microscopy

In order to investigate a potential role of the p6 T8N mutant on virus assembly and budding, virion morphology was examined by thin-section electron microscopy. HeLa cells were transfected with WT and p6 T8N mutant proviral constructs and chemically fixed at 24 h pi and subjected to electron microscopy. In addition, HeLa cells transfected with the

proviral constructs p6 T8I and PTAP- served as negative controls. To compare the effect of p6 mutations on virion assembly to HIV-1 wildtype and HIV-1 lacking PTAP, virus-like structures at or near the plasma membrane were quantified and sorted into three classes (budding arrested, immature and mature) (Figure 3.23).

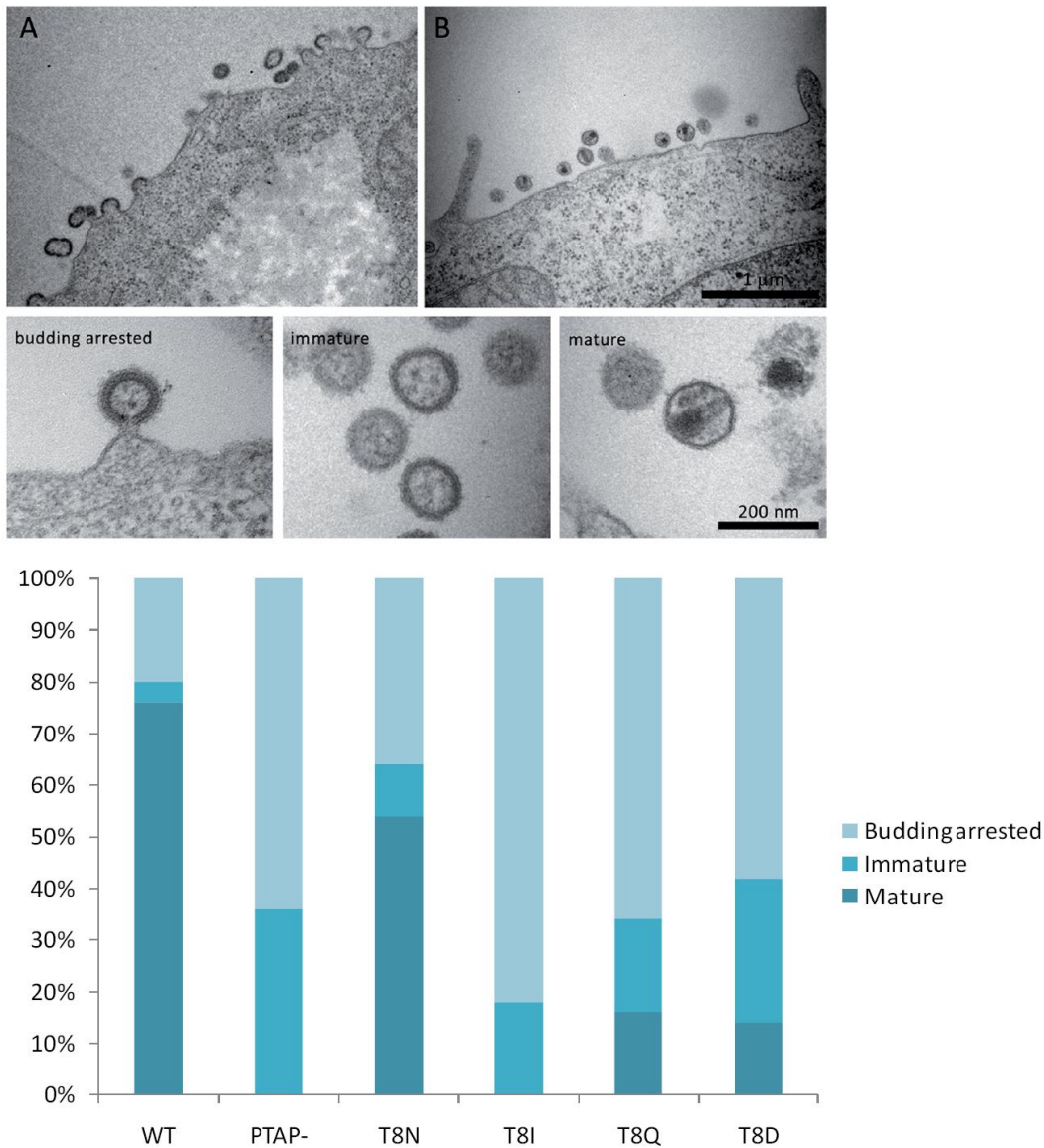


**Figure 3.23 Visualization of p6 T8N virions by thin-section electron microscopy.**

HeLa cells were transfected with the proviral constructs WT, T8N, T8I, T8D, T8Q and PTAP- and chemically fixed 48 h pt and processed for thin-section electron microscopy. (A) and (B) Low-magnification images showing the morphological features of immature, budding arrested virions (A) at the plasma membrane and (B) mature wildtype virions at the periphery of the cell. The lower panels contain high-magnification images of the 3 main assembly phenotypes used to categorize virus particles generated from the different proviral constructs. The percentage of virus-like structures under each category was quantified by systematic uniform random sampling (50 virions were quantified per category) and are indicated in the graph.

The assembly of the p6 T8N mutant was closest to that of wildtype HIV. More than 50 % of virus-like structures consisted of mature virions with conical-shaped cores compared to

75 % in the case of wildtype HIV-1. In contrast, the p6 T8I mutant was strongly inhibited in release and maturation of these virions was similar to that typically seen during the assembly of virions lacking a PTAP motif. 80 % of virions were budding arrested compared to 65 % for PTAP- viruses. No mature virion was observed in the case of the T8I mutant. The p6 mutants T8Q and T8D showed a lower number of mature particles (10-20 %) in contrast to wild-type HIV-1 Gag.

Taken together, these results confirm our data obtained with the virus release assay, indicating that the p6 T8N mutant is capable of achieving levels of wildtype release; moreover, it shows that the majority of viruses that are released are mature and appear morphologically identical to the wildtype virus.

### ***3.8 Characterization of the interaction properties between the p6 T8N mutant and the Tsg101 UEV domain***

Because the T8N mutation in the PT<sub>8</sub>AP motif results in wildtype levels of virus release and gag processing and seems to be as infectious as the wildtype, we wanted to further characterize this mutant to reveal the biological and molecular basis of HIV-1 PNAP late domain function. To study the molecular basis of PNAP late domain function, we sought to study the structural properties between the Tsg101 UEV domain and a PNAP peptide in principal two ways: by crystallization of the complex and Isothermal Titration Calorimetry (ITC). Through the latter one can compare the binding affinity of a wildtype PTAP p6 peptide for its interacting cellular partner Tsg101 UEV domain to that of a PNAP p6 peptide and those of other p6 T8 mutants.

#### **3.8.1 Analysis of the crystal structure of the Tsg101 UEV domain in complex with a PNAP p6 peptide**

Obtaining the crystal structure of the complex formed between a PN<sub>8</sub>AP peptide and the Tsg101 UEV domain, may reveal the molecular basis of HIV PNAP late domain function. Moreover, it will help examine in detail the contacts made between the complex and how these compare to the well-characterized PTAP-Tsg101 UEV interaction (71, 117). For this purpose, a histidine (his)-tagged version of the Tsg101 UEV domain was cloned into a

bacterial expression vector and transformed into *Escherichia coli* (*E. coli*) BL21 cells. Protein expression was induced with IPTG (Isopropyl  $\beta$ -D-1-thiogalactopyranoside); the cleared supernatant was loaded onto a Ni-NTA resin, eluted and dialyzed. Subsequently, the His tag was cleaved off and the untagged protein was purified by gel filtration. The Tsg101 UEV protein yield was concentrated to 43 mg/ml (Figure 3.24).

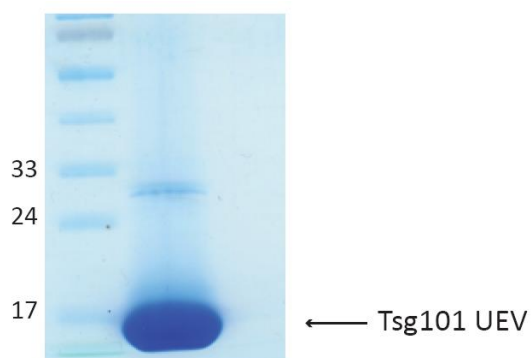


**Figure 3.24 Gel filtration purified Tsg101 UEV.**

A his-tagged version of the 145 amino acid residue Tsg101 UEV domain was synthetically produced, cloned into a bacterial expression vector and transformed into *E. coli* BL21 cells. Protein expression was induced with 100  $\mu$ M IPTG. Cells were harvested and the cleared supernatant was loaded onto a Ni-NTA resin, eluted and dialyzed against 50 mM Tris pH 8.0/150 mM NaCl. Subsequently, the his-tag was removed by treatment with TEV protease and the untagged protein was purified by gel filtration and concentrated to 43 mg/ml. The resulting purified Tsg101 UEV protein is indicated by an arrow. Positions of molecular mass markers in kDa are shown at the left.

In addition, a nine amino acid residue PEPNAPPEE p6 peptide was synthetically produced. The p6 peptide and the Tsg101 UEV protein sample were sent for crystallization trials to the group of Dr. Winfried Weissenhorn in Grénoble. Overall, eight different crystals were obtained under two sets of conditions: 28 % PEG 8000, 0.1 M sodium cacodylate, 0.2 M ammonium sulfate, and 26 % PEG 4000, 100 mM Tris pH 8.5, 220 mM lithium sulfate. Diffraction of the crystals identified the Tsg101 UEV domain occurring in two different arrangements: either as a dimer or a dodecamer (Figure 3.25).

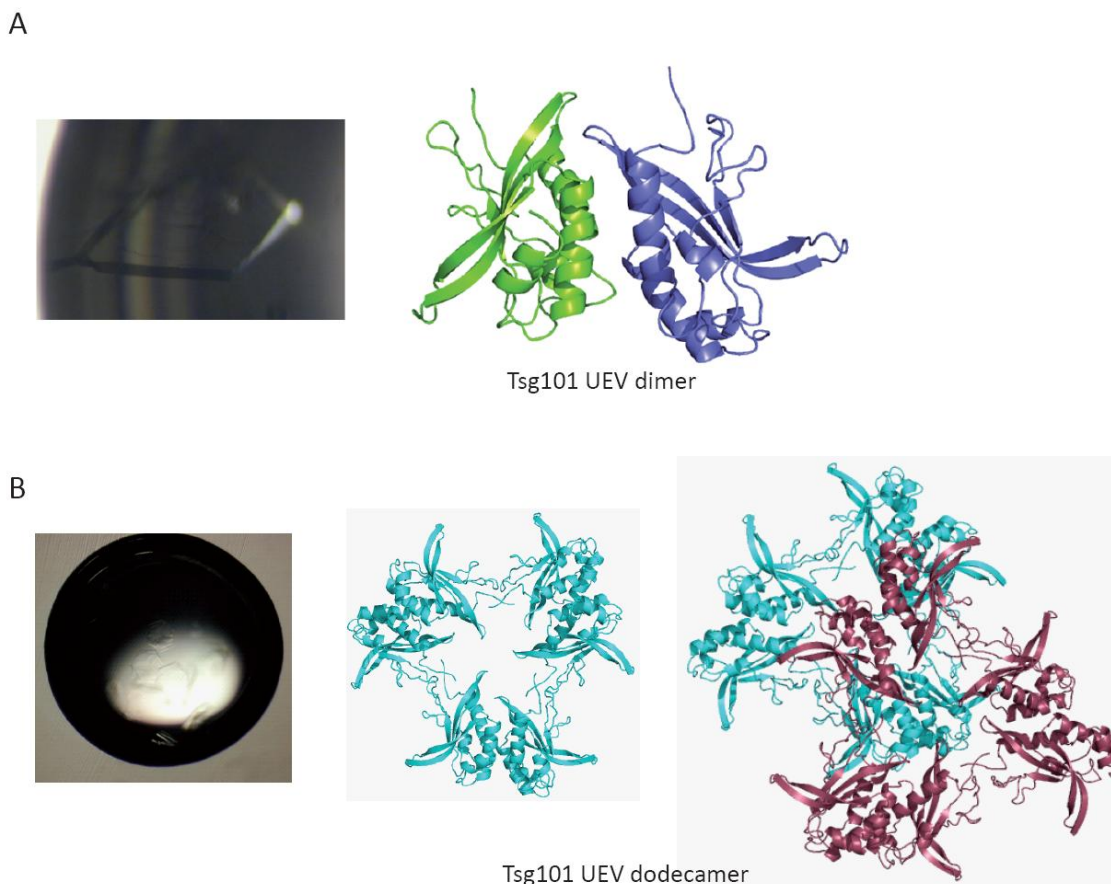


**Figure 3.25 Tsg101 UEV crystal structure.**

Tsg101 UEV microcrystals were obtained under two different conditions: (A) 28 % PEG 8000, 0.1 M sodium cacodylate, 0.2 M ammonium sulfate yielded three 2 Å resolution crystals in which Tsg101 UEV was found as a dimer; (B) 26 % PEG 4000, 100 mM Tris pH 8.5, 220 mM lithium sulfate yielded 2.8 Å resolution crystals in which Tsg101 UEV occurred as a dodecamer.

However, as shown in Figure 3.25 no peptide was found in complex with it. The PTAP binding pocket in Tsg101 UEV is highlighted in Figure 3.26 A superimposing the known NMR structure (117) of the Tsg101 UEV-PTAP complex onto the crystal structure of the Tsg101 UEV domain obtained in this study. An electron density map of the peptide binding site region indicates that no peptide is present in this area (Figure 3.26 B). One reasonable explanation of why no peptide was found complexed to Tsg101 UEV could be that suboptimal concentrations of peptide were used. Therefore, two approaches were used to introduce the peptide into the structure: 1) soaking of the crystals in the peptide solution; or 2) recrystallization with a higher peptide to protein ratio. However, no crystal structure of the complex has been obtained so far.

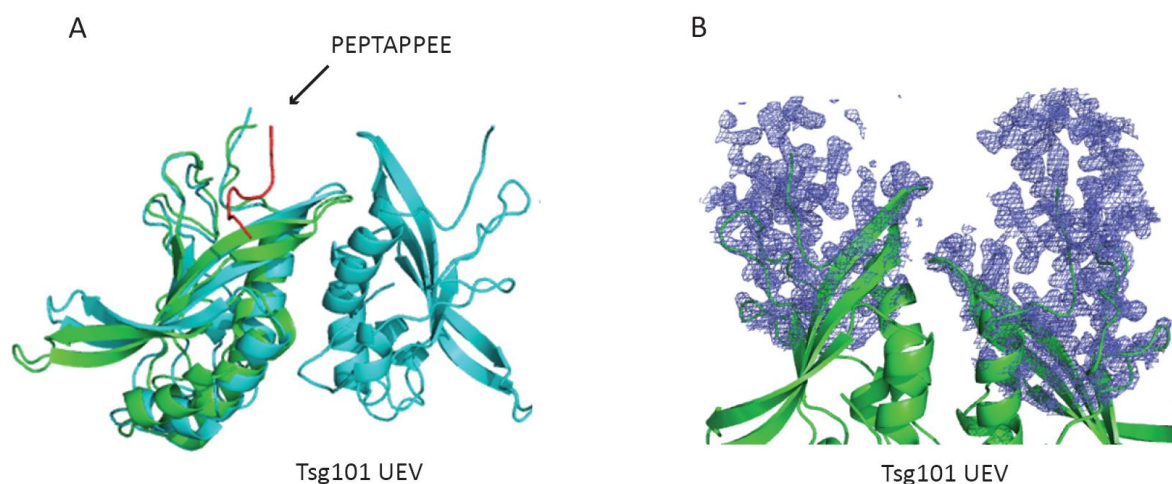


**Figure 3.26 Crystal structure of the Tsg101 UEV-PTAP complex.**

(A) The image of the known NMR structure of the Tsg101 UEV (blue) and the wildtype PTAP p6 peptide (red) (117) was superimposed onto the crystal structure of the crystallized Tsg101 UEV during this study (green). The location of the PTAP peptide binding site in Tsg101 UEV is indicated by an arrow. (B) Electron density map of the top portion of the crystal structure of Tsg101 UEV shows that no peptide is present.

### ***3.9 Binding affinity between a PNAP p6 peptide and Tsg101 UEV***

Isothermal titration calorimetry (ITC) is a highly sensitive tool to measure the thermodynamic properties of protein-protein and protein-ligand interactions. ITC measures directly the binding equilibrium by determining the heat evolved upon association of a ligand with its binding partner (112). A typical power compensation calorimeter is depicted in Figure 3.27. In such an instrument, the reference cell is kept at a constant temperature, hence the term isothermal. In modern ITC instruments, a titrant is delivered at defined time intervals into the sample cell that contains the binding partner. Then as ligand and protein interact in the sample cell, any heat evolved or consumed from the reaction is sensed and a proportional amount of power is applied to keep the temperature between the sample and reference cells constant. The raw calorimetric signal is equal to the power ( $\mu\text{cal}/\text{sec}$  or  $\mu\text{J}/\text{sec}$ ) that must be applied to keep the sample cell from changing temperature as a function of time. The heat change or  $\Delta H$  is equivalent to the time required for the temperature of the sample cell to return to a baseline value and is in proportion to the amount of binding that takes place. Thus, as the reaction reaches saturation the heat change is diminished until only the background heat of dilution is detected.

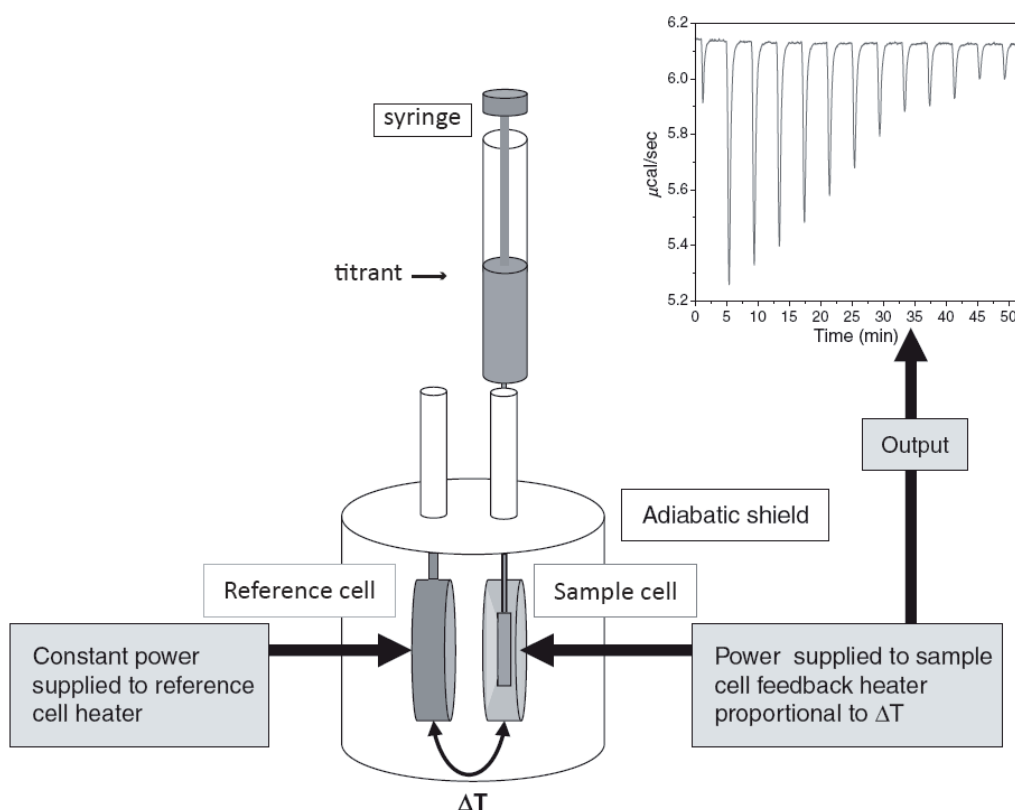


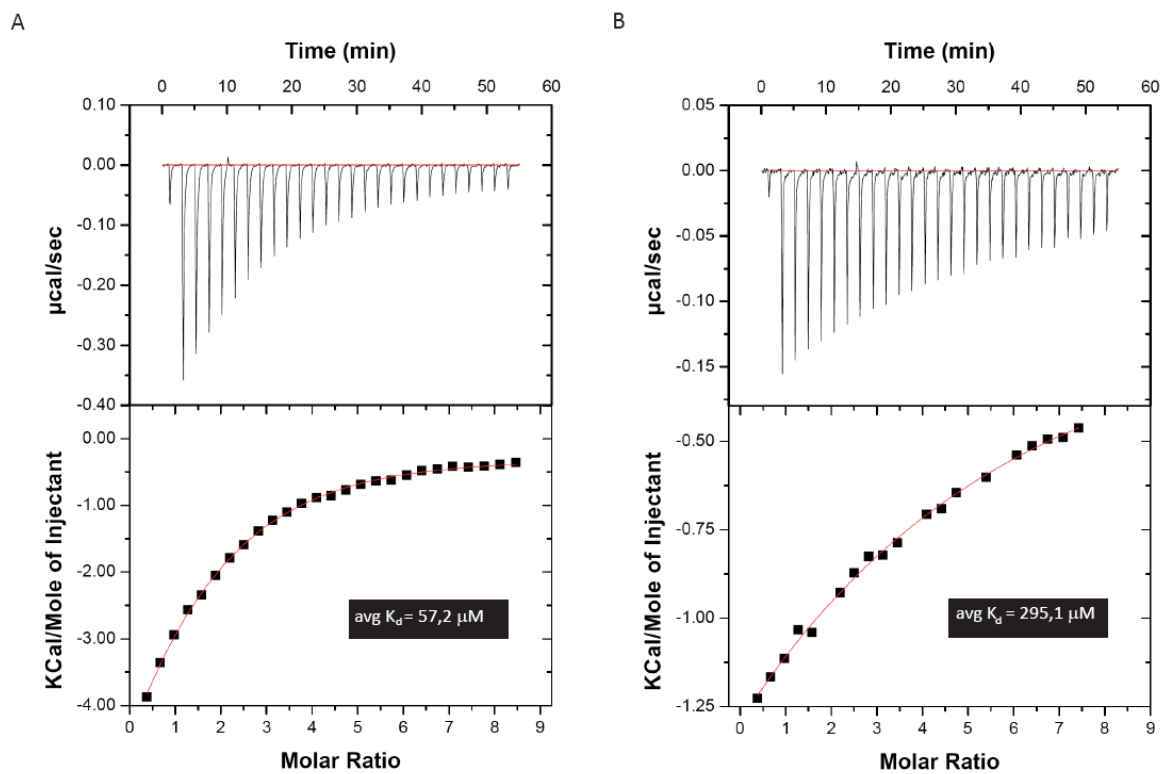
**Figure 3.27 Schematic representation of a power compensation calorimeter.**

In a typical experiment, a solution of a ligand is titrated into a solution of its binding partner. The heat released upon their interaction is measured over time. The output signal is in the form of peaks that represent a heat change proportional to the amount of binding and power required to keep the sample cell temperature equal to that of the reference cell, which is kept constant. As consecutive injections are delivered and the system reaches saturation, the heat change becomes smaller, hence the smaller peaks, until only the heats of dilution are observed. A binding curve is then obtained from the heats of each injection against the ratio of ligand and macromolecule in the sample cell. Adapted from (44).

We employed this method to measure and compare the binding affinities between Tsg101 UEV and three p6 peptides: the wildtype PTAP peptide, the PNAP peptide and a PAAP peptide. For this purpose, nine amino acid residue peptides containing the basic sequence PEPXAPPEE were synthetically produced and Tsg101 UEV protein was purified. The concentration of Tsg101 UEV was measured by two independent methods: by the Bradford Assay and by extinction coefficient. The peptide concentration was measured by infrared spectroscopy. In ITC, it is of utmost importance that both the ligand and protein are in the same buffer. Thus, both Tsg101 UEV and peptides were resuspended in a buffer containing 150 mM NaCl and 1X PBS at pH 8.0, they were aliquoted and kept at  $-80^{\circ}\text{C}$ . The protein and peptides were quick-thawed at  $37^{\circ}\text{C}$ , protein concentration was measured and appropriate

dilutions of both protein and ligand were made before each experiment. Samples were degassed by applying vacuum before being loaded into the ITC machine. The ITC machine was thoroughly washed before and in between experiments to reduce the occurrence of anomalous signals generated during the experiment. Starting concentrations of 25 mM Tsg101 UEV and 500  $\mu$ M peptide were used. About 250  $\mu$ l of Tsg101 UEV were injected into the sample cell and around 50  $\mu$ l of peptide were loaded into the syringe, which resulted in about 18 injections of titrant. Peptides were tested at a concentration range between 500  $\mu$ M and 2 mM while the concentration of Tsg101 UEV remained constant throughout the experiments performed. A representative experiment for each peptide is shown in Figure 3.28. The  $K_d$  values result from the average of at least 3 independent experiments per peptide. The average  $K_d$  obtained for the wildtype PTAP p6 peptide was 57.2  $\mu$ M which is in good agreement with that recently reported by Im et al (71). The other naturally occurring residue in the PT<sub>8</sub>AP position is Ser and although the binding affinity between a PSAP p6 peptide and Tsg101 UEV has reportedly been measured, the actual  $K_d$  value has not been published before. Thus, we were interested in comparing the binding affinity between the PSAP and PTAP p6 peptides for Tsg101 UEV. As shown in Figure 3.28 C, the average  $K_d$  for the PSAP-Tsg101UEV interaction was 46.9  $\mu$ M and is thus as strong as the one exhibited by the PTAP peptide. On the other hand, the binding affinity between a PNAP p6 peptide and Tsg101 UEV (Figure 3.28 B) was 5 times lower than the wildtype interaction. Titration of the PAAP p6 peptide (Figure 3.28 C) gave rise to small peaks of equal and negligible size and had a correspondingly negligible binding affinity. Overall, the naturally occurring PTAP and PSAP p6<sup>Gag</sup> motifs bind Tsg101 with similar affinity and these motifs seem to be equally efficient in recruiting Tsg101 (54, 132). Although the binding affinity between a PNAP peptide and Tsg101 UEV was 5 times lower than the wildtype PT/SAP interaction, this binding affinity is clearly and significantly stronger than that displayed by the PAAP peptide. Moreover, the fact that the p6 T8N mutant can support HIV-1 release suggests that the binding affinity between Tsg101 UEV and p6<sup>Gag</sup> need not to be so tight to be able to recruit Tsg101 to sites of virus budding. In support of this observation, it has been shown that the interaction between Ub and Tsg101 UEV is rather weak, around 500  $\mu$ M (see section 1.4) while the interaction between Tsg101 and the ESCRT-0 component, Hrs is around 290  $\mu$ M. Moreover, the fact that simultaneous binding of Ub and a p6 peptide increases the binding affinity

between the Tsg101 UEV and p6 about 10-fold, suggests that if the affinity between a PNAP peptide and Tsg101 UEV is not tight enough to recruit Tsg101 to sites of virus budding, binding of a Ub moiety could solve this problem.



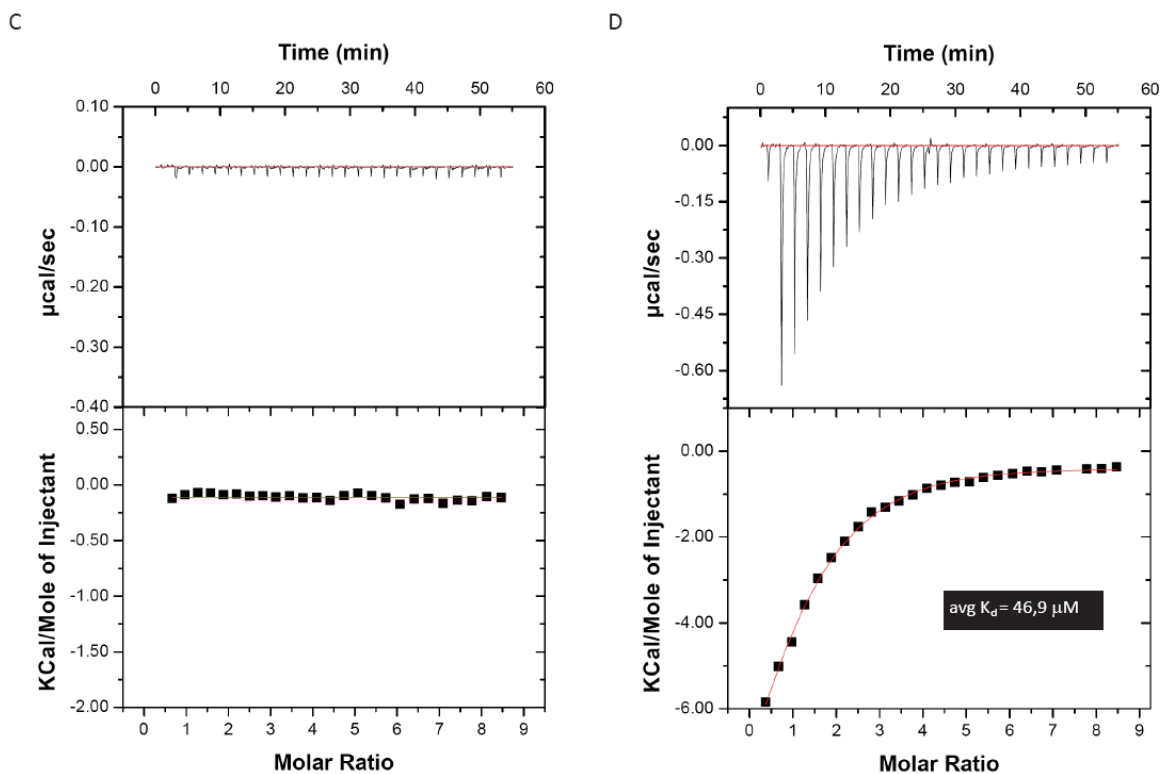


**Figure 3.28 Isothermal titration calorimetry of the Tsg101 UEV-p6 peptide interaction.**

The upper panels represent the ITC thermograms and the lower panels represent the fitted binding isotherms. The isotherm curves were fit to a 1:1 binding model. Values from at least 3 independent titration experiments were averaged to yield the indicated  $K_d$  values. p6 peptides (A) PTAP, (B) PNAP, (C) PAAP, (D) PSAP were titrated at a concentration range between 500  $\mu\text{M}$  to 2 mM into the cell containing Tsg101 UEV at 25  $\mu\text{M}$  at 25°C in 150 mM NaCl, 1X PBS (pH 8.0). Shown are thermograms for peptides titrated at 1 mM.

## 4 Discussion

Protein phosphorylation is a widely used posttranslational modification by the cell to convey specific messages in response to particular stimuli. It allows the coordination of a myriad of cellular processes in a timely and specific manner. It is no wonder that viruses have adapted the use of such a modification to their own advantage. This is evidenced by the fact that several families of DNA viruses encode their own kinases (74). In other instances, cellular kinases have been detected within purified virus particles. These virion-associated protein kinases (VAPKs) usually phosphorylate viral proteins and contribute to the infectivity of the virus (65). Alternatively, viruses can engage the signaling activity of cellular kinases within their hosts such as that directed by mitogen-activated protein kinases (MAPKs) through a viral effector protein. This is particularly evident in the RNA viruses of the *orthomyxoviridae*, *retroviridae*, *filoviridae*, and *flaviviridae* (113). Viruses can recruit kinase activity by carrying consensus phosphorylation sequences in their genomes (140). There is evidence that structural proteins of HIV-1 such as CA, MA as well as the accessory proteins vif, vpr, rev, nef, tat and vpr are phosphorylated (19, 24, 26, 75, 101, 102). It is now becoming apparent how this viral peculiarity represents motif mimicry used as a tactic to reprogram the host cell. Viruses are able to recruit protein kinases, ligases or eukaryotic adaptor proteins by mimicking eukaryotic short linear motifs or SLiMs within disordered regions of their genetic sequence. Some of the most obvious examples are the eukaryotic motifs mimicked by viruses known as late domains (33). The PT/SAP and LYPXnL late domains of p6 HIV-1 redirect components of the ESCRT machinery to sites of virus assembly and budding, facilitating the catalysis of the last scission step that releases the nascent virion from its host cell. The HIV-1 p6 protein is an ideal example of a docking protein: it is highly flexible and unstructured—although it exhibits some regions of secondary structure under hydrophobic conditions (40)—and not only does it recruit diverse cellular and viral proteins but is also subject to several posttranslational modifications. For instance, p6 has been reported to be ubiquitinated at conserved Lys residues in positions 27 and 33 (107) and sumoylated at position 27 (57). An interesting observation is that p6 has 13 potential phosphorylation sites and in fact, p6 was previously identified by our group to exist as the

major phosphoprotein in HIV-1 particles (101). However, an in-depth study of the functional role of p6 phosphorylation has not been conducted to this date. Therefore, these observations prompted us to conduct a comprehensive analysis of the consequences of potential p6 phosphorylation in the HIV-1 replication cycle.

#### **4.1 Comprehensive analysis of HIV-1 p6<sup>Gag</sup> phosphorylation**

HIV-1 p6<sup>Gag</sup> contains 13 potentially phosphorylated residues: eight Ser, four Thr, and one Tyr. We made use of 3 phosphorylation prediction programs available on the web (NetPhos/NetPhosK, GPS, and DISPHOS) to select residues within p6 that were highly predicted to be phosphorylated. In addition, Ser, Thr and Tyr p6 residues that are highly conserved among HIV-1 subtypes were selected (Table 3.1 and Table 3.2). Information derived from these analyses was combined to choose the following p6 residues for mutational analysis: S14 and S25, as well as T8 and T23. We found that mutation of the p6 S14 and S25 residues had no effect on virus maturation or production as assayed in 293T cells (Figure 3.1). Moreover, the replication capacity observed for these p6 mutants was comparable to that of the wildtype virus in both C8166 cells and primary lymphocytes (Figure 3.4 and Figure 3.5). Thus, although these Ser residues are rather highly conserved and have high scores for phosphorylation, they do not seem to play a role in the replication cycle of the virus. The p6 T23 residue had been previously analyzed by our group and was included in this study to further characterize it and to confirm previous observations obtained with this mutant. Like the S14 and S25 p6 residues, we can conclude that the T23 residue plays no role in virus maturation, production or replication capacity of the virus. This contradicts results published by Hemonnot et al (60), who provided data that implicated the p6 T23 in HIV-1 release, maturation and infectivity. Reportedly, the p6 T23 residue was observed to be phosphorylated *in vitro* by the HIV-1 VAPK, ERK-2. Mutation of this residue to Ala resulted in multiple aberrant viruses, the majority of which were released but displayed an immature morphology. Although the same cell system and HIV-1 strain have been used in both studies, we failed to observe any effect of the p6 T23 mutant on any aspect of the viral replication cycle. Although we did not examine the morphology of the released virions, our release and infectivity data for this mutant suggests that they are not morphologically

aberrant since we did not observe accumulation of processing intermediates in these virions nor was their replicative capacity compromised. Moreover, although creating a Thr to Ala point mutation in p6 at this position results in an amino acid change within the *pol* frame, the inhibitory effect of the T23 mutation observed by Hemonnot et al cannot be attributed to this fact, since 1) our mutant also results in a change in *pol* and 2) most importantly, it has been published that deletion of residues T21-T23 in p6<sup>Gag</sup> or equivalent mutations in *pol* are dispensable for the virus, at least in cell culture systems (13, 111). So far, the reason for these discrepancies is not evident.

The p6 T8 residue has a high phosphorylation prediction score and is strongly conserved among HIV-1 subtypes. Moreover, given that this residue is part of the critical p6 PTAP late domain and that p6 is subject to various posttranslational modifications, there seemed to be a high likelihood that phosphorylation of this residue could be involved in the late domain activity of p6. It has also been shown before by biochemical methods that the late domain proteins of other viruses such as MLV, MPMV, and VSV are phosphorylated (29, 133, 154, 155). Thus, to approach the potential role of p6 T8 phosphorylation we attempted to emulate a phosphorylated state of this residue by creating a point mutant containing an Asp instead of the Thr. We observed that the p6 T8D mutant virus was released to a slightly greater extent than the T8I, T8A, and PTAP<sup>-</sup> mutants in 293T cells. Moreover, we examined its ability to establish a productive spreading infection in C8166 cells. In these cells, the T8D mutant achieved virus titers that were at least 2- to 4-fold higher than the T8I and T8A mutants (Figure 3.4). When analyzed in a more relevant cell system such as primary lymphocytes, the T8D mutant exhibited delayed kinetics and reached virus titers comparable to the wildtype virus (Figure 3.5). However, it cannot be excluded that the delayed kinetics of virus production displayed by the T8D mutant could be due to the emergence of viral revertants. In fact, closer examination by thin-section EM revealed a significant proportion of immature and budding-arrested viruses (Figure 3.23) suggesting that the high virus titers exhibited by this mutant are likely due to reversion.

As expected, the PTAP<sup>-</sup> mutant was strongly impaired in replication, while the T8I mutant exhibited an initial delay that did not reach wildtype virus titers at later timepoints.

To investigate whether the improved ability of the p6 T8D virus to exit the cell could be due to the mimicked phosphorylation state of the mutation, we replaced the T8 residue

by a Glu residue. Since this residue is bulkier than Asp and might better emulate a phosphorylated state of the residue, we reasoned that release might become even more efficient. However, the T8E mutant was not more efficiently released relative to the T8D mutant (Figure 3.7); on the contrary, the T8E mutant seemed to be even more impaired in release. Phosphorylation is a highly dynamic process, and it seems plausible that if phosphorylation would function as an 'on' signal in this scenario, a T8D or T8E mutant could presumably be in a constitutively active 'on' state without the possibility of 'switching-off' the signal. This could interfere with putative signaling events potentially required to facilitate virus release. This possibility, however, seems inconsistent with other observations as along with the T8E mutant we tested a p6 T8N mutant that was included as a negative control in our experiments. Unexpectedly, this mutant behaved similarly to the wildtype virus both in release and in single-round infection. This finding strongly argues against a role for p6 T8 phosphorylation in virus release. Further supporting this conclusion is the p6 mass spectrometry data obtained from 3 independent 293T cell-derived virus preparations and 2 independent MT-4 cell-derived virus preparations that indicate that this residue does not undergo phosphorylation. Thus, the improved ability of the T8D mutant to exit the host cell could be due to an overall slightly greater affinity for the cellular interaction partner, Tsg101 relative to the T8I and T8A mutants. Importantly, this putative affinity of interaction between a T8D virion and Tsg101 is likely to be much lower than the wildtype interaction and could result in an overall less efficient recruitment of Tsg101 to sites of virus assembly and budding. This could result in Tsg101 and the ESCRT machinery reaching those sites when the Gag shell is almost complete. This could give rise to mainly immature, dead-end viruses as postulated by Carlson et al (see section 1.3.2.1.3) and as indicated by our EM data (Figure 3.23).

#### ***4.2 Uncoupling of the gag and pol overlapping reading frames to perform extensive mutations in p6<sup>Gag</sup>***

The HIV-1 genome has three main coding regions: *gag* which directs the synthesis of the internal structural proteins, *pol* which encodes the viral enzymes and *env* which gives rise to the envelope proteins. In HIV-1 the *pol* gene lacks an initiation codon and partially

overlaps with the *gag* reading frame. To support translation of the *pol* products, a small number of ribosomes undergo a -1 ribosomal frameshift event once every 20 *gag* translation events. The frameshift required for the translation of HIV-1 Gag-Pol is promoted by two *cis*-active signals on the genomic RNA: a UUUUUUA heptamer termed the 'slippery' sequence and a stem-loop. These elements are located in the overlapping region of the *gag* and *pol* genes directly following the coding region for NC (62). C-terminal residues within p6<sup>Gag</sup> have been shown to be required for proper separation of the PR from the p6\* (transframe) (111). Moreover, C-terminal residues within p6<sup>Gag</sup> also overlap with the PR sequence. Thus, extensive mutational analysis of p6<sup>Gag</sup> is hindered by this viral property. To overcome this limitation we applied a strategy recently described by Leiherer et al (89) in which the *gag* and *pol* overlapping reading frames are separated or 'uncoupled.' This is achieved by abrogating the frameshift signal at the N-terminus of the p6\* and reintroducing it at the end of the *gag* codon (Figure 3.9). This results in an extended Gag by 5 amino acid residues, while the p6\* is extended by 70 amino acid residues. A synthetic fragment containing the changes in the frameshift signal was introduced into the backbone of the HIV-1 NL4-3 infectious clone. In agreement with the published study, we observed that such uncoupled viruses retain wildtype levels of virus production, protein processing and maturation as well as being infectious (Figure 3.10 and Figure 3.11). Since our main goal was to use this uncoupled construct to analyse the effect of extensive mutations in potentially phosphorylated residues in p6<sup>Gag</sup>, we further mutated extensive segments within the uncoupled construct's p6<sup>Gag</sup> sequence, generating three main proviruses in which either all Ser, Thr and Tyr residues were mutated with the exception of Thr8 (FL) or in which only the N-terminal (Nter) or C-terminal (Cter) Ser, Thr, and Tyr residues were mutated (Figure 3.12). Initial analysis of these mutants revealed that both the FL and Cter p6 mutations were detrimental to virus release. However, further analysis of these mutants proved difficult to reach a conclusion since it appeared that cumulative Ser, Thr, and Tyr mutations within the p6 sequence had no significant effect on virus production. Thus, careful interpretation of these observations is warranted until further analysis clearly distinguishes whether virus release is affected or not. Nevertheless, some assumptions can be made in each possible scenario: first of all, if potential p6 phosphorylation proves not to be required for virus release, then the infectivity and replicative fitness of these virions must be examined, since it

is plausible that p6 phosphorylation is not required for virus release but for the association of cellular factors or viral proteins that are important during viral entry and replication. For instance, the HIV-1 accessory protein Vpr protein is incorporated into virions by recognition of two motifs within p6<sup>Gag</sup>, one of which is localized at the C-terminus of p6 and involves the <sup>41</sup>LRSLF sequence. Vpr is a highly basic protein which is itself phosphorylated (102) and has been implicated in nuclear import of the viral PIC (pre-integration complex) as well as in activation of transcription, cell-cycle arrest and in the induction of apoptosis (45). p6<sup>Gag</sup> phosphorylation (for instance by inducing a negatively charged environment) might specifically serve as an activation signal to recruit Vpr to sites of virus assembly and budding. To test this, one could determine the degree of Vpr incorporation into p6 mutants and the effect this might have on viral replication. Importantly, the p6 mass spectrometry analysis identified S43 as a phosphoresidue which is part of the <sup>41</sup>LRSLF motif. Furthermore, the MS analysis suggests that this modification is only present in p6<sup>Gag</sup> and is lost once p6 is cleaved off from the precursor protein (Table 3.3). This would imply that transient modification of p6 could result in the recruitment of Vpr shortly before or concomitant with initiation of proteolytic cleavage of the Gag polyprotein precursor. Loss of the phosphorylation signal would induce the disassociation of Vpr from p6<sup>Gag</sup> which could be important for Vpr association with the PIC during viral entry.

Alternatively, p6 phosphorylation could occur 'accidentally' due to sequence similarities with preferred substrate-binding sites. Yet another possibility is that phosphorylation could occur within the virus particle and have its effect during the early stages of virus entry. It has been reported that the ERK-2 kinase is incorporated into HIV-1 particles (24). This suggests that kinases incorporated within HIV-1 particles can control the phosphorylation status of the substrate protein and catalyze its modification at a later stage during the infectious cycle of the virus. For instance, phosphorylation of the HIV-1 MA protein by virion-associated ERK/MAPK has been reported to be involved in the uncoating process during virus entry (75).

Considering the second scenario where the FL and Cter mutants reflect a true phenotype suggesting that p6 phosphorylation would indeed play a role in virus release, this would suggest that the potential phosphorylation of Ser, Thr, and Tyr residues within the C-terminus of p6 might be relevant for virus release. Impact on other viral processes such as

maturation, infectivity and replication capacity would require further examination. Although a defect in virus maturation was not readily detected by Western blot analysis in any of the experiments performed, a closer and more detailed look at these mutants should be conducted by EM. In addition, one could further discriminate between these residues to identify the particular residue(s) involved in the phenotype by narrowing down the extent of residues mutated within the C-terminus of p6. Moreover, the mass spectrometry analysis performed for wildtype NL4-3 viruses derived from two different cell lines suggests that p6 C-terminal Ser residues 40, 43, and 51 could potentially be involved in the putative phenotype. Phosphorylation prediction programs such as NetPhosK can be used to identify kinases that might be involved in phosphorylating specific residues. According to this program, the S40 residue is putatively phosphorylated by the PKC kinase, S43 by CKI while three different kinases could in theory phosphorylate S51: CKII, DNAPK and ATM. The involvement of these kinases in viral processes is not without precedent. For instance, PKC has been reported to phosphorylate the viral P proteins of human parainfluenza virus type 3 (HPIV3) and Sendai virus (34, 67). This modification is important for virus replication. In addition, PKCs have also been reported to phosphorylate the HIV-1 accessory protein Nef, resulting in increased viral replication (152). Both CKI and CKII are involved in regulating the gene repressive activity of the immediate early protein 63 (IE63) of varicella-zoster virus (VZV) (14) while the ATM kinase has been reported to enhance HIV-1 replication through enhanced Rev function (3). The DNAPK has been implicated in retroviral DNA integration (32). There is evidence that the late domains of other retroviruses are phosphorylated: The p24 protein of MPMV, the M protein of VSV and the p12 protein of MLV (101). In the case of MLV, it has been shown that phosphorylation of serines within this domain are required during early events of viral infection (156); alternatively, it has been suggested that phosphorylation of p12 might serve to bind to WW domain-containing proteins, such as E3 Ub ligases (155). A direct role for phosphorylation in the late-domain activity of retroviral proteins has only been demonstrated for HTLV-1 and reportedly for HIV-1. HTLV-1 MA protein contains PTAP and PPPY L-domain motifs. A Ser residue in the vicinity to the L-domain was observed to be phosphorylated by virion-associated ERK-2. This modification was found to decrease virus release and impair viral infectivity (61). The same group showed

that p6<sup>Gag</sup> Thr23 residue is phosphorylated by the ERK-2 kinase and that phosphorylation of this residue is important for virus release and infectivity (60).

Phosphorylation and ubiquitination are posttranslational modifications that exhibit considerable crosstalk. For instance, phosphorylation may serve as a signal for the addition or removal of a second posttranslational modification or for recognition by a binding protein that carries out a second modification. In addition to phosphorylation, HIV-1 Gag is monoubiquitinated at Lys residues present in all of its domains (55). Moreover, Gag modification with Ub and an intact proteasome have been shown to be important for late domain activity (93). In this context, p6 phosphorylation might serve to recruit Ub ligase activity that in turn serves to recruit ESCRT components to sites of virus assembly and budding. The ESCRT-I component and cellular interaction partner of p6<sup>Gag</sup>, Tsg101 contains an UEV domain that serves to recognize and bind Ub during the sorting process of cargo proteins. Interestingly, it has been shown that the affinity between the p6 PTAP L-domain and Tsg101 is increased about 10-fold when a Ub-moiety is attached to the C-terminus of p6 (49). Hence, p6<sup>Gag</sup> phosphorylation-directed Gag ubiquitination might serve to recruit more efficiently or bind Tsg101 more tightly. However, it has been shown that p6 ubiquitination is not required for the p6-Tsg101 association (35, 118). Another possibility is that ubiquitination of a nearby, yet unidentified protein would serve as a substrate and this would lead to the recruitment of ESCRT components, as suggested by Zhadina et al (157). Another scenario is set forth by the fact that Ub ligase activity can be regulated by phosphorylation as that reported for Nedd4-2 (135). In this context, p6 would be subject to adventitious phosphorylation by being in close proximity to kinases that control the activity of Ub ligases or due to ESCRT-III component phosphorylation. Indeed, the ESCRT-III components Vps4b and CHMP3 have been shown to be phosphorylated (105).

### ***4.3 p6 phosphopeptide analysis by mass spectrometry***

To unequivocally determine sites in p6 that are actual substrates to kinase-mediated phosphorylation we conducted a mass spectrometry analysis of HIV-1<sub>NL4-3</sub> virus-derived protein bands. This study allowed us to identify phosphoresidues within p6 as well as in other viral structural proteins, such as MA and CA. The relevance and possible significance of the MA and CA modifications is beyond the scope of this study and will thus not be

addressed in more detail. The analysis permitted us to compare the p6 phosphorylation pattern obtained from viruses-derived either from 293T or MT-4 cells. It also allowed us to follow the phosphorylation pattern of p6 throughout its processing stages: from its existence as part of the Gag polyprotein precursor to its cleaved, processed form as p6. The analysis of virions derived from 293T cells indicates that p6 is phosphorylated as part of the Gag precursor in residues (residue positions are given in relation to p6) T22/23, S40, S43, and S51 while the NCSP1p6 processing intermediate is phosphorylated at T21, T22/23. Finally, the free form of p6 is phosphorylated at T22/23, S40, and S51. The fact that both p6<sup>Gag</sup> and free p6 repeatedly showed phosphoresidues at S40 and S51 suggests that these phosphorylations are maintained during the processing step that yields the free form of p6. Nevertheless, it is possible that these modifications were not detected in the analysis of the NCSP1p6 processing intermediate due to the low stoichiometry of the modification. Alternatively, it may actually reflect a regulatory activity by cellular kinases associated with the virion. As mentioned in section 4.2, S40 is putatively phosphorylated by the PKC kinase and S51 by one of these kinases: DNAPK, ATM or CKII. It would be of interest to know whether these kinases are packaged into the virion. This might hint at the timepoint at which phosphorylation takes place. For instance, if the kinases are not packaged within the virion, it could indicate that association of Gag with these kinases must occur at an early timepoint, prior to completion of the nascent virion scission reaction. Alternatively, if the kinases are packaged into the virion, it could suggest that phosphorylation during Gag processing could be regulated within it. ATP molecules could inadvertently become incorporated into viral particles during the AAA+ ATPase Vps4-catalyzed disassembly of ESCRT-III components. In the case of T22/23 it was not possible to pinpoint the phosphorylated residue due to the close proximity of their signals. The T23 is within a consensus sequence for phosphorylation by the ERK-2 kinase. There is biochemical evidence that ERK-2 is incorporated into HIV-1 particles and that the phosphorylation of T23 plays an important role in HIV-1 release and infectivity (24, 60). However, our own studies indicated that although T23 seems to be phosphorylated, this modification does not seem to play a role in the release or replication capacity of HIV-1. The T21 residue was consistently identified as a phosphoresidue exclusively in the context of the NCSP1p6 processing intermediate in 2 out of 3 virus preparations; this could suggest that this modification might positively regulate further processing of Gag intermediates by the

viral protease. The p6 phosphorylation pattern obtained from MT-4-derived virions was in principle similar to that obtained from 293T-derived virions with respect to the phosphoresidues identified. Although fewer residues were observed to be phosphorylated in MT-4-derived virions, no new phosphoresidues were identified in comparison to 293T-derived virions. Hence, in MT-4-derived viruses, p6<sup>Gag</sup> was phosphorylated at T22/23 and S40; NCSP1p6 contained the phosphoresidues T22/23 and S51, while cleaved p6 was phosphorylated at S40 and S50/51. This could suggest that all p6 phosphorylations observed take place in p6 as part of the Gag precursor; alternatively, the phosphorylation at S51 might be acquired to signal activation of further processing. To better distinguish between the modifications taking place at the level of p6<sup>Gag</sup>, p6 as a cleavage intermediate or in its free form, an additional analysis from another independent virus preparation should aid in the interpretation of these results. Overall, the differences in phosphorylation patterns observed between 293T-derived and MT-4-derived viruses could either indicate that there is a true difference in p6 phosphorylation or that simply the analysis missed the identification of additional residues and it must be repeated in a different virus preparation. In addition, mass spectrometry analysis of p6 phosphosite mutants can help corroborate the identified phosphorylated residues. In summary, in agreement with the study published by Müller et al (101) we could detect p6 as a phosphoprotein that can exist in a multiply phosphorylated form, given the number of phosphoresidues we identified in the cleaved form of p6. Although phosphoamino acid analysis identified Tyr as a phosphoresidue in their study, our mass spec analysis did not detect such a modification in the single Tyr residue present within p6. In contrast to Müller et al, we could clearly identify Gag as a phosphoprotein, suggesting phosphorylation could take place during the assembly/budding reaction. Overall, mass spectrometry proved to be a powerful tool to identify phosphoresidues in p6.

#### ***4.4 Interaction properties between a p6 T8N mutant and the Tsg101 UEV domain***

During our study of potential p6 phosphorylation mutants observed that a p6 T8N mutant that was constructed as a negative control for our release assay, surprisingly showed wildtype behavior both in release and in single-round infectivity. Moreover, the ability of this mutant virus to support virus release was confirmed by electron microscopy and we could

ascertain that a considerable amount of particles displayed mature capsid morphology. It is known that among different HIV-1 subtypes, the C-terminal p6<sup>Gag</sup> domain is the most variable in length and sequence. A PXXP amino acid sequence motif, occurring as PTAP or PSAP is highly conserved and has even been observed to be duplicated within HIV-1 subtype C strains (145). The integrity of this motif is critical for proper nascent virus detachment from the host cell membrane (53, 64). Hence, our results with the p6 T8N mutant were unexpected and we therefore sought to characterize this mutant in further detail to understand the basis for its activity. Biochemically, we could confirm that it can support virus release similar to the wildtype virus. Moreover, this mutant proved to be infectious by single-round infectivity. To determine whether more subtle differences in replication might explain the reason why this mutant does not occur in nature, we analyzed its ability in establishing a spreading infection, however, results await analysis. It was also possible that changing the T8 residue to an Asn would change the specificity for an interaction partner. Normally, the PT/SAP L-domain recruits the ESCRT-I component, Tsg101 to sites of virus budding facilitating virus release. We could prove, albeit indirectly, that the mutant PNAP L-domain retains its Tsg101 recruiting activity. This was further supported by our binding affinity studies that showed that the Tsg101 UEV domain and a PNAP-containing p6 peptide interact with an average  $K_d$  of 295.1  $\mu$ M. Although this affinity is 5-fold lower than what we observed between the PT/SAP peptide and Tsg101 UEV, it is significantly higher than that measured between a PAAP peptide and UEV, which was negligible (Figure 26). Moreover, the ITC measurements are in agreement with the biochemical data obtained with the p6 T8A and T8N mutants. The fact that Tsg101 UEV and PNAP can interact with 5-fold less affinity and still support HIV-1 release indicates that the interaction need not be so tight and that this affinity is sufficient to mediate recruitment of Tsg101 and catalyze release. In fact, the affinity of the interaction that occurs between Tsg101 UEV and a PSAP peptide derived from the ESCRT-0 component Hrs is 6-fold lower than the p6 PT/SAP-Tsg101 UEV interaction (71). It is also possible that ubiquitination of p6<sup>Gag</sup> or other domains in Gag may increase the affinity of the interaction. It has been shown that fusion of a Ub moiety to the C-terminus of p6 increases the affinity of the interaction 10-fold (49). The present study, however, did not address the role of Gag ubiquitination in the recruiting activity of Tsg101 by the PNAP L-domain. This could be tested by using a Tsg101 mutant for Ub binding. Although Tsg101

binds to both Ub and PT/SAP through its UEV domain, different interfaces are used to recognize the respective ligands. Moreover, it has been shown that mutation of the Tsg101 UEV Ub-binding site does not interfere with p6 binding (49). To obtain more structural information regarding the mode of interaction between PNAP and Tsg101 UEV we attempted to crystallize the complex. However, so far we have only obtained crystals of the uncomplexed protein. It is possible that due to the lower affinity of the interaction, it is harder to obtain a crystal of the complex. We recently obtained new crystals of the protein which will be incubated with high concentrations of the PNAP peptide in an effort to force the peptide into the structure.

The question that still remains elusive is why the PNAP L-domain does not occur in natural HIV-1 isolates? It could be that a PNAP in place of a PT/SAP has a replicative disadvantage. This could be resolved by comparing the replicative fitness of such viruses. Another simple explanation could be that it is just a matter of structural conservation. In the wildtype interaction, the main-chain amide of the critical PTAP T8 residue forms a hydrogen bond with the main-chain carbonyl of Asn69 in UEV. In addition, the side-chain hydroxyl group of T8 forms a hydrogen bond with the main-chain amide of Asn69, while the methyl of T8 makes no direct contacts to the UEV domain (71). In principle, an Asn residue conserves structural properties of a Thr residue (9). Importantly, Asn has a high propensity to hydrogen bond since the amide group can accept two and donate two hydrogen bonds. Thus, in principle, the N8 residue could still maintain the hydrogen bonding interactions of the T8 residue necessary to interact with the UEV domain. Importantly, the lower affinity resulting from the PNAP-UEV interaction suggests that the structural properties of the complex are nevertheless altered. The only other existing evidence that interaction between a PNAP residue and Tsg101 UEV can take place comes from a p6 peptide substitution study where the affinity of p6 mutants for GST-UEV is tested on a SPOT membrane. It is observed that binding still exists, albeit to a lesser extent when the T8 residue is replaced by an Asn residue (130). Another, perhaps more interesting, possibility is that PNAP functionality in the context of HIV-1 release, has been preferentially replaced by residues of higher affinity throughout evolution. In support of this assumption it the fact that, at least in the context of main-chain to side-chain hydrogen bonding patterns in proteins, asparagine and aspartate residues frequently interconvert, as do the serine and threonine residues. It is also clear that the two

pairs of residues often interconvert from S/T to D/N, more often than with any of the other amino acid residues. The rate is lower than S to T or D to N, but is nevertheless highly significant. In contrast, asparagine residues rarely interchange to glutamine (147). This correlates well with the effect we observed with the p6 T8Q mutant, which was not able to rescue virus release as the p6 T8N mutant did. To explore the likelihood that the PNAP motif has been evolutionarily replaced by a motif of higher affinity, such as PT/SAP we conducted a search for viral and eukaryotic proteins containing the P-N-A-P motif. The most relevant eukaryotic proteins identified were the voltage-dependent calcium channel and the melanoma antigen recognized by T cells 1 (MART-1). The MART-1 protein, for example, contains tandem PNAPPAY motifs predicted to interact with WW domain-containing ligases. In fact, both of these proteins interact and are regulated by Nedd4 ligases (92, 123). The adaptor-related protein complex 4, beta 1 subunit (AP4B1) was also identified to contain a PNAP motif. The AP4B1 is a subunit of the AP-4 protein. The AP proteins in general recruit cytosolic components of the transport machinery to assemble into protein coats and form the budding vesicle on the membrane of a donor organelle (6). The PNAP motif was prominently found in two unrelated viruses: EIAV and human hepatitis B virus (HBV). In EIAV, the PNAP motif is within an accessible loop in the CA protein. EIAV contains a YPDL L-domain within the C-terminal p9 domain that is known to be required to mediate virus release. However, it has also been reported that EIAV Gag is able to use not only Alix, but also Tsg101 or Vps28 for efficient budding. (138). As a lentivirus, it is intriguing why this virus does not possess a PT/SAP L-domain as in HIV-1. The finding that the PNAP motif can provide L-domain function could suggest that preference towards domains of higher affinity or that provide an evolutionary advantage could substitute for its function. Interestingly, although EIAV seems to bypass the need for ubiquitin in YPDL-mediated virus release (93), fusion of a Ub moiety to the C-terminus of an EIAV L-domain mutant is capable of rescuing virus production. Moreover, fusion of Ub rendered EIAV release sensitive to Tsg101 depletion (78). Thus, it is tempting to speculate that the PNAP motif present in the EIAV CA could be responsible for this phenotype, acting as a remnant ancestral L-domain. As mentioned above, concomitant binding of Ub and a PTAP peptide increases the Tsg101 UEV-PTAP interaction by 10-fold. Thus, it is plausible that Ub fusion to EIAV functions in the same way, strengthening the interaction between its PNAP motif and Tsg101. The HBV core contains

two candidate late domain-like motifs, PPAY<sub>132</sub> and PN<sub>136</sub>AP (82). Interestingly, a study conducted by Ponsel et al (114) showed that mutation of the N136 residue allowed virus nucleocapsid formation but inhibited particle envelopment and virion release. Nevertheless, this motif has not been recognized as a true L-domain since it was found that a P135A mutant did not prevent HBV virion release (114) presumably questioning the relevance of the whole motif in virus release. However, as reported by Im et al (71), at least in the context of the PTAP motif, the P7 is not so critical for binding and thus, a P7A mutant leads to a less than 3-fold reduction in affinity for Tsg101 UEV. Thus, it is not surprising that HBV production can still take place in this context. Moreover, there is evidence that inhibition of the ESCRT-associated factor Vps4 inhibits HBV replication and secretion (82), hinting at the possibility that ESCRT components might be engaged through the HBV core.

In summary, the finding that a PNAP p6 peptide is able to support wildtype levels of HIV-1 release invokes further exploration into the interaction properties that mediate this interaction. This is especially relevant in the design of p6-UEV peptide inhibitors. Perhaps, a high affinity PNAP-containing peptide could be designed in the future that would act as a competitive inhibitor of the PTAP-UEV interaction. Importantly, this inhibition is unlikely to disturb other endocytic process involving Tsg101 as shown by Im et al (71). Hence, the unprecedented functionality of the PNAP-UEV interaction should be an important addition to the future design of small molecule inhibitors.

#### ***4.5 Future directions***

HIV-1 is a virus that greatly benefits from usurping cellular factors at different stages of its replication cycle. It can achieve this by effectively mimicking cellular protein motifs. In this way, it has become a substrate to varied posttranslational modifications, including phosphorylation, thus engaging key machinery that helps orchestrate a myriad of cellular processes. Elucidation of the detailed role of HIV-1 p6 phosphorylation in the viral replication cycle must be pursued further. It will be necessary to unequivocally determine the effect potential p6 phosphorylation site mutants have in virus release, maturation and replication. This will eventually help pinpoint the relevant residue(s) involved in the phenotype, if any. The uncoupled constructs were designed in a way to contain additional restriction sites, facilitating the exchange of fragments with a selected amount of mutations

and enabling further site-directed mutagenesis. Furthermore, the results obtained by the mass spectrometry analysis will help corroborate the observations and will provide additional information regarding the putative kinases that could phosphorylate them. In this regard, an additional preparation from MT-4 cell-derived HIV-1 virions should be analyzed. Detected phosphoresidues should be compared to the other two virus preparations to help define whether there is an actual difference in the phosphorylation pattern between HIV-1 virions derived from 293T cells as compared to those derived from MT-4 cells. It is also possible to ascertain the apparent absence of a morphological defect of the p6 mutants by visualizing them through electron microscopy. The uncoupled *gag-pol* construct proved to be an excellent tool to generate extensive mutations in p6 without affecting the partially overlapping *pol* frame and it allows further exploration of Gag domains that could not be studied in detail before, such as SP1.

Regarding the p6 PNAP mutant, it will be important to analyze its ability to support a spreading infection in primary lymphocytes. The experiments have been conducted and only the analysis is pending. It will be interesting to see if such mutants revert to the wildtype motif. This might shed light on the reason why this motif does not occur in natural HIV-1 isolates. On the other hand, the crystal structure of the Tsg101-UEV complex will provide critical information regarding the interaction properties between the two which will provide us with a better understanding of the flexibility of residues that can exist within this position. At the same time, this information might help in the future design of peptides that can effectively interfere with the HIV-1 budding reaction. New crystals of Tsg101 UEV have been obtained and the peptide will be forced into the structure by using high concentrations of it. Analysis of the crystals will be carried out in Grénoble.

## 5 References

1. **Adachi, A., H. E. Gendelman, S. Koenig, T. Folks, R. Willey, A. Rabson, and M. A. Martin.** 1986. Production of acquired immunodeficiency syndrome-associated retrovirus in human and nonhuman cells transfected with an infectious molecular clone. *J Virol* **59**:284-91.
2. **Ammosova, T., R. Berro, M. Jerebtsova, A. Jackson, S. Charles, Z. Klase, W. Southerland, V. R. Gordeuk, F. Kashanchi, and S. Nekhai.** 2006. Phosphorylation of HIV-1 Tat by CDK2 in HIV-1 transcription. *Retrovirology* **3**:78.
3. **Ariumi, Y., and D. Trono.** 2006. Ataxia-telangiectasia-mutated (ATM) protein can enhance human immunodeficiency virus type 1 replication by stimulating Rev function. *J Virol* **80**:2445-52.
4. **Babst, M., T. K. Sato, L. M. Banta, and S. D. Emr.** 1997. Endosomal transport function in yeast requires a novel AAA-type ATPase, Vps4p. *EMBO J* **16**:1820-31.
5. **Babst, M., B. Wendland, E. J. Estepa, and S. D. Emr.** 1998. The Vps4p AAA ATPase regulates membrane association of a Vps protein complex required for normal endosome function. *EMBO J* **17**:2982-93.
6. **Barois, N., and O. Bakke.** 2005. The adaptor protein AP-4 as a component of the clathrin coat machinery: a morphological study. *Biochem J* **385**:503-10.
7. **Barre-Sinoussi, F., J. C. Chermann, F. Rey, M. T. Nugeyre, S. Chamaret, J. Gruest, C. Dauguet, C. Axler-Blin, F. Vezinet-Brun, C. Rouzioux, W. Rozenbaum, and L. Montagnier.** 1983. Isolation of a T-lymphotropic retrovirus from a patient at risk for acquired immune deficiency syndrome (AIDS). *Science* **220**:868-71.
8. **Berg, J., J. Tymoczko, and L. Stryer.** 2007. *Biochemistry*, 6th ed. W.H. Freeman and Company, New York.
9. **Betts, M., and R. Russell.** 2003. *Amino acid properties and consequences of substitutions*. Wiley.
10. **Bhattacharyya, R. P., A. Remenyi, B. J. Yeh, and W. A. Lim.** 2006. Domains, motifs, and scaffolds: the role of modular interactions in the evolution and wiring of cell signaling circuits. *Annu Rev Biochem* **75**:655-80.
11. **Bieniasz, P. D.** 2009. The cell biology of HIV-1 virion genesis. *Cell Host Microbe* **5**:550-8.
12. **Bieniasz, P. D.** 2006. Late budding domains and host proteins in enveloped virus release. *Virology* **344**:55-63.
13. **Bleiber, G., S. Peters, R. Martinez, D. Cmarko, P. Meylan, and A. Telenti.** 2004. The central region of human immunodeficiency virus type 1 p6 protein (Gag residues S14-I31) is dispensable for the virus in vitro. *J Gen Virol* **85**:921-7.
14. **Bontems, S., E. Di Valentin, L. Baudoux, B. Rentier, C. Sadzot-Delvaux, and J. Piette.** 2002. Phosphorylation of varicella-zoster virus IE63 protein by casein kinases influences its cellular localization and gene regulation activity. *J Biol Chem* **277**:21050-60.
15. **Bossemeyer, D.** 1995. Protein kinases--structure and function. *FEBS Lett* **369**:57-61.
16. **Brugger, B., B. Glass, P. Haberkant, I. Leibrecht, F. T. Wieland, and H. G. Krausslich.** 2006. The HIV lipidome: a raft with an unusual composition. *Proc Natl Acad Sci U S A* **103**:2641-6.
17. **Brun, S., L. Chaloin, B. Gay, E. Bernard, C. Devaux, C. Lionne, N. Chazal, and L. Briant.** 2010. Electrostatic repulsion between HIV-1 capsid proteins modulates hexamer plasticity and in vitro assembly. *Proteins* **78**:2144-56.
18. **Bukrinskaya, A.** 2007. HIV-1 matrix protein: a mysterious regulator of the viral life cycle. *Virus Res* **124**:1-11.

19. **Burnette, B., G. Yu, and R. L. Felsted.** 1993. Phosphorylation of HIV-1 gag proteins by protein kinase C. *J Biol Chem* **268**:8698-703.
20. **Calistri, A., C. Salata, C. Parolin, and G. Palu.** 2009. Role of multivesicular bodies and their components in the egress of enveloped RNA viruses. *Rev Med Virol* **19**:31-45.
21. **Carlson, L. A., J. A. Briggs, B. Glass, J. D. Riches, M. N. Simon, M. C. Johnson, B. Muller, K. Grunewald, and H. G. Krausslich.** 2008. Three-dimensional analysis of budding sites and released virus suggests a revised model for HIV-1 morphogenesis. *Cell Host Microbe* **4**:592-9.
22. **Carlton, J. G., and J. Martin-Serrano.** 2009. The ESCRT machinery: new functions in viral and cellular biology. *Biochem Soc Trans* **37**:195-9.
23. **Carlton, J. G., and J. Martin-Serrano.** 2007. Parallels between cytokinesis and retroviral budding: a role for the ESCRT machinery. *Science* **316**:1908-12.
24. **Cartier, C., M. Deckert, C. Grangeasse, R. Trauger, F. Jensen, A. Bernard, A. Cozzone, C. Desgranges, and V. Boyer.** 1997. Association of ERK2 mitogen-activated protein kinase with human immunodeficiency virus particles. *J Virol* **71**:4832-7.
25. **Cartier, C., B. Hemonnot, B. Gay, M. Bardy, C. Sanchiz, C. Devaux, and L. Briant.** 2003. Active cAMP-dependent protein kinase incorporated within highly purified HIV-1 particles is required for viral infectivity and interacts with viral capsid protein. *J Biol Chem* **278**:35211-9.
26. **Cartier, C., P. Sivard, C. Tranchat, D. Decimo, C. Desgranges, and V. Boyer.** 1999. Identification of three major phosphorylation sites within HIV-1 capsid. Role of phosphorylation during the early steps of infection. *J Biol Chem* **274**:19434-40.
27. **Chen, B. J., and R. A. Lamb.** 2008. Mechanisms for enveloped virus budding: can some viruses do without an ESCRT? *Virology* **372**:221-32.
28. **Cimarelli, A., and J. Luban.** 1999. Translation elongation factor 1-alpha interacts specifically with the human immunodeficiency virus type 1 Gag polyprotein. *J Virol* **73**:5388-401.
29. **Clinton, G. M., and A. S. Huang.** 1981. Distribution of phosphoserine, phosphothreonine and phosphotyrosine in proteins of vesicular stomatitis virus. *Virology* **108**:510-4.
30. **Coffin, J. M., S. H. Hughes, and H. E. Varmus (ed.).** 1997. *Retroviruses*. Cold Spring Harbor Laboratory Press, Cold Spring Harbor, NY.
31. **Craven, R. C., R. N. Harty, J. Paragas, P. Palese, and J. W. Wills.** 1999. Late domain function identified in the vesicular stomatitis virus M protein by use of rhabdovirus-retrovirus chimeras. *J Virol* **73**:3359-65.
32. **Daniel, R., R. A. Katz, and A. M. Skalka.** 1999. A role for DNA-PK in retroviral DNA integration. *Science* **284**:644-7.
33. **Davey, N. E., G. Trave, and T. J. Gibson.** 2010. How viruses hijack cell regulation. *Trends Biochem Sci*.
34. **De, B. P., S. Gupta, and A. K. Banerjee.** 1995. Cellular protein kinase C isoform zeta regulates human parainfluenza virus type 3 replication. *Proc Natl Acad Sci U S A* **92**:5204-8.
35. **Demirov, D. G., and E. O. Freed.** 2004. Retrovirus budding. *Virus Res* **106**:87-102.
36. **Demirov, D. G., J. M. Orenstein, and E. O. Freed.** 2002. The late domain of human immunodeficiency virus type 1 p6 promotes virus release in a cell type-dependent manner. *J Virol* **76**:105-17.
37. **Dilley, K. A., D. Gregory, M. C. Johnson, and V. M. Vogt.** 2010. An LYP SL late domain in the gag protein contributes to the efficient release and replication of Rous sarcoma virus. *J Virol* **84**:6276-87.
38. **Endo-Munoz, L., T. Warby, D. Harrich, and N. A. McMillan.** 2005. Phosphorylation of HIV Tat by PKR increases interaction with TAR RNA and enhances transcription. *Virol J* **2**:17.
39. **Fiorentini, S., E. Marini, S. Caracciolo, and A. Caruso.** 2006. Functions of the HIV-1 matrix protein p17. *New Microbiol* **29**:1-10.
40. **Fossen, T., V. Wray, K. Bruns, J. Rachmat, P. Henklein, U. Tessmer, A. Maczurek, P. Klinger, and U. Schubert.** 2005. Solution structure of the human immunodeficiency virus type 1 p6 protein. *J Biol Chem* **280**:42515-27.

41. **Freed, E. O.** 1998. HIV-1 gag proteins: diverse functions in the virus life cycle. *Virology* **251**:1-15.
42. **Freed, E. O.** 2003. The HIV-TSG101 interface: recent advances in a budding field. *Trends Microbiol* **11**:56-9.
43. **Freed, E. O.** 2002. Viral late domains. *J Virol* **76**:4679-87.
44. **Freyer, M. W., and E. A. Lewis.** 2008. Isothermal titration calorimetry: experimental design, data analysis, and probing macromolecule/ligand binding and kinetic interactions. *Methods Cell Biol* **84**:79-113.
45. **Fritz, J. V., D. Dujardin, J. Godet, P. Didier, J. De Mey, J. L. Darlix, Y. Mely, and H. de Rocquigny.** 2010. HIV-1 Vpr oligomerization but not that of Gag directs the interaction between Vpr and Gag. *J Virol* **84**:1585-96.
46. **Gallo, R. C., P. S. Sarin, E. P. Gelmann, M. Robert-Guroff, E. Richardson, V. S. Kalyanaraman, D. Mann, G. D. Sidhu, R. E. Stahl, S. Zolla-Pazner, J. Leibowitch, and M. Popovic.** 1983. Isolation of human T-cell leukemia virus in acquired immune deficiency syndrome (AIDS). *Science* **220**:865-7.
47. **Ganser-Pornillos, B. K., M. Yeager, and W. I. Sundquist.** 2008. The structural biology of HIV assembly. *Curr Opin Struct Biol* **18**:203-17.
48. **Garnier, L., J. W. Wills, M. F. Verderame, and M. Sudol.** 1996. WW domains and retrovirus budding. *Nature* **381**:744-5.
49. **Garrus, J. E., U. K. von Schwedler, O. W. Pornillos, S. G. Morham, K. H. Zavitz, H. E. Wang, D. A. Wettstein, K. M. Stray, M. Cote, R. L. Rich, D. G. Myszka, and W. I. Sundquist.** 2001. Tsg101 and the vacuolar protein sorting pathway are essential for HIV-1 budding. *Cell* **107**:55-65.
50. **Gheysen, D., E. Jacobs, F. de Foresta, C. Thiriart, M. Francotte, D. Thines, and M. De Wilde.** 1989. Assembly and release of HIV-1 precursor Pr55gag virus-like particles from recombinant baculovirus-infected insect cells. *Cell* **59**:103-12.
51. **Gomez, C., and T. J. Hope.** 2005. The ins and outs of HIV replication. *Cell Microbiol* **7**:621-6.
52. **Gottlieb, M. S., J. E. Groopman, W. M. Weinstein, J. L. Fahey, and R. Detels.** 1983. The acquired immunodeficiency syndrome. *Ann Intern Med* **99**:208-20.
53. **Gottlinger, H. G., T. Dorfman, J. G. Sodroski, and W. A. Haseltine.** 1991. Effect of mutations affecting the p6 gag protein on human immunodeficiency virus particle release. *Proc Natl Acad Sci U S A* **88**:3195-9.
54. **Gottwein, E., J. Bodem, B. Muller, A. Schmechel, H. Zentgraf, and H. G. Krausslich.** 2003. The Mason-Pfizer monkey virus PPPY and PSAP motifs both contribute to virus release. *J Virol* **77**:9474-85.
55. **Gottwein, E., and H. G. Krausslich.** 2005. Analysis of human immunodeficiency virus type 1 Gag ubiquitination. *J Virol* **79**:9134-44.
56. **Grimsrud, P. A., D. L. Swaney, C. D. Wenger, N. A. Beauchene, and J. J. Coon.** 2010. Phosphoproteomics for the masses. *ACS Chem Biol* **5**:105-19.
57. **Gurer, C., L. Berthoux, and J. Luban.** 2005. Covalent modification of human immunodeficiency virus type 1 p6 by SUMO-1. *J Virol* **79**:910-7.
58. **Harty, R. N., M. E. Brown, G. Wang, J. Huibregtse, and F. P. Hayes.** 2000. A PPxY motif within the VP40 protein of Ebola virus interacts physically and functionally with a ubiquitin ligase: implications for filovirus budding. *Proc Natl Acad Sci U S A* **97**:13871-6.
59. **Harty, R. N., J. Paragas, M. Sudol, and P. Palese.** 1999. A proline-rich motif within the matrix protein of vesicular stomatitis virus and rabies virus interacts with WW domains of cellular proteins: implications for viral budding. *J Virol* **73**:2921-9.
60. **Hemonnot, B., C. Cartier, B. Gay, S. Rebuffat, M. Bardy, C. Devaux, V. Boyer, and L. Briant.** 2004. The host cell MAP kinase ERK-2 regulates viral assembly and release by phosphorylating the p6gag protein of HIV-1. *J Biol Chem* **279**:32426-34.

61. **Hemonnot, B., D. Molle, M. Bardy, B. Gay, D. Laune, C. Devaux, and L. Briant.** 2006. Phosphorylation of the HTLV-1 matrix L-domain-containing protein by virus-associated ERK-2 kinase. *Virology* **349**:430-9.
62. **Hill, M., G. Tachedjian, and J. Mak.** 2005. The packaging and maturation of the HIV-1 Pol proteins. *Curr HIV Res* **3**:73-85.
63. **Howley, D. M. K. a. P. M. (ed.).** 2007. *Fields' Virology*, 5th ed, vol. 2. Lippincott Williams & Wilkins, Philadelphia.
64. **Huang, M., J. M. Orenstein, M. A. Martin, and E. O. Freed.** 1995. p6Gag is required for particle production from full-length human immunodeficiency virus type 1 molecular clones expressing protease. *J Virol* **69**:6810-8.
65. **Hui, E. K.** 2002. Virion-associated protein kinases. *Cell Mol Life Sci* **59**:920-31.
66. **Hunter, T.** 2007. The age of crosstalk: phosphorylation, ubiquitination, and beyond. *Mol Cell* **28**:730-8.
67. **Huntley, C. C., B. P. De, and A. K. Banerjee.** 1997. Phosphorylation of Sendai virus phosphoprotein by cellular protein kinase C zeta. *J Biol Chem* **272**:16578-84.
68. **Hurley, J. H., and S. D. Emr.** 2006. The ESCRT complexes: structure and mechanism of a membrane-trafficking network. *Annu Rev Biophys Biomol Struct* **35**:277-98.
69. **Hurley, J. H., and P. I. Hanson.** 2010. Membrane budding and scission by the ESCRT machinery: it's all in the neck. *Nat Rev Mol Cell Biol* **11**:556-66.
70. **Im, Y. J., and J. H. Hurley.** 2008. Integrated structural model and membrane targeting mechanism of the human ESCRT-II complex. *Dev Cell* **14**:902-13.
71. **Im, Y. J., L. Kuo, X. Ren, P. V. Burgos, X. Z. Zhao, F. Liu, T. R. Burke, Jr., J. S. Bonifacino, E. O. Freed, and J. H. Hurley.** 2010. Crystallographic and functional analysis of the ESCRT-I /HIV-1 Gag PTAP interaction. *Structure* **18**:1536-47.
72. **Ingham, R. J., G. Gish, and T. Pawson.** 2004. The Nedd4 family of E3 ubiquitin ligases: functional diversity within a common modular architecture. *Oncogene* **23**:1972-84.
73. **Ivanchenko, S., W. J. Godinez, M. Lampe, H. G. Krausslich, R. Eils, K. Rohr, C. Brauchle, B. Muller, and D. C. Lamb.** 2009. Dynamics of HIV-1 assembly and release. *PLoS Pathog* **5**:e1000652.
74. **Jacob, T., C. Van den Broeke, and H. W. Favoreel.** 2010. Viral serine/threonine protein kinases. *J Virol* **85**:1158-73.
75. **Jacque, J. M., A. Mann, H. Enslin, N. Sharova, B. Brichacek, R. J. Davis, and M. Stevenson.** 1998. Modulation of HIV-1 infectivity by MAPK, a virion-associated kinase. *EMBO J* **17**:2607-18.
76. **Jayakar, H. R., K. G. Murti, and M. A. Whitt.** 2000. Mutations in the PPPY motif of vesicular stomatitis virus matrix protein reduce virus budding by inhibiting a late step in virion release. *J Virol* **74**:9818-27.
77. **Joshi, A., H. Garg, K. Nagashima, J. S. Bonifacino, and E. O. Freed.** 2008. GGA and Arf proteins modulate retrovirus assembly and release. *Mol Cell* **30**:227-38.
78. **Joshi, A., U. Munshi, S. D. Ablan, K. Nagashima, and E. O. Freed.** 2008. Functional replacement of a retroviral late domain by ubiquitin fusion. *Traffic* **9**:1972-83.
79. **Jouvenet, N., S. J. Neil, C. Bess, M. C. Johnson, C. A. Virgen, S. M. Simon, and P. D. Bieniasz.** 2006. Plasma membrane is the site of productive HIV-1 particle assembly. *PLoS Biol* **4**:e435.
80. **Katzmann, D. J., M. Babst, and S. D. Emr.** 2001. Ubiquitin-dependent sorting into the multivesicular body pathway requires the function of a conserved endosomal protein sorting complex, ESCRT-I. *Cell* **106**:145-55.
81. **Katzmann, D. J., C. J. Stefan, M. Babst, and S. D. Emr.** 2003. Vps27 recruits ESCRT machinery to endosomes during MVB sorting. *J Cell Biol* **162**:413-23.
82. **Kian Chua, P., M. H. Lin, and C. Shih.** 2006. Potent inhibition of human Hepatitis B virus replication by a host factor Vps4. *Virology* **354**:1-6.

83. **Kikonyogo, A., F. Bouamr, M. L. Vana, Y. Xiang, A. Aiyar, C. Carter, and J. Leis.** 2001. Proteins related to the Nedd4 family of ubiquitin protein ligases interact with the L domain of Rous sarcoma virus and are required for gag budding from cells. *Proc Natl Acad Sci U S A* **98**:11199-204.
84. **Kostelansky, M. S., C. Schluter, Y. Y. Tam, S. Lee, R. Ghirlando, B. Beach, E. Conibear, and J. H. Hurley.** 2007. Molecular architecture and functional model of the complete yeast ESCRT-I heterotetramer. *Cell* **129**:485-98.
85. **Krebs FC, H. T., Quiterio S, Gartner S, Wigdahl B (ed.).** 2001. Lentiviral LTR-directed Expression, Sequence Variation, and Disease Pathogenesis. Theoretical Biology and Biophysics Group, Los Alamos National Laboratory, Los Alamos, NM.
86. **Kuiken C, F. B., Leitner T, Hahn B, Mizrachi I, Mullins J, Rambaut A, Wolinsky S, Korber B (ed.).** 2010. HIV Sequence Compendium 2010. Los Alamos National Laboratory, Theoretical Biology and Biophysics, Los Alamos, New Mexico.
87. **Kutluay, S. B., and P. D. Bieniasz.** 2010. Analysis of the initiating events in HIV-1 particle assembly and genome packaging. *PLoS Pathog* **6**:e1001200.
88. **Langelier, C., U. K. von Schwedler, R. D. Fisher, I. De Domenico, P. L. White, C. P. Hill, J. Kaplan, D. Ward, and W. I. Sundquist.** 2006. Human ESCRT-II complex and its role in human immunodeficiency virus type 1 release. *J Virol* **80**:9465-80.
89. **Leiharer, A., C. Ludwig, and R. Wagner.** 2009. Uncoupling human immunodeficiency virus type 1 Gag and Pol reading frames: role of the transframe protein p6\* in viral replication. *J Virol* **83**:7210-20.
90. **Leonard, T. A., B. Rozycki, L. F. Saidi, G. Hummer, and J. H. Hurley.** 2011. Crystal structure and allosteric activation of protein kinase C betaII. *Cell* **144**:55-66.
91. **Lever, A. M., and K. T. Jeang.** 2006. Replication of human immunodeficiency virus type 1 from entry to exit. *Int J Hematol* **84**:23-30.
92. **Levy, F., K. Muehlethaler, S. Salvi, A. L. Peitrequin, C. K. Lindholm, J. C. Cerottini, and D. Rimoldi.** 2005. Ubiquitylation of a melanosomal protein by HECT-E3 ligases serves as sorting signal for lysosomal degradation. *Mol Biol Cell* **16**:1777-87.
93. **Martin-Serrano, J.** 2007. The role of ubiquitin in retroviral egress. *Traffic* **8**:1297-303.
94. **Martin-Serrano, J., S. W. Eastman, W. Chung, and P. D. Bieniasz.** 2005. HECT ubiquitin ligases link viral and cellular PPXY motifs to the vacuolar protein-sorting pathway. *J Cell Biol* **168**:89-101.
95. **Martin-Serrano, J., A. Yarovoy, D. Perez-Caballero, and P. D. Bieniasz.** 2003. Divergent retroviral late-budding domains recruit vacuolar protein sorting factors by using alternative adaptor proteins. *Proc Natl Acad Sci U S A* **100**:12414-9.
96. **Martin-Serrano, J., T. Zang, and P. D. Bieniasz.** 2001. HIV-1 and Ebola virus encode small peptide motifs that recruit Tsg101 to sites of particle assembly to facilitate egress. *Nat Med* **7**:1313-9.
97. **Mervis, R. J., N. Ahmad, E. P. Lillehoj, M. G. Raum, F. H. Salazar, H. W. Chan, and S. Venkatesan.** 1988. The gag gene products of human immunodeficiency virus type 1: alignment within the gag open reading frame, identification of posttranslational modifications, and evidence for alternative gag precursors. *J Virol* **62**:3993-4002.
98. **Miyauchi, K., Y. Kim, O. Latinovic, V. Morozov, and G. B. Melikyan.** 2009. HIV enters cells via endocytosis and dynamin-dependent fusion with endosomes. *Cell* **137**:433-44.
99. **Miyoshi, I., H. Taguchi, M. Fujishita, K. Niiya, T. Kitagawa, Y. Ohtsuki, and T. Akagi.** 1982. Asymptomatic type C virus carriers in the family of an adult T-cell leukemia patient. *Gann* **73**:339-40.
100. **Morita, E., and W. I. Sundquist.** 2004. Retrovirus budding. *Annu Rev Cell Dev Biol* **20**:395-425.

101. **Muller, B., T. Patschinsky, and H. G. Krausslich.** 2002. The late-domain-containing protein p6 is the predominant phosphoprotein of human immunodeficiency virus type 1 particles. *J Virol* **76**:1015-24.
102. **Muller, B., U. Tessmer, U. Schubert, and H. G. Krausslich.** 2000. Human immunodeficiency virus type 1 Vpr protein is incorporated into the virion in significantly smaller amounts than gag and is phosphorylated in infected cells. *J Virol* **74**:9727-31.
103. **Nelson, D., and M. Cox (ed.).** 2007. *Lehninger: Principles of Biochemistry*, 4th ed.
104. **Niefind, K., and D. Schomburg.** 1991. Amino acid similarity coefficients for protein modeling and sequence alignment derived from main-chain folding angles. *J Mol Biol* **219**:481-97.
105. **Olsen, J. V., B. Blagoev, F. Gnad, B. Macek, C. Kumar, P. Mortensen, and M. Mann.** 2006. Global, in vivo, and site-specific phosphorylation dynamics in signaling networks. *Cell* **127**:635-48.
106. **Ono, A., and E. O. Freed.** 2004. Cell-type-dependent targeting of human immunodeficiency virus type 1 assembly to the plasma membrane and the multivesicular body. *J Virol* **78**:1552-63.
107. **Ott, D. E., L. V. Coren, E. N. Chertova, T. D. Gagliardi, and U. Schubert.** 2000. Ubiquitination of HIV-1 and MuLV Gag. *Virology* **278**:111-21.
108. **Ott, D. E., L. V. Coren, B. P. Kane, L. K. Busch, D. G. Johnson, R. C. Sowder, 2nd, E. N. Chertova, L. O. Arthur, and L. E. Henderson.** 1996. Cytoskeletal proteins inside human immunodeficiency virus type 1 virions. *J Virol* **70**:7734-43.
109. **Palencia, A., J. C. Martinez, P. L. Mateo, I. Luque, and A. Camara-Artigas.** 2006. Structure of human TSG101 UEV domain. *Acta Crystallogr D Biol Crystallogr* **62**:458-64.
110. **Parent, L. J., R. P. Bennett, R. C. Craven, T. D. Nelle, N. K. Krishna, J. B. Bowzard, C. B. Wilson, B. A. Puffer, R. C. Montelaro, and J. W. Wills.** 1995. Positionally independent and exchangeable late budding functions of the Rous sarcoma virus and human immunodeficiency virus Gag proteins. *J Virol* **69**:5455-60.
111. **Paulus, C., C. Ludwig, and R. Wagner.** 2004. Contribution of the Gag-Pol transframe domain p6\* and its coding sequence to morphogenesis and replication of human immunodeficiency virus type 1. *Virology* **330**:271-83.
112. **Pierce, M. M., C. S. Raman, and B. T. Nall.** 1999. Isothermal titration calorimetry of protein-protein interactions. *Methods* **19**:213-21.
113. **Pleschka, S.** 2008. RNA viruses and the mitogenic Raf/MEK/ERK signal transduction cascade. *Biol Chem* **389**:1273-82.
114. **Ponsel, D., and V. Bruss.** 2003. Mapping of amino acid side chains on the surface of hepatitis B virus capsids required for envelopment and virion formation. *J Virol* **77**:416-22.
115. **Popov, S., E. Popova, M. Inoue, and H. G. Gottlinger.** 2008. Human immunodeficiency virus type 1 Gag engages the Bro1 domain of ALIX/AIP1 through the nucleocapsid. *J Virol* **82**:1389-98.
116. **Popova, E., S. Popov, and H. G. Gottlinger.** 2010. Human immunodeficiency virus type 1 nucleocapsid p1 confers ESCRT pathway dependence. *J Virol* **84**:6590-7.
117. **Pornillos, O., S. L. Alam, D. R. Davis, and W. I. Sundquist.** 2002. Structure of the Tsg101 UEV domain in complex with the PTAP motif of the HIV-1 p6 protein. *Nat Struct Biol* **9**:812-7.
118. **Pornillos, O., S. L. Alam, R. L. Rich, D. G. Myszka, D. R. Davis, and W. I. Sundquist.** 2002. Structure and functional interactions of the Tsg101 UEV domain. *EMBO J* **21**:2397-406.
119. **Puffer, B. A., L. J. Parent, J. W. Wills, and R. C. Montelaro.** 1997. Equine infectious anemia virus utilizes a YXXL motif within the late assembly domain of the Gag p9 protein. *J Virol* **71**:6541-6.
120. **Raiborg, C., and H. Stenmark.** 2009. The ESCRT machinery in endosomal sorting of ubiquitylated membrane proteins. *Nature* **458**:445-52.

121. **Raymond, C. K., I. Howald-Stevenson, C. A. Vater, and T. H. Stevens.** 1992. Morphological classification of the yeast vacuolar protein sorting mutants: evidence for a prevacuolar compartment in class E vps mutants. *Mol Biol Cell* **3**:1389-402.
122. **Rieder, S. E., L. M. Banta, K. Kohrer, J. M. McCaffery, and S. D. Emr.** 1996. Multilamellar endosome-like compartment accumulates in the yeast vps28 vacuolar protein sorting mutant. *Mol Biol Cell* **7**:985-99.
123. **Rougier, J. S., M. Albesa, H. Abriel, and P. Viard.** 2011. Neuronal precursor cell-expressed developmentally down-regulated 4-1 (NEDD4-1) controls the sorting of newly-synthesized Cav1.2 calcium channels. *J Biol Chem.*
124. **Roxrud, I., H. Stenmark, and L. Malerod.** 2010. ESCRT & Co. *Biol Cell* **102**:293-318.
125. **Saad, J. S., A. Kim, R. H. Ghanam, A. K. Dalton, V. M. Vogt, Z. Wu, W. Lu, and M. F. Summers.** 2007. Mutations that mimic phosphorylation of the HIV-1 matrix protein do not perturb the myristyl switch. *Protein Sci* **16**:1793-7.
126. **Saad, J. S., J. Miller, J. Tai, A. Kim, R. H. Ghanam, and M. F. Summers.** 2006. Structural basis for targeting HIV-1 Gag proteins to the plasma membrane for virus assembly. *Proc Natl Acad Sci U S A* **103**:11364-9.
127. **Saksena, S., J. Sun, T. Chu, and S. D. Emr.** 2007. ESCRTing proteins in the endocytic pathway. *Trends Biochem Sci* **32**:561-73.
128. **Salahuddin, S. Z., P. D. Markham, F. Wong-Staal, G. Franchini, V. S. Kalyanaraman, and R. C. Gallo.** 1983. Restricted expression of human T-cell leukemia-lymphoma virus (HTLV) in transformed human umbilical cord blood lymphocytes. *Virology* **129**:51-64.
129. **Scherer, W. F., J. T. Syverton, and G. O. Gey.** 1953. Studies on the propagation in vitro of poliomyelitis viruses. IV. Viral multiplication in a stable strain of human malignant epithelial cells (strain HeLa) derived from an epidermoid carcinoma of the cervix. *J Exp Med* **97**:695-710.
130. **Schlundt, A., J. Sticht, K. Piotukh, D. Kosslick, N. Jahnke, S. Keller, M. Schuemann, E. Krause, and C. Freund.** 2009. Proline-rich sequence recognition: II. Proteomics analysis of Tsg101 ubiquitin-E2-like variant (UEV) interactions. *Mol Cell Proteomics* **8**:2474-86.
131. **Schmitt, A. P., G. P. Leser, E. Morita, W. I. Sundquist, and R. A. Lamb.** 2005. Evidence for a new viral late-domain core sequence, FPIV, necessary for budding of a paramyxovirus. *J Virol* **79**:2988-97.
132. **Segura-Morales, C., C. Pescia, C. Chatellard-Causse, R. Sadoul, E. Bertrand, and E. Basyuk.** 2005. Tsg101 and Alix interact with murine leukemia virus Gag and cooperate with Nedd4 ubiquitin ligases during budding. *J Biol Chem* **280**:27004-12.
133. **Sen, A., C. J. Sherr, and G. J. Todaro.** 1977. Phosphorylation of murine type C viral p12 proteins regulates their extent of binding to the homologous viral RNA. *Cell* **10**:489-96.
134. **Sena-Esteves, M., Y. Saeki, S. M. Camp, E. A. Chiocca, and X. O. Breakefield.** 1999. Single-step conversion of cells to retrovirus vector producers with herpes simplex virus-Epstein-Barr virus hybrid amplicons. *J Virol* **73**:10426-39.
135. **Snyder, P. M.** 2009. Down-regulating destruction: phosphorylation regulates the E3 ubiquitin ligase Nedd4-2. *Sci Signal* **2**:pe41.
136. **Strack, B., A. Calistri, S. Craig, E. Popova, and H. G. Gottlinger.** 2003. AIP1/ALIX is a binding partner for HIV-1 p6 and EIAV p9 functioning in virus budding. *Cell* **114**:689-99.
137. **Sundquist, W. I., H. L. Schubert, B. N. Kelly, G. C. Hill, J. M. Holton, and C. P. Hill.** 2004. Ubiquitin recognition by the human TSG101 protein. *Mol Cell* **13**:783-9.
138. **Tanzi, G. O., A. J. Piefer, and P. Bates.** 2003. Equine infectious anemia virus utilizes host vesicular protein sorting machinery during particle release. *J Virol* **77**:8440-7.
139. **Trauger SA, J. T., Siuzdak G.** 2003. Investigating viral proteins and intact viruses with mass spectrometry. *Top Curr Chem* **225**:265-282.
140. **Ubersax, J. A., and J. E. Ferrell, Jr.** 2007. Mechanisms of specificity in protein phosphorylation. *Nat Rev Mol Cell Biol* **8**:530-41.

141. **UNAIDS** 2010, posting date. Report on the global AIDS epidemic UNAIDS. [Online.]
142. **Usami, Y., S. Popov, and H. G. Gottlinger.** 2007. Potent rescue of human immunodeficiency virus type 1 late domain mutants by ALIX/AIP1 depends on its CHMP4 binding site. *J Virol* **81**:6614-22.
143. **Veronese, F. D., T. D. Copeland, S. Oroszlan, R. C. Gallo, and M. G. Sarngadharan.** 1988. Biochemical and immunological analysis of human immunodeficiency virus gag gene products p17 and p24. *J Virol* **62**:795-801.
144. **VerPlank, L., F. Bouamr, T. J. LaGrassa, B. Agresta, A. Kikonyogo, J. Leis, and C. A. Carter.** 2001. Tsg101, a homologue of ubiquitin-conjugating (E2) enzymes, binds the L domain in HIV type 1 Pr55(Gag). *Proc Natl Acad Sci U S A* **98**:7724-9.
145. **Wadekar, K., S. Pandey, P. Jain, V. Roy, A. Asthana, and R. Paranjape.** 2010. Frequency of P/S(XX)P duplication and FRFE, absence of LYP in p6Gag of Indian human immunodeficiency virus-1 subtype c isolates. *American Medical Journal* **1**:114-121.
146. **Waheed, A. A., and E. O. Freed.** 2010. The Role of Lipids in Retrovirus Replication. *Viruses* **2**:1146-1180.
147. **Wan, W. Y., and E. J. Milner-White.** 1999. A recurring two-hydrogen-bond motif incorporating a serine or threonine residue is found both at alpha-helical N termini and in other situations. *J Mol Biol* **286**:1651-62.
148. **Wei, X., J. M. Decker, H. Liu, Z. Zhang, R. B. Arani, J. M. Kilby, M. S. Saag, X. Wu, G. M. Shaw, and J. C. Kappes.** 2002. Emergence of resistant human immunodeficiency virus type 1 in patients receiving fusion inhibitor (T-20) monotherapy. *Antimicrob Agents Chemother* **46**:1896-905.
149. **Welsch, S., O. T. Keppler, A. Habermann, I. Allespach, J. Krijnse-Locker, and H. G. Krausslich.** 2007. HIV-1 buds predominantly at the plasma membrane of primary human macrophages. *PLoS Pathog* **3**:e36.
150. **Wills, J. W., C. E. Cameron, C. B. Wilson, Y. Xiang, R. P. Bennett, and J. Leis.** 1994. An assembly domain of the Rous sarcoma virus Gag protein required late in budding. *J Virol* **68**:6605-18.
151. **Witze, E. S., W. M. Old, K. A. Resing, and N. G. Ahn.** 2007. Mapping protein post-translational modifications with mass spectrometry. *Nat Methods* **4**:798-806.
152. **Wolf, D., S. I. Giese, V. Witte, E. Krautkramer, S. Trapp, G. Sass, C. Haller, K. Blume, O. T. Fackler, and A. S. Baur.** 2008. Novel (n)PKC kinases phosphorylate Nef for increased HIV transcription, replication and perinuclear targeting. *Virology* **370**:45-54.
153. **Xiang, Y., C. E. Cameron, J. W. Wills, and J. Leis.** 1996. Fine mapping and characterization of the Rous sarcoma virus Pr76gag late assembly domain. *J Virol* **70**:5695-700.
154. **Yasuda, J., and E. Hunter.** 1998. A proline-rich motif (PPPY) in the Gag polyprotein of Mason-Pfizer monkey virus plays a maturation-independent role in virion release. *J Virol* **72**:4095-103.
155. **Yuan, B., X. Li, and S. P. Goff.** 1999. Mutations altering the moloney murine leukemia virus p12 Gag protein affect virion production and early events of the virus life cycle. *EMBO J* **18**:4700-10.
156. **Yueh, A., and S. P. Goff.** 2003. Phosphorylated serine residues and an arginine-rich domain of the moloney murine leukemia virus p12 protein are required for early events of viral infection. *J Virol* **77**:1820-9.
157. **Zhadina, M., and P. D. Bieniasz.** 2010. Functional interchangeability of late domains, late domain cofactors and ubiquitin in viral budding. *PLoS Pathog* **6**:e1001153.

## **Appendix A: Analysis of the role of E3 ubiquitin ligase recruitment in retrovirus formation**

Special domains within the major structural retroviral protein Gag play a central role in the fission process that separates a budding retrovirus from the host cell membrane. These highly conserved peptide motifs are termed late domains and recruit cellular factors, such as components of the ESCRT (endosomal sorting complex required for transport) pathway. This pathway consists of a complex of proteins that participates in the sorting of ubiquitinated cargo proteins into multivesicular bodies (MVBs). In analogy to its role in MVB formation, the ESCRT system is required to separate the nascent virion from the infected cell. How enveloped viruses access the ESCRT system depends on the type of late domain present. There are 3 types of late domains, PT/SAP, YPDL and PPXY that recruit the ESCRT component Tsg101, the ESCRT-associated protein AIP1/Alix or interact with HECT E3 Ubiquitin ligases of the Nedd4 family, respectively. While the connection between Tsg101 and AIP1/Alix to the ESCRT system is well studied, the mechanism by which HECT Ubiquitin ligases mediate viral budding is not clearly understood. Although HIV-1 does not possess an L-domain of the PPXY type, it has been shown that overexpression of a specific isoform of the Nedd4 HECT E3 ubiquitin-ligase can enhance release of an HIV-1 clone lacking both of its known L-domains (22).

This study was aimed at providing evidence that interaction of Gag with ubiquitin and HECT E3 ligases facilitate virus release. By making use of a heterodimerizer system (ARIAD Pharmaceuticals) Figure A 1, which allows induction of interaction between proteins through a small molecule we sought to assay the contribution of different HECT Ub ligases and their subdomains to virus release and analyze the different requirements for E3 ligases among different retroviruses. A scheme of the dimerizer-inducible system for Gag budding is shown in Figure A 2.

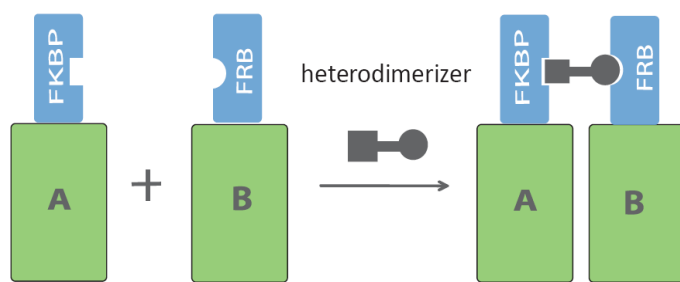


**Figure A 1 The heterodimerizer system:**

The FKBP (12 kDa) and FRB (11 kDa) domains can be each fused to a protein of interest A and B. Addition of the bivalent small chemical compound AP21967, the heterodimerizer, links the FKBP and FRB domains thereby bringing protein A and B into close proximity.

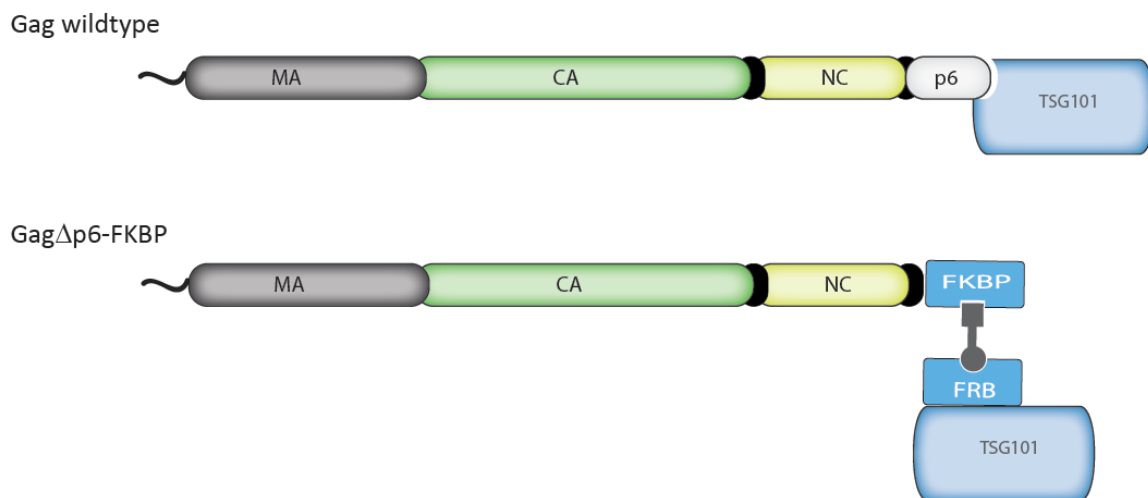


**Figure A 2 Schematic of the dimerizer-inducible system for Gag budding.**

The naturally occurring HIV-1 Gag-ESCRT interaction mediated by the Gag late domain and a Gag-binding domain of the relevant cellular factor is replaced by the heterodimerizer-inducible interaction of the FKBP and FRB domains, respectively. The p6 domain of HIV-1 Gag, containing the late domain motif was replaced by the FKBP domain while the FRB domain was fused to cellular factors that play a role in HIV-1 release such as Tsg101. In the presence of the dimerizer molecule, budding of the HIV-1 Gag $\Delta$ p6-FKBP should be reconstituted when a promoting factor such as Tsg101-FRB is coexpressed.

The ability of the Nedd4 family of E3 Ub ligases: WWP1, WWP2, Nedd4L and Itch were tested as FRB fusion proteins for their ability to rescue HIV-1 Gag $\Delta$ -FKBP release. 293T cells were cotransfected with each of the ligases at various concentrations and with the HIV-1 Gag $\Delta$ -FKBP. Cell lysates and virus supernatants were harvested and virus-like particles were pelleted over a 20 % sucrose cushion 24 h after transfection. The levels of released VLPs were determined by quantitative western blotting of the viral Gag protein. Initial experiments showed that the WWP2 and Itch ligases partially enhance VLP production (Figure A 3).

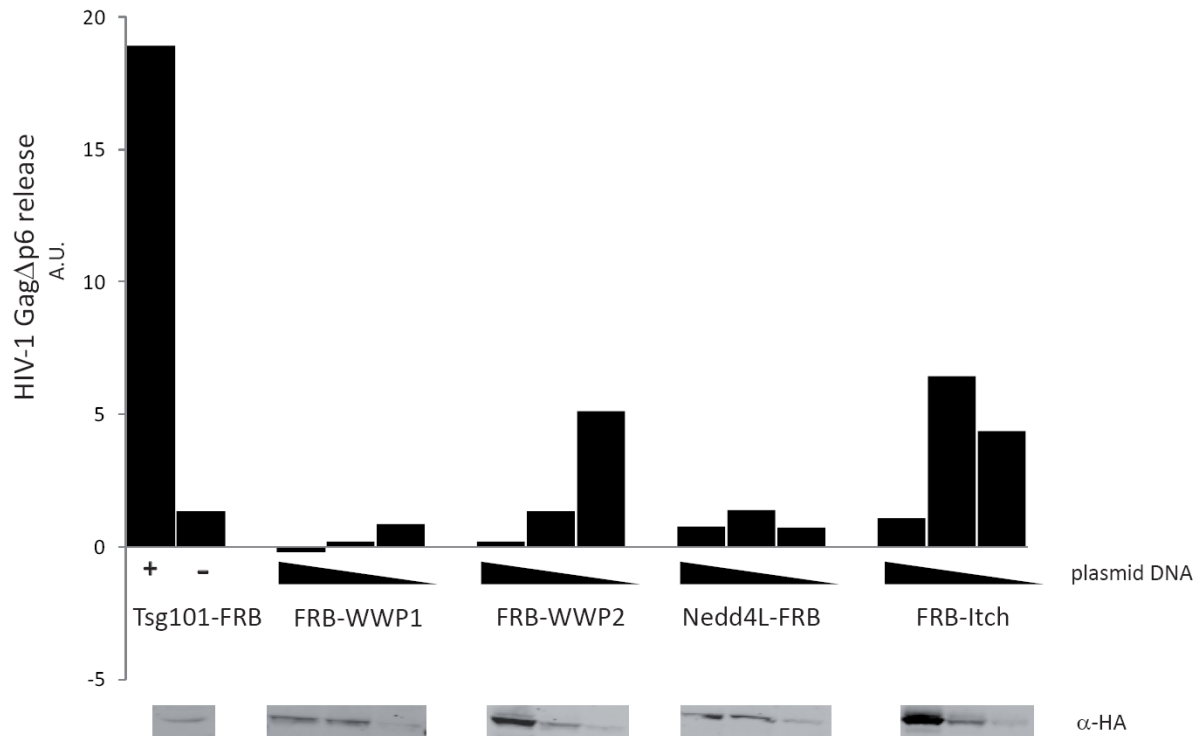


**Figure A 3 Effect of HECT Ub ligases in HIV-1 GagΔp6 release.**

293T cells were cotransfected with HIV-1 GagΔp6-FKBP and various amounts of plasmid DNA (100 ng-20 ng-5 ng) of the WWP1-, WWP2-, Nedd4L- and Itch-FRB tagged ligases. 50 nM AP21967 dimerizer were added 6 h after transfection. Gag release was determined 24 h after transfection by quantitative Western blotting of pelleted supernatants and expressed as arbitrary units (AU). As a positive control, FRB-tagged Tsg101 was tested in the presence (+) or absence (-) of dimerizer. Cell lysates were probed for HA to check for the expression of the ligase-FRB-HA fusion protein.

The FRB-tagged Itch and WWP2 constructs were selected for further analysis and tested at an additional range of concentrations. While the WWP2 construct failed to achieve higher levels of virus production (data not shown), the Itch construct efficiently rescued HIV-1 GagΔp6 release up to 50 % of wildtype levels (Figure A 4).

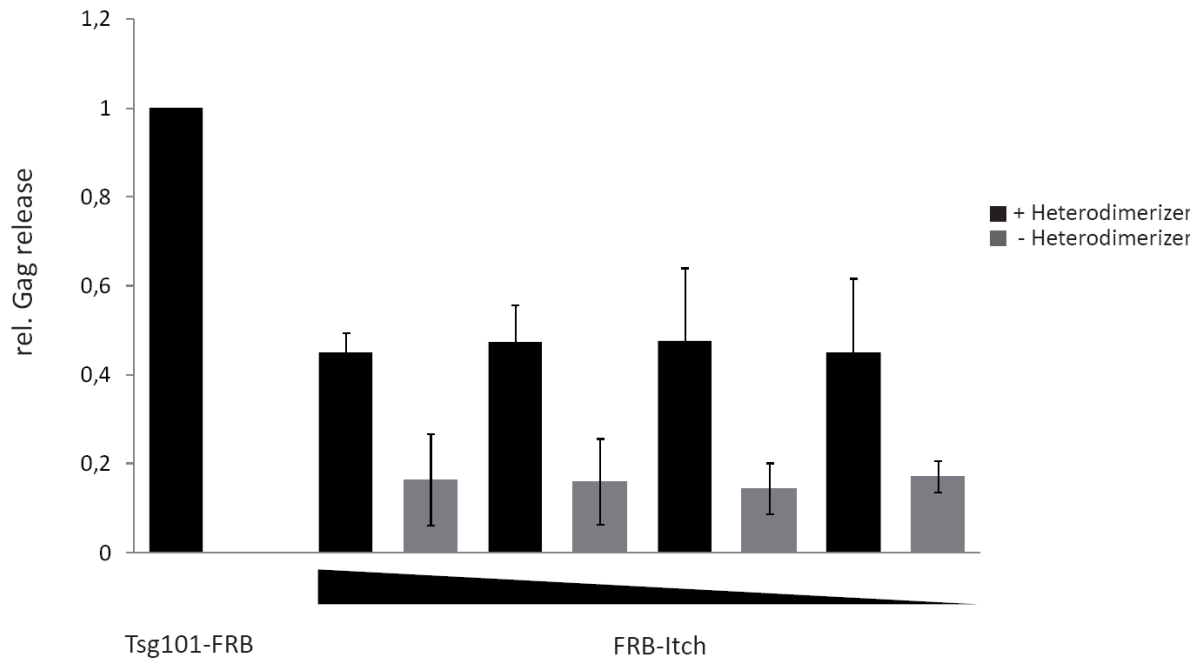


**Figure A 4 Effect of the FRB-tagged Itch ligase in rescuing HIV-1 Gag  $\Delta$ p6-FKBP release.**

293T cells were cotransfected with HIV-1 Gag $\Delta$ p6-FKBP and various amounts of FRB-Itch plasmid DNA (12.5 ng-10 ng-7.5 ng-5 ng) Cells were incubated either in the presence or absence of heterodimerizer as indicated. 50 nM AP21967 dimerizer was added 6 h after transfection. Gag release was determined 24 h after transfection by quantitative Western blotting of cell lysates and pelleted supernatants and expressed as the relative Gag release. The release efficiency of HIV-1 Gag $\Delta$ p6-FKBP in presence of Tsg101-FRB and dimerizer was set to 1.0.

The role of the HECT ubiquitin ligases was also tested in the context of a L-domain mutant rous sarcoma virus (RSV). Hence, the FRB-tagged WWP1, WWP2, Nedd4L and Itch were cotransfected with a L-domain mutant FKBP-tagged RSV Gag $\Delta$ PPPY $\Delta$ LYPSL and their ability to rescue RSV release was tested. None of the ligases was able to promote release of the mutant RSV Gag (data not shown).

Although ubiquitination of retroviral Gag proteins has been extensively researched, the precise role of Gag ubiquitination is still unclear. Given the similarities between MVB sorting and viral budding, and the fact that fusion of Ub to the C-terminus of HIV-1 Gag enhanced its interaction with Tsg101 *in vitro* (49), a direct relevance of Gag ubiquitination appears plausible. We sought to address the role of ubiquitin overexpression and delivery to sites of HIV-1 Gag $\Delta$ p6-FKBP assembly and budding through the dimerizer system. The ability of the FRB-Ub fusion protein in rescuing release of HIV-1 Gag $\Delta$ p6-FKBP is shown in Figure A5. Experiments conducted using Tsg101-FRB as a positive control showed that overexpression of a Ub moiety can rescue release up to 50 % of the wildtype levels. The Alix protein can mediate release of L-domain mutant HIV-1 when overexpressed, thus we also included this

construct in some of the analyses as an additional positive control (data not shown). While the FRB-tagged Tsg101 control provided the most consistent results and was able to rescue release of L-domain deficient HIV-1 Gag, Alix-FRB did not. I repeatedly observed inconsistencies in the behavior of this construct in the absence of heterodimerizer.

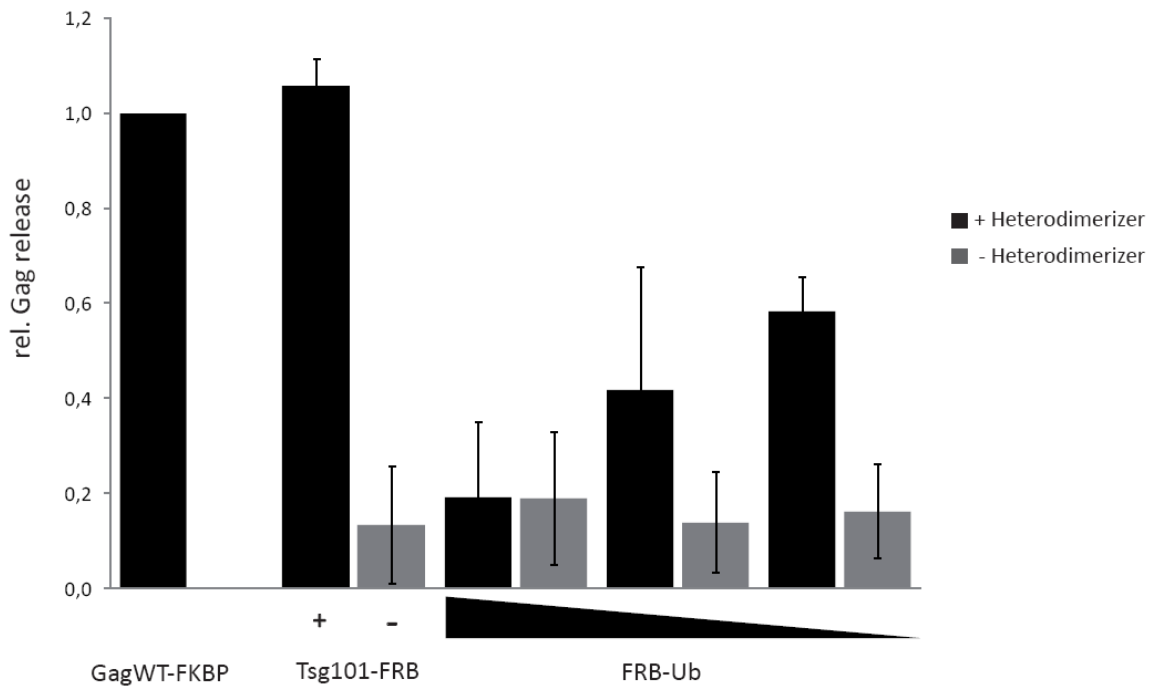


**Figure A 5 Effect of FRB-Ub overexpression in the rescue of HIV-1 Gag $\Delta$ p6-FKBP particles.**

293T cells were cotransfected with HIV-1 Gag $\Delta$ p6-FKBP and various amounts of FRB-Ub plasmid DNA (100 ng-20 ng-5 ng) Cells were incubated either in the presence or absence of heterodimerizer as indicated. 50 nM AP21967 dimerizer was added 6 h after transfection. Gag release was determined 24 h after transfection by quantitative Western blotting of cell lysates and pelleted supernatants and expressed as the relative Gag release. The release efficiency of HIV-1 Gag $\Delta$ p6-FKBP in presence of Tsg101-FRB and dimerizer was set to 1.0.

Taken together, out of the HECT E3 ligases tested the Itch ligase most efficiently rescued L-domain deficient HIV-1 Gag but not RSV in this system. In addition, Ub overexpression seemed to help HIV-1 Gag $\Delta$ p6 overcome part of its late domain deficiency; however we obtained conflicting results with the Alix control (see above). These inconsistencies must be considered in the final interpretation of the data and the behavior of the Alix construct must be evaluated carefully.

## List of publications

### Journal papers:

Morales I., Carbajal, MA., Bohn, S., Holzer, D., Kato, SE., Greco, FA., Moussatché, N., Krijnse-Locker, J. 2008. The vaccinia virus F11L product facilitates cell detachment and promotes migration. *Traffic* **9**: 1283-98.

Kienitz, A., Vogel, C., Morales, I., Müller, R., Bastians, H. 2005. Partial downregulation of MAD1 causes spindle checkpoint inactivation and aneuploidy, but does not confer resistance towards taxol. *Oncogene* **24**: 4301-10.

### Oral presentations:

Morales, I., Müller, B., Kräusslich, HG. Functional relevance of p6<sup>Gag</sup> phosphorylation in HIV-1's replication cycle. Workshop "Cell Biology of Viral Infections," September 2009, Deidesheim, Germany.

Morales, I., Jäger, S., Kräusslich, H. Role of cellular ESCRT factors and E3 ubiquitin ligases in retroviral release. SFB 638 Spring meeting: "Dynamics of macromolecular complexes in biosynthetic transport," April 2008, Lindenfels-Winkel, Germany.

Jäger, S., Morales, I., Habermann, A., Kräusslich, HG. A heterodimerizer-based approach to analyze the role of cellular factors in retrovirus formation. Cold Spring Harbor Retrovirus Meeting, May 2008, Cold Spring Harbor, NJ, USA.

Morales, I., Habermann, A., Kräusslich, HG. Role of cytoskeletal elements in HIV-1 budding. Workshop "Cell Biology of Viral Infections," September 2009, Deidesheim, Germany.

### Poster presentations:

Morales, I., Müller, B., Kräusslich, HG. Functional analysis of potential phosphorylation sites in the p6 domain of HIV-1 Gag. 1<sup>st</sup> Cellular Networks Conference, September 2010, Heidelberg, Germany.

Morales, I., Müller, B., Kräusslich, HG. Functional analysis of potential phosphorylation sites in the p6 domain of HIV-1 Gag. Centennial Retrovirus Meeting, April 2010, Prague, Czech Republic.

Jäger, S., Morales, I., Habermann, A., Kräusslich, HG. Dissecting the role of cellular factors in retroviral budding using heterodimerizer-mediated virus-host protein interaction. Retrovirus Assembly Meeting, October 2008, Prague, Czech Republic.

Jäger, S., Morales, I., Habermann, A., Kräusslich, HG. A heterodimerizer-based approach to analyze the role of cellular factors in retrovirus formation. Annual Meeting of the German Society of Virology (GfV), March 2008, Heidelberg, Germany.

## 6 List of abbreviations

aa	amino acid
AA	acrylamide
AAA+ ATPase	ATPase associated with a variety of cellular activities
AIDS	acquired immunodeficiency virus
ALG-2	apoptosis-linked gene 2
ALIX	ALG-2 interacting protein X
AMSH	associated molecule with the SH3 domain of STAM
app.	<i>approximately</i>
APS	ammonium peroxodisulfate
BIS	N,N'-methylene bisacrylamide
CA	capsid
CHMP	charged multivesicular body protein
CIAP	calf intestine alkaline phosphatase
CTD	C-terminal domain
DMEM	dulbecco's Modified Eagle Medium
DNA	desoxyribonucleic acid
dNTPs	deoxy-nucleoside-triphosphates
DUB	deubiquitinase
EAP	ELL-associated protein
ECL	enhanced chemiluminescence
EDTA	ethylene-diamine-tetra-acetic acid
EGFR	epidermal growth factor receptor
EIAV	equine infectious anemia virus
ELISA	enzyme-linked immunosorbent assay
EM	electron microscopy
Env	envelope
ESCRT	endosomal trafficking complex required for transport

FCS	fetal calf serum
Fig.	figure
FKBP	FK506 binding protein
FRB	FKBP12 rapamycin-binding domain
Gag	group specific antigen
GLUE	GRAM-like ubiquitin binding in EAP45
h	hour
HA	hemagglutinin
HECT	homologous to E6-AP C-terminus
HIV-1	human immunodeficiency virus-1
HRS	hepatocyte growth factor-regulated tyrosine kinase substrate
Hsp	heat shock protein
HTLV	human T cell leukemia virus
ILV	intraluminal vesicle
IPTG	isopropyl- $\beta$ -D-thiogalactopyranosid
kDa	kilo Dalton
LB	lysogeny broth
LC-MS/MS	liquid chromatography-tandem mass spectrometry
LTR	long terminal repeat
LTR	long terminal repeat
MA	matrix
MLV	murine leukemia virus
MPMV	mason pfizer monkey virus
mRNA	messenger RNA
MVB	multivesicular body
NC	nucleocapsid
Nedd4L	neural precursor cell expressed, developmentally down-regulated 4
NEM	N-ethylmaleimide
NMR	nuclear magnetic resonance

nt	nucleotide
NTD	N-terminal domain
p	protein
p24	alternative designation of the HIV-1 CA protein
PAGE	polyacrylamide gel electrophoresis
PBMC	peripheral blood mononuclear <i>cell</i>
PBS	phosphate buffered saline
PCR	polymerase chain reaction
PIC	preintegration complex
pol	polymerase
PR	protease
RNA	ribonucleic acid
rpm	rotations per minute
RRE	Rev responsive element
RSV	rouv sarcoma virus
RT	room temperature
RT	room temperature
RTC	reverse transcription complex
SDS	sodium dodecyl sulfate
siRNA	small interfering RNA
SP1	spacer 1
SP2	spacer 2
TBS	tris buffered saline
TMB	3,3',5,5' tetramethylbenzidine
Tris	tris(hydroxymethyl)aminomethane
TSG101	tumor suppressor gene 101
U	unit
Ub	ubiquitin
UBD	ubiquitin binding domain
UEV	ubiquitin E2 variant

UIM	ubiquitin interacting motif
UTR	untranslated terminal region
Vps	vacuolar protein sorting

## Acknowledgements

I would like to sincerely thank my advisor Prof. Hans-Georg Kräusslich for giving me the opportunity to learn to conduct independent research with the HIV-1 virus, which although has been studied for several decades still holds many surprises for the researcher, always evolving new ways to keep propagating. I would also like to thank the members of my PhD committee: Dr. Jacomine Krijnse-Locker for her support, optimism and critical reading of this work, to Prof. Dieter Kübler for participating again yet in a different level of my studies in Germany and to Dr. Freddy Frischknecht for taking part in the evaluation of this work.

I am thankful to to Dr. Barbara Müller for initiating this exciting project, for her contribution of constructs and her valuable input. I would like to thank our collaborators, Dr. Albert Sickmann and Dr. René Zahedi at the ISAS institute for the mass spectrometry analysis of p6 and Dr. Winfried Weissenhorn and Pauline Machebouef for their crystallization assays. In addition, I would like to thank Kishore Rajagopalan for giving me essential advice on how to use an ITC machine, to Sergio Perez Acebrón for invaluable discussions on ITC data analysis, to Norman Davey for his interest in the project and his detailed analysis of the PNAP motif, to Prof. Matthias Mayer for help with the peptide measurements. I would specially like to thank my dear friend Arzu Sandicki for facilitating the use of the ITC machine at the ZMBH and for introducing me to Kishore and Prof. Mayer.

My wholehearted thanks go to my very special manager, Petrificado Chancla for contributing his expertise in EM and whose enormous support and good humor made everything much easier, to my very dear friend Maier Chorizate for her great support, stimulating discussions, and for sharing her love of Marquess, to Nacho Libre for teaching me how to purify proteins, help with columns and for setting up crystallization trials in Heidelberg, to Jessy Jane for support and critical reading of this work, to Heike Oberwinkler and Bärbel Glass for sharing their technical expertise and to Xabi Contreras for facilitating the use of their gel system at the BZH .

Finally, I am deeply grateful to my parents Antonio and Martha, for their tremendous support in each of my undertakings and for their unconditional belief in me.

This work was financially supported by the German Research Foundation (DFG) within the scope of the SFB 638.